AIR GAPS IN PROTECTIVE CLOTHING

DURING FLASH FIRE EXPOSURE

A Thesis Submitted to

the College of Graduate Studies and Research

in Partial Fulfillment of the Requirements for the Degree of

Doctor of Philosophy

in the Department of Mechanical Engineering

University of Saskatchewan

Saskatoon, Saskatchewan

By

AHMED GHAZY

PERMISSION TO USE

In presenting this thesis in partial fulfillment of the requirements for a Postgraduate degree from the University of Saskatchewan, I agree that the Libraries of this University may make it freely available for inspection. I further agree that permission for copying of this thesis in any manner, in whole or in part, for scholarly purposes may be granted by the professor or professors who supervised my thesis work or, in their absence, by the Head of the Department or the Dean of the College in which my thesis work was done. It is understood that any copying or publication or use of this thesis or parts thereof for financial gain shall not be allowed without my written permission. It is also understood that due recognition shall be given to me and to the University of Saskatchewan in any scholarly use which may be made of any material in my thesis.

Requests for permission to copy or to make other uses of materials in this thesis in whole or part should be addressed to:

Head of the Department of Mechanical Engineering

University of Saskatchewan

Saskatoon, Saskatchewan S7N 5A9

Canada

ABSTRACT

Protective clothing is widely used in many industries and applications to provide protection against fire exposure. Exposure to fire can result in skin burn injuries that range from first-degree to third-degree burn injury depending on the exposure intensity and duration. Within the firefighting community, and especially the petroleum and petrochemical industries flash fire is one of the possible fire hazards for workers. Exposure to flash fire is usually of short duration (a few seconds) until the worker runs away from the fire location. The typical protective clothing system consists of a fire resistant fabric, the human skin, and an air gap between the fabric and skin. The protective performance of the clothing is evaluated based on the total energy transfer from the fabric to the skin through the air gap causing burn injury to the skin. Therefore the air gap between the protective clothing and skin plays an important role in determining the protection level provided by the clothing since the energy transfer through the air gap determines the amount of energy received by the skin. The more realistic the analysis of the air gap, the more reliable the evaluation of the protective performance of the clothing.

This study introduces a more realistic analysis for the air gap between protective clothing and the skin compared to that found in the literature. More specifically, the study accounts for the combined conduction-radiation heat transfer through the air gap, which was treated as a thermal radiation participating medium with temperature dependent thermophysical properties. A finite volume model was developed to simulate the transient heat transfer in a single layer protective clothing system with radiation heat transfer. The model was employed to investigate the influence of the conduction-radiation heat transfer through the air gap on the overall heat transfer through the protective clothing system and hence on its protective performance. The influence of different protective clothing parameters on the combined

conduction-radiation heat transfer through the air gap such as the air gap absorption coefficient, air gap width, fabric thickness, and fabric backside emissivity was studied. A comprehensive study of the influence of a periodic variation in the air gap width and associated inflow of cool air due to the motion of the person wearing the clothing on its protective performance was carried out. A wide range of variation in the frequency and amplitude of the fabric periodic movement was considered to capture different scenarios for the wearer's motion. Finally, a finite volume model was developed to simulate the transient heat transfer in multiple layers firefighters' protective clothing. The model considered the combined conduction-radiation heat transfer in the air gaps entrapped between the clothing layers, which were treated as thermal radiation participating media. The influence of each air gap on the overall performance of the clothing was investigated as well.

The improved air gap model is a significant improvement for modeling heat transfer in protective clothing. It was used to obtain a more detailed knowledge of the theoretical performance of such clothing, e.g. it was found that reducing the fabric backside emissivity was more effective in improving the clothing protective performance than increasing the fabric thickness. It was also observed that the motion of the person wearing the clothing has a significant effect on the performance of the clothing: an increase in the frequency of the fabric movement improves the protection provided by the clothing, primarily due to the more frequent inflow of cool air, while an increase in the amplitude of the fabric movement reduces the protection provided by the clothing by concentrating the exposure on the skin. Finally, the air gaps entrapped between the clothing layers in firefighters' protective clothing were found to improve the clothing performance, and the influence of the air gap between the moisture barrier

and the thermal liner is greater than that of the air gap between the outer shell and the moisture barrier.

ACKNOWLEDGMENT

First of all, I would like to express my sincere appreciation and gratitude to my supervisor Prof. Donald J. Bergstrom for his unlimited support, encouragement, and guidance. I admit that his wise supervision permitted to me and guided me to grow up safely as an independent researcher. His advice and positive comments were always there to add significantly to the quality of the research work. In addition, his kind compliments were invaluable in reviving my enthusiasm at the moments of frustration.

I would like also to extend my thank and appreciation to my advisory committee members; Prof. James D. Bugg, Prof. Carey J. Simonson, Prof. Richard W. Evitts, Prof. David A. Torvi, and Prof. David Sumner for their suggestions and advices for my research program.

As the family is always the Unknown Soldier behind the success in the graduate program, I would like to take the opportunity to acknowledge my beloved small family; my wife, Hanaa and my two sons, Moataz and Saifeddean for their continuous patience and sacrifice during my study program. An equivalent acknowledgement goes to our big family in Egypt for their encouragement and support.

Finally, I acknowledge the financial support from the Department of Mechanical Engineering through the departmental scholarship. I also acknowledge the financial support provided to me by Prof. Donald J. Bergstrom during the last few months of my Ph.D. program.

TABLE OF CONTENTS

CHAPTER 1

INTRODUCTION

1. BACKGROUND

Flash fire is one of the possible hazards for workers in many industries and applications such as petroleum and petrochemical industries, firefighting, and sport car driving. Flash fires typically release heat fluxes of the order of 80 kW/m^2, which are partially convective and partially radiative. Exposures to flash fire are usually of short duration (a few seconds) and typically end when the individual escapes from the location of the fire. Exposure to fire can result in skin burn injuries that range from first-degree burn injury to third-degree burn injury depending on the exposure intensity and duration.

Protective clothing made of fire resistant fabrics is widely used in many industries and applications in order to provide protection from fire exposure. The type of protective clothing varies from one application to another depending on the probability of exposure, and expected exposure intensity and duration. Evaluating the performance of protective clothing usually involves estimating the total energy transfer through the fabric that causes burn injury to the human skin on the other side of the fabric.

The typical protective clothing system consists of a single layer or multiple layers of fire resistant fabric, the human skin, and the air gap between the clothing and the skin. Energy transfers from the flame to clothing during the exposure in the form of convective and radiative heat fluxes. A portion of this energy is stored in the clothing in the form of a temperature rise while another portion is released from the exposed surface of the clothing to the ambient in the form of radiation losses. If the air gap between the clothing and the skin is less than 6.35 mm

(1/4 in.), energy transfers by combined conduction-radiation heat transfer from the backside of the clothing to the skin. This release of the energy stored in the clothing to the skin during the exposure and cool down periods raises the skin temperature and potentially causes skin burn injury.

2. MOTIVATION

The numerical modeling of heat and mass transfer in protective clothing aims at (i) predicting the protective performance of the clothing as an alternative to the experimental models that are costly and time consuming; (ii) investigating potential approaches to improve the clothing performance and to avoid or minimize skin burn injuries. In addition, the more realistic the analysis adopted by the numerical model, the more reliable the prediction of the clothing performance.

The various numerical models developed in the literature for heat and mass transfer in protective clothing during fire exposure clearly demonstrated the importance of the air gap between the fabric and the skin and its effect on the performance of protective clothing. However, most models have focused on providing a careful analysis of both the fabric and the skin behaviour and only dealt with the air gap in an approximate way. For example, they often decouple the conduction and radiation heat transfer through the air gap, and instead assume steady state conduction and only surface radiation heat transfer through the air gap. A more careful and realistic model for the heat transfer through the air gap would contribute to a more accurate prediction of the clothing performance.

Given this context, the overall objective of this research project is to investigate the influence of the air gap between the protective clothing and the skin on the clothing performance. This requires the development of an improved model for the air gap between the protective

clothing and skin that considers the combined conduction-radiation heat transfer through the air gap which is treated as a radiation participating medium.

3. RESEARCH OBJECTIVES

The specific objectives of the present thesis are highlighted as follows where the air gap model is the critical and unifying aspect of these objectives.

1- To develop a numerical model for the transient heat transfer in a protective clothing system during flash fire exposure that accounts for the combined conduction-radiation heat transfer in the air gap between the clothing and the skin, which is treated as a thermal radiation participating medium with temperature dependent properties.

2- To further investigate the influence of different clothing system parameters on the combined conduction-radiation heat transfer in the air gap, as a radiation participating medium, and hence their influence on the clothing performance during flash fire exposure.

3- To investigate the influence of a periodic variation in the air gap width due to the motion of the person wearing the clothing on the transient heat transfer through the clothing and hence the clothing protective performance during flash fire exposure.

4- To develop a numerical model for the transient heat transfer in a multiple layer protective clothing system during flash fire exposure that takes into account the combined conduction-radiation heat transfer in the air gaps between clothing layers, which are treated as thermal radiation participating media with temperature dependent properties.

4. NUMERICAL CHALLENGES

The implementation of numerical methods for modeling radiation heat transfer in a thermal radiation participating medium is the main research theme pursued in this project. In particular, modeling transient conduction-radiation heat transfer in a thermal radiation

participating medium using the Finite Volume Method for both conduction and radiation parts is the specific expertise developed in the research work.

One numerical challenge encountered in modeling conduction-radiation heat transfer within the air gap of protective clothing is the simultaneously determined boundary conditions for conduction-radiation compared to the defined boundary conditions adopted in the typical conduction-radiation approach. In other words, the typical conduction-radiation problem which considers enclosures of thermal radiation participating medium is solved in the literature for defined boundary conditions such as constant temperatures or constant heat fluxes at the boundary. However, the conduction-radiation heat transfer through the air gap of protective clothing is located in the middle of the protective clothing system. Therefore, the temperatures at the air gap boundaries are directly dependent on the value of the conduction-radiation heat transfer through the air gap. On the other hand, the value of the conduction-radiation heat transfer through the air gap depends on the temperatures at the boundaries of the air gap.

Additional numerical complexity has been added to the conduction-radiation model adopted for the air gap(s) of protective clothing by considering temperature dependent thermal properties (objectives 1, 2, 3, 4), varying the conduction-radiation domain periodically (objective 3), and having multiple conduction-radiation domains with simultaneously determined boundary conditions (objective 4).

5. THESIS ORGANIZATION

The layout of the thesis consists of six chapters that include four journal manuscripts. The present chapter introduces the research motivation, objectives, and challenges. Chapters two to five contain the four journal manuscripts that address the four objectives of the thesis as follows. Chapter two describes a numerical model for heat transfer in protective clothing during

flash fire exposure that accounts for the combined conduction-radiation heat transfer in the air gap between the clothing and the skin. Chapter three introduces a parametric study for different protective clothing parameters that affect the conduction-radiation heat transfer through the air gap and their influence on the clothing performance. Chapter four addresses the influence of the motion of the person wearing the clothing on the heat transfer through the clothing and hence the clothing protective performance. Chapter five describes a numerical model for heat transfer in multiple layer protective clothing considering the conduction-radiation heat transfer in the air gaps between the clothing layers.

6. CONTRIBTIONS OF AUTHORS

The journal manuscripts included in chapter two to five are co-authored by Ahmed Ghazy as the first author and Prof. Donald J. Bergstrom as the corresponding author. However, all the research work documented in the manuscripts was accomplished by Ahmed Ghazy, with Prof. Donald J. Bergstrom providing some technical advice. The text of each manuscript was prepared by Ahmed Ghazy, with Prof. Donald J. Bergstrom critically reviewing the manuscripts and providing editorial feedback.

CHAPTER 2

NUMERICAL SIMULATION OF TRANSIENT HEAT TRANSFER IN A PROTECTIVE CLOTHING SYSTEM DURING A FLASH FIRE EXPOSURE

Published as

A. Ghazy and D.J. Bergstrom, Numerical Simulation of Transient Heat Transfer in a Protective Clothing System during a Flash Fire Exposure, Numerical Heat Transfer A, vol. 58(9), pp.702-724, 2010.

Contribution of this Chapter to the Thesis

The research work presented in this chapter aims at achieving the first objective of the thesis. More specifically, the chapter describes a numerical model for heat transfer in protective clothing systems that implements a more sophisticated model for the air gap between the fabric and the skin. A comparison between the predictions of the present model to that of the typical model in the literature is included in the chapter, which demonstrates the effect of the present air gap model on predicting the clothing performance. The model was used to provide insight into the mechanism of heat transfer in protective clothing that could potentially improve the performance of the clothing and/or lead to new protection strategies.

Numerical Simulation of Transient Heat Transfer in a Protective Clothing System during a Flash Fire Exposure

Ahmed Ghazy and Donald J. Bergstrom

Department of Mechanical Engineering, University of Saskatchewan, Saskatoon, Saskatchewan, Canada

Address correspondence to Donald J. Bergstrom, Department of Mechanical Engineering, University of Saskatchewan, 57 Campus Dr., Saskatoon, SK S7N 5A9, Canada. E-mail: Don.Bergstrom@usask.ca

ABSTRACT

A finite volume model was developed to simulate the transient heat transfer in a protective clothing system. The model domain consists of a fire-resistant fabric, the human skin, and the air gap between the fabric and the skin. The model uses a more sophisticated treatment of the air gap compared to previous models: it accounts for transient combined conduction-radiation heat transfer within the air gap and includes the variation in the air gap properties with temperature. Predictions were obtained for the temperature and heat flux distributions in the fabric, skin, and air gap as a function of time, as well as the time to receive skin burn injuries. The numerical model was used to explore the physics of heat transfer in protective clothing, which could potentially be used to improve the performance of this clothing. This study illustrates the dependence of the temporal behavior of the heat fluxes on the specific model assumptions, as well as the associated sensitivity of skin burn predictions to these assumptions.

NOMENCLATURE

A	surface area, m^2

a, b	finite volume discrete equation coefficient, source term
C	heat capacity, J/kg K
c_P	specific heat at constant pressure, J/kg K
D_c^l	directional cosine integrated over $\Delta\Omega^l$
$\hat{e}$	unit vector in coordinate direction
G	incident radiation, W/m^2
h	convective heat transfer coefficient, W/m^{2}K
I	Intensity, W/m^2
k	thermal conductivity, W/m K
L	thickness, m
P	pre-exponential factor, 1/s
q''	heat flux, W/m^2
$\vec{r}$	position vector, m
R	ideal gas constant, J/mol K
$\hat{s}$	unit vector in a given direction
S	source function
s	geometric distance, m
T	temperature, K
t	time, s
W	fabric width, m
y	linear vertical coordinate, m

Greek Symbols

Ω	solid angle, sr

Ψ	quantitative measure of skin damage
θ	polar angle, rad
ϕ	azimuthal angle, rad
ΔE	activation energy of skin, J/kmol
ΔV	volume of control volume, m^3
$\Delta\Omega^l$	control angle
α	air gap absorptivity
ε	emissivity
γ	extinction coefficient of the fabric, 1/m
κ	air gap absorption coefficient, 1/m
ρ	density, kg/m^3
σ	Stefan-Boltzmann constant, 5.67×10^{-8} W/m^2K^4
τ	transmissivity
ω	blood perfusion rate, $(m^3/s)/m^3$ of human tissue

Subscripts

air	air
amb	ambient conditions
b	human blood / black body
cnv	convection heat transfer
cr	human body core
ep, ds, sc	epidermis , dermis, subcutaneous human skin layers
exp	exposure

fab	fabric
fbr	fabric fiber
fl	flame
g	hot gases
ib, ie	first, last computational control volume
N, S	north, south neighbor control volumes
n, s	north, south control volume faces
P	control volume central point
R , rad	radiation heat transfer
x, y, z	coordinate directions

Superscripts

A	apparent
l	index for direction

1. INTRODUCTION

Accidental exposure to fire may occur in diverse fields including the petroleum and petrochemical industries. One possible hazard is a flash fire, which may result from the sudden ignition of combustible gases that are released from a leak in pipelines or plant components. Flash fires typically release heat fluxes of the order of 80 kW/m^2 [1], which are partially convective and partially radiative. Exposures to flash fire are usually of short duration (less than 5 s) and end when the worker escapes from the location of the fire. Municipal firefighters face a variety of convective and/or radiative exposures of different duration and intensity. Exposure to fire can result in skin burn injuries. These injuries range from first-degree burn injury to third-degree burn injury depending on the exposure intensity and duration. One of the methods used to

predict skin burns is the criterion developed by Stoll and Chianta [2] to estimate the time of exposure necessary for a rectangular heat flux wave of a given intensity incident on a bare skin to cause second-degree burn.

Protective clothing made of fire resistant fabrics is widely used in many industries in order to provide protection from fire. The type of protective clothing varies from one application to another depending on the probability of exposure, and expected exposure intensity and duration. For the fabric used in this clothing, breaking the chemical bonds between molecules requires a large amount of energy, which thus explains the survival of the clothing for a finite time during fire exposure.

Evaluating the performance of protective clothing typically involves estimating the total energy transfer through the fabric that is necessary to cause burn injury to human skin on the other side of the fabric. Bench top tests such as the Thermal Protective Performance (TPP) test are used to evaluate the performance of protective fabrics. In this test, fabric is examined by radiant exposure [3], convective exposure [4], or a combination of both exposures [5]. The TPP rating of a fabric is defined as the amount of energy in cal/cm^2 that must be supplied to the fabric for a second-degree burn of the skin behind the fabric to occur based on the Stoll criterion. A standard air gap width of 6.35 mm (1/4 in.) is used in the test to separate the fabric specimen and the test sensor that is used to measure the heat flux incident on the skin. In order to test the protective performance of the entire garment rather than a specimen of the fabric, manikin tests are conducted according to ASTM F 1930 [6]. An instrumented manikin wearing the garment is subjected to a simulated flash fire and then using many skin simulant heat flux gauges installed on different parts of the manikin's body, the heat fluxes at these locations are measured. From

this information, the extent to second and third degree burns can be predicted using the Henriques burn integral [7].

Safety precautions notwithstanding, a large number of industrial workers receive skin burn injuries during fire exposure every year. This statistic has stimulated research towards developing both experimental and numerical models to simulate heat and moisture transfer in protective clothing and to predict their performance. Torvi [1, 8] developed a one-dimensional finite element model to simulate heat transfer in a single layer of fire-resistant fabric during a contact flame bench top test. The fabric was exposed to approximately 80 kW/m^2 for a short duration. The thermal degradation in the fabric at high temperatures was included by Zhu et al. [9] in a one-dimensional model to simulate heat transfer in heat-resistant fabrics during radiant exposure. Their model was able to predict the rate of mass loss in the fabric due to pyrolysis with good agreement compared to experimental data.

By combining heat transfer in the protective fabric and human skin, Song et al. [10] developed a one-dimensional finite difference model to simulate heat transfer in a single layer protective garment worn by an instrumented manikin (PyroMan®) that was exposed to a laboratory flash fire. The model accounted for the variation in the air gap width between the fabric and the manikin body with location (leg, arm, shoulder, etc.) that was measured using a three-dimensional body scanning technique. Zhu et al. [11] applied a more realistic model for heat transfer in human skin that allows for a finite speed of heat transfer in the skin in a one-dimensional model to evaluate the thermal performance of flame-resistant fabrics during radiant exposure. Their study compared skin burn predictions using the new model to that using Pennes's model [12] where a significant deviation was noticed between the two models at high heat flux exposure.

The simulation of coupled heat and mass transfer in porous textiles has been reported in the literature by many researchers [13-15]. The coupled heat and moisture transfer in multiple layer firefighters' clothing during flash fire exposure was numerically investigated by Chitrphiromsri et al. [16, 17]. The model was used to predict both temperature and moisture content distributions within the firefighters' clothing during both the exposure and the cool down periods. Song et al. [18] also developed a one-dimensional finite volume model to study heat and moisture transfer in multiple layer firefighters' clothing during the contact flame TPP test. Their model also investigated the sensor (skin) temperature for a configuration where the fabric and the skin were in direct contact.

The modes of heat transfer within the air gap between the fabric and the test sensor were studied by Torvi et al. [19] using his previously developed model [1, 8]. Based on a theoretical investigation for the transient Rayleigh number across the air gap for different gap widths, the study predicted natural convection heat transfer to occur within air gap widths of 7 mm or higher. The numerical results were validated using flow visualization technique where natural convection occurred for gap widths higher than 6.35 mm (1/4 in.).

The models in the literature clearly demonstrate the importance of the air gap between the fabric and the skin and its effect on the performance of protective clothing. However, most models have focused on providing a careful analysis of both the fabric and the skin behavior and only dealt with the air gap in an approximate way. Given this context, this paper introduces a numerical model for the transient heat transfer in a protective clothing system that implements a more sophisticated model for the air gap between the fabric and the skin. More specifically, the model accounts for the transient combined conduction-radiation heat transfer in the gap. The variation in the air gap thermal properties and its energy content during both the exposure and

the cool down periods is also included. The simulation results are used to provide insight into the mechanism of heat transfer in protective clothing that could potentially improve the performance of the clothing and/or lead to new protection strategies. The model will also be used in future studies to address some real life features of fire exposure.

2. PROBLEM DESCRIPTION

Consider a protective clothing system that consists of a single layer of Kevlar®/PBI fire-resistant fabric, the human skin which consists of epidermis, dermis, and subcutaneous layers, and an air gap between the fabric and the skin, as shown in Figure 1. The system, which is in a horizontal orientation, is exposed to localized flame contact with a nominal heat flux of 83 kW/m^2. Energy is transferred by both convection and radiation from the flame to the fabric. A portion of this energy is stored inside the fabric raising its temperature and causing thermochemical reactions within the fabric, while another portion of this energy is transferred by radiation from the fabric to the ambient. In this study, the standard TPP test's air gap width of 6.35 mm (1/4 in.) was used. For this size of air gap, energy is transferred by both conduction and radiation from the backside of the fabric to the skin raising the skin temperature and potentially causing skin burn injury. After exposure ends, energy is transferred by convection and radiation from the fabric to the ambient.

The analysis of the protective clothing system used five elements: fabric, air gap, epidermis, dermis, and subcutaneous, and the energy equations for these elements were solved simultaneously. The continuity of temperature and heat flux represents the internal boundary conditions between these elements.

2.1. Heat Transfer in the Fabric

The energy equation for the fabric is expressed [8, 20] as

$$\rho C^A(T)\frac{\partial T}{\partial t} = \frac{\partial}{\partial y}\left(k(T)\frac{\partial T}{\partial y}\right) - \frac{\partial}{\partial y}q_{rad}^{"}(y) \qquad 0 < t \le t_{exp} \qquad (1a)$$

$$\rho c_P(T)\frac{\partial T}{\partial t} = \frac{\partial}{\partial y}\left(k(T)\frac{\partial T}{\partial y}\right) \qquad t > t_{exp} \qquad (1b)$$

Where ρ, c_P and k are the fabric density, specific heat, and thermal conductivity, respectively, and t_{exp} is the exposure duration. The fabric apparent heat capacity, C^A has been measured [1] using a Differential Scanning Calorimeter (DSC) and then modeled as a function of the fabric temperature. It includes the evaporation of the fabric moisture content and the fabric thermal degradation. The Kevlar®/PBI specific heat is calculated [20] as

$$c_P(T) = 1300 + 1.6(T - 300K) \qquad (2)$$

The Kevlar®/PBI thermal conductivity is determined from the fiber to air fraction of the fabric [1] as follows.

$$k(T) = 0.8\,k_{air}(T) + 0.2\,k_{fbr}(T) \qquad (3)$$

where k_{fbr} and k_{air} are the fiber thermal conductivity and the thermal conductivity of the air contained in the fabric's pores, which are defined [1] as

$$\begin{aligned} k_{air}(T) &= 0.026 + 0.000068(T - 300K) && T \le 700K \\ &= 0.053 + 0.000054(T - 700K) && T > 700K \end{aligned} \qquad (4a)$$

$$\begin{aligned} k_{fbr}(T) &= 0.13 + 0.0018(T - 300K) && T \le 700K \\ &= 1 && T > 700\ K \end{aligned} \qquad (4b)$$

Beer's law [21] was employed [1, 8] to account for the absorption of the incident thermal radiation, $q_{rad}^{"}(y)$ as it penetrates the pores of the fabric, i.e.

$$q_{rad}^{"}(y) = q_{rad\,fl}^{"}\,exp(-\gamma y) \qquad (5)$$

The term $q_{rad\,fl}^{"}$, which represents the radiant portion of exposure, is written as

$$q''_{rad\,fl} = \sigma \varepsilon_g T_g^4 \tag{6}$$

where σ is the Stefan-Boltzmann constant, ε_g is the hot gases emissivity, and T_g is the hot gases temperature. The extinction coefficient of the fabric γ is given [1, 8] by

$$\gamma = \frac{-ln(\tau)}{L_{fab}} \tag{7}$$

where τ is the fabric transmissivity, and L_{fab} is the fabric thickness.

The fabric boundary conditions are as follows.

$$-k(T)\frac{\partial T}{\partial y}\Big|_{y=0} = h_{fl}\left(T_g - T_{fab(y=0)}\right) - \sigma \varepsilon_{fab1}\left(1-\varepsilon_g\right)\left(T_{fab(y=0)}^4 - T_{amb}^4\right) \qquad 0 < t \le t_{exp} \tag{8a}$$

$$k(T)\frac{\partial T}{\partial y}\Big|_{y=0} = h_{cnv}\left(T_{fab(y=0)} - T_{amb}\right) + \sigma \varepsilon_{fab1}\left(T_{fab(y=0)}^4 - T_{amb}^4\right) \qquad t > t_{exp} \tag{8b}$$

$$-k(T)\frac{\partial T}{\partial y}\Big|_{y=L_{fab}} = q''_y(\vec{r})\Big|_{y=L_{fab}} - k_{air}(T)\frac{\partial T_{air}}{\partial y}\Big|_{y=L_{fab}} \qquad t > 0 \tag{9}$$

where ε_{fab1} is the fabric exposed surface emissivity; T_{amb} is the ambient temperature that is taken as 300 K; $q''_y(\vec{r})$, which will be discussed later, is the emitted radiation from the fabric backside surface; h_{fl} is the convective heat transfer coefficient from the flame to the fabric; and h_{cnv} is the convective heat transfer coefficient from the fabric to the ambient during the cool down period. The latter is estimated from an empirical correlation for natural convection heat transfer from a horizontal heated plate facing downwards to air at atmospheric pressure [21] as

$$h_{cnv} = 0.59\left(\frac{T_{fab(y=0)} - T_{amb}}{W_{fab}}\right)^{1/4} \tag{10}$$

The first term on the right hand side of Eq. (8a) is the convection portion of the exposure from the hot gases to the fabric while the second term represents the radiant losses from the fabric to

the ambient during the exposure. However, the term $(1-\varepsilon_g)$ represents the influence of the flame hot gases on the radiation exchange between the fabric and the ambient. Note that the radiant portion of the exposure is accounted for in Eq. (1a). The first term on the right hand side of Eq. (8b) represents the convection losses from the fabric to the ambient, while the second term represents the radiant losses to the ambient during the cool down of the fabric. The right hand side of Eq. (9) represents the combined conduction-radiation heat transfer in the air gap at the fabric-air interface.

Most previous models accounted for the absorption of the thermal radiation through the fabric, $\frac{\partial}{\partial y}q_{rad}^{"}(y)$ as the exponential decay of the net incident radiation on the fabric exposed surface, i.e. the radiant portion of exposure minus the radiant loss from the fabric exposed surface to the ambient. However, as will be shown later, the radiant loss from the fabric to the ambient is close to double the radiant portion of the exposure. Using the resultant of these two values in Eq. (1a) would then treat the radiation loss to the ambient, which is the fabric boundary condition, as originating from the inside structure of the fabric rather than from the fabric surface.

The fabric initial condition is

$$T_{fab}(x, t=0) = T_{amb} \tag{11}$$

2.2. Heat Transfer in the Air Gap

The energy equation for the air gap between the fabric and the skin can be written as

$$\rho(T)c_P(T)\frac{\partial T}{\partial t} = \frac{\partial}{\partial y}\left(k(T)\frac{\partial T}{\partial y}\right) - \frac{\partial q_R^{"}}{\partial y} \tag{12}$$

where ρ, c_P and k are the air density, specific heat, and thermal conductivity, respectively, and $q_R^{"}$ is the radiative heat flux through the air gap, which can be obtained by solving the Radiative Transfer Equation (RTE) of the air gap as described below.

Considering the air gap as a gray, absorbing, and emitting medium, the change in the intensity along a radiation ray path is written [22] as

$$\frac{dI(\vec{r},\hat{s})}{ds} = -\kappa(\vec{r})I(\vec{r},\hat{s}) + \kappa(\vec{r})I_b(\vec{r}) \tag{13}$$

where I is the radiation intensity, which varies with the spatial position $\vec{r}$ and the angular direction $\hat{s}$, κ is the air gap absorption coefficient, s is the geometric distance, and I_b is the black body intensity. The unit direction $\hat{s}$ is defined as

$$\hat{s} = (sin\theta\ cos\phi)\hat{e}_x + (sin\theta\ sin\phi)\hat{e}_y + (cos\theta)\hat{e}_z \tag{14}$$

where $\hat{e}_x$, $\hat{e}_y$, and $\hat{e}_z$ are unit vectors in the x, y, and z directions, θ is the polar angle measured from $\hat{e}_z$, and ϕ is the azimuthal angle measured from $\hat{e}_x$. The black body intensity is defined as

$$I_b = \frac{\sigma T^4}{\pi} \tag{15}$$

where σ is the Stephan-Boltzmann constant, and T is the medium temperature. An absorption coefficient of κ = 5 m^{-1} is used for the air gap based on an estimation of the absorptivity,α, of the hot gases in the gap using Hottel's method [23] i.e.

$$\alpha = 1 - exp(-\kappa L_{air}) \tag{16}$$

where L_{air} is the air gap thickness. The properties of dry air [23] are used to account for the variation in the thermal properties of the hot gases in the gap with temperature.

The divergence of the radiative heat flux in Eq. (12) is obtained from the relation

$$\frac{\partial q_R^{"}}{\partial y} = \kappa\left(4\pi I_b(\vec{r}) - G(\vec{r})\right) \tag{17}$$

where G is the incident radiation, which is defined as

$$G(\vec{r}) = \int_{4\pi} I(\vec{r}, \hat{s}) d\,\Omega \tag{18}$$

where $d\Omega$ is the solid angle surrounding the radiation ray.

The radiation intensity distribution within the air gap is calculated by solving the RTE (Eq. (13)) numerically along with its boundary conditions. Assuming both the fabric backside and the skin surface to behave as opaque gray surfaces, the boundary conditions for the air gap RTE are written as

$$I_{fab}(\vec{r}, \hat{s}) = \varepsilon_{fab2}(\vec{r}) I_{b,fab}(\vec{r}) \qquad at\ y = L_{fab} \tag{19}$$

$$I_{ep}(\vec{r}, \hat{s}) = \varepsilon_{ep}(\vec{r}) I_{b,ep}(\vec{r}) \qquad at\ y = L_{fab} + L_{air} \tag{20}$$

where ε_{fab2} is the fabric backside emissivity, and ε_{ep} is the epidermis surface emissivity.

The emitted radiation from the fabric backside surface, Eq. (9), is estimated as

$$q_y''(\vec{r})\big|_{y=L_{fab}} = \int_{4\pi} I(\vec{r}, \hat{s})(\hat{s} \cdot \hat{e}_y) d\,\Omega \Bigg|_{y=L_{fab}} \tag{21}$$

The boundary conditions for the air gap energy equation (Eq. (12)) are obtained from the continuity of temperature on both sides of the air gap with the fabric and the skin as follows

$$T_{air}|_{y=L_{fab}} = T_{fab}\big|_{y=L_{fab}} \qquad t > 0 \tag{22}$$

$$T_{air}|_{y=L_{fab}+L_{air}} = T_{ep}\big|_{y=L_{fab}+L_{air}} \qquad t > 0 \tag{23}$$

where T_{ep} is the epidermis layer temperature.

The air gap initial condition is

$$T_{air}(y, t = 0) = T_{amb} \tag{24}$$

2.3. Heat Transfer in the Human Skin

Skin consists of three layers: epidermis, dermis, and subcutaneous where blood perfusion takes place in the latter two layers. The bioheat equation developed by Pennes [12] was used to model heat transfer in the skin tissues.

The energy equation for the epidermis layer is written as

$$(\rho c_P)_{ep} \frac{\partial T}{\partial t} = \frac{\partial}{\partial y}\left(k_{ep} \frac{\partial T}{\partial y}\right) \tag{25}$$

where ρ, c_P, and k have their conventional meaning. The epidermis boundary conditions are

$$-k_{ep} \frac{\partial T_{ep}}{\partial y}\Big|_{y=L_{fab}+L_{air}} = q_y^{"}(\vec{r})\big|_{y=L_{fab}+L_{air}} - k_{air}(T) \frac{\partial T_{air}}{\partial y}\Big|_{y=L_{fab}+L_{air}} \qquad t > 0 \tag{26}$$

$$T_{ep}\big|_{y=L_{fab}+L_{air}+L_{ep}} = T_{ds}\big|_{y=L_{fab}+L_{air}+L_{ep}} \qquad t > 0 \tag{27}$$

where L_{ep} is the epidermis layer thickness, and T_{ds} is the dermis layer temperature.

The energy equation for the dermis layer is written as

$$(\rho c_P)_{ds} \frac{\partial T}{\partial t} = \frac{\partial}{\partial y}\left(k_{ds} \frac{\partial T}{\partial y}\right) + (\rho c_P)_b \omega_b (T_{cr} - T) \tag{28}$$

where $(\rho c_P)_{ds}$ is the volumetric heat capacity of the dermis layer, ω_b is the blood perfusion rate within the dermis layer, and T_{cr} is the human core body temperature. The dermis boundary conditions are

$$k_{ep} \frac{\partial T_{ep}}{\partial y}\Big|_{y=L_{fab}+L_{air}+L_{ep}} = k_{ds} \frac{\partial T_{ds}}{\partial y}\Big|_{y=L_{fab}+L_{air}+L_{ep}} \qquad t > 0 \tag{29}$$

$$T_{ds}\big|_{y=L_{fab}+L_{air}+L_{ep}+L_{ds}} = T_{sc}\big|_{y=L_{fab}+L_{air}+L_{ep}+L_{ds}} \qquad t > 0 \tag{30}$$

where, L_{ds} is the dermis layer thickness, and T_{sc} is the subcutaneous layer temperature.

The energy equation for the subcutaneous layer is written as

$$(\rho c_P)_{sc}\frac{\partial T}{\partial t} = \frac{\partial}{\partial y}\left(k_{sc}\frac{\partial T}{\partial y}\right) + (\rho c_P)_b \omega_b (T_{cr} - T) \tag{31}$$

where, $(\rho c_P)_{sc}$ is the volumetric heat capacity of the subcutaneous layer. The subcutaneous boundary conditions are

$$k_{ds}\frac{\partial T_{ds}}{\partial y}\Big|_{y=L_{fab}+L_{air}+L_{ep}+L_{ds}} = k_{sc}\frac{\partial T_{sc}}{\partial y}\Big|_{y=L_{fab}+L_{air}+L_{ep}+L_{ds}} \qquad t > 0 \tag{32}$$

$$T_{sc}|_{y=L_{fab}+L_{air}+L_{ep}+L_{ds}+L_{sc}} = T_{cr} \qquad t > 0 \tag{33}$$

where, L_{sc} is the subcutaneous layer thickness.

The skin initial condition is expressed as a linear temperature distribution between 32.5ºC at the epidermis surface and 37ºC at the subcutaneous base (core body temperature).

2.4. Skin Burn Model

Henriques' integral [7] was adopted in this study to predict times to skin burn injuries. According to Henriques' model, the thermal damage of the skin tissues occurs when the temperature at the interface between the epidermis and the dermis layers (basal layer) reaches 44^{o}C. To predict first and second degree burn injuries, the temperature at the basal layer is used in the following integral expression

$$\Psi = \int_0^t P\, exp\left(-\frac{\Delta E}{RT}\right) dt \tag{34}$$

A first-degree burn occurs when the value of Ψ reaches 0.53, and a second-degree burn occurs when the value of Ψ reaches 1. To predict third degree burn injury, the temperature at the interface between the dermis and the subcutaneous (dermal base) is used in the integral. A third degree burn is predicted to occur when the value of Ψ reaches 1. The values for the pre-exponential factor P and the activation energy ΔE of the skin were determined by Weaver and

Stoll [24] for second-degree burn injury. Takata [25] determined the corresponding values for third-degree burn injury. These values are listed in Table 3.

3. NUMERICAL SOLUTION

The numerical discretization of the RTE (Eq. (13)) was performed by the finite volume method [26-29] while the step scheme was employed to relate the face intensity to the nodal intensity as follows

$$a_P^l I_P^l = a_N^l I_N^l + a_S^l I_S^l + b^l \tag{35}$$

where $I^l \equiv I(\vec{r}, \hat{s})$ and

$$a_N^l = max(-A_n D_{cn}^l, 0) \tag{36}$$

$$a_S^l = max(-A_s D_{cs}^l, 0) \tag{37}$$

$$a_P^l = ma\,x(A_n D_{cn}^l, 0) + ma\,x(A_s D_{cs}^l, 0) + \kappa_P \Delta V_P \Delta\Omega^l \tag{38}$$

$$b^l = S_P^l \Delta V_P \Delta\Omega^l \tag{39}$$

where

$$D_{cs}^l = -D_{cn}^l \tag{40}$$

$$D_{cn}^l = \int_{\Delta\Omega^l} (\hat{s}^l \cdot \hat{e}_y)\, d\Omega \tag{41}$$

$$\Delta\Omega^l = \int_{\Delta\Omega^l} d\Omega \tag{42}$$

$$A_n = A_s = \Delta x \tag{43}$$

$$\Delta V_P = \Delta x\, \Delta y \tag{44}$$

$$S_P^l = \kappa_P I_{b,P} \tag{45}$$

The discretization of the energy equations for the fabric, air gap, epidermis, dermis, and subcutaneous were also performed by the finite volume method [30]. A fully implicit scheme was employed for the temporal discretization. The boundary conditions were applied using fictitious nodes, as shown in Figure 2, while uniform grids were used within each domain. Due to the nonlinearity that comes from the conduction-radiation coupling within the air gap, the radiation boundary condition, and the variation in the thermal properties of both the fabric and the air gap with temperature, the Gauss-Seidel point-by-point iterative scheme was used to solve the system discrete equations. The solution marches as follows. For each time step, temperatures from the previous time step are used as initial values for the iteration loop. The air gap, fabric backside, and epidermis surface temperatures are used to estimate the radiation intensity distribution within the air gap. Then the divergence of radiative heat flux within the air gap is calculated to use in the air gap energy equation, while the radiation heat fluxes at both sides of the air gap are used for the boundary conditions of the fabric backside surface and the epidermis surface. New temperatures are calculated by visiting each grid starting from the fabric surface to the subcutaneous base. The thermal properties for the fabric and the air gap, the temperature values in the source terms, and the divergence of radiative heat flux and the radiation heat fluxes on both sides of the air gap are updated based on the current temperature within the iteration loop. The iterative solver continues until the non-dimensional change in the temperature field becomes less than 10^{-5}. The influence of the grid size and time step were studied in order to reduce their influence on the solution to acceptable level. After the system temperature distribution at a given time step is obtained, the basal layer and the dermal base temperatures are substituted in the Henriques integral (Eq. (34)) to predict the time to receive skin burn injuries.

4. RESULTS AND DISCUSSION

The fabric and hot gas parameters used in the simulation are listed in Table 1. The human skin thermophysical properties are listed in Table 2. The simulation assumes an exposure to localized flame contact with a nominal heat flux of 83 kW/m^2 for 10 s followed by 60 s of cool down.

The model validation is accomplished by simulating the specific flame TPP test performed by Torvi [1] using a skin simulant test sensor. The model closely predicted the change in the skin simulant's surface temperature during both the exposure and the cool down periods as shown in Figure 3. The source of the small discrepancy between the prediction and measurements is difficult to determine without a more specific and comprehensive set of measurements, e.g. spatial temperature distributions. This discrepancy might be attributed to the model assumptions to simulate the test, and/or to other influences that are not considered in the model such as the reduction in the fabric thickness due to pyrolysis and the reduction in the air gap width due to fabric shrinkage.

The overall performance of the air gap model is assessed by comparing the skin burn predictions using the present model to that produced using a simpler air gap model for different air gap widths. The present model was simplified to the typical model found in the literature by: (i) using an air gap absorption coefficient value of zero (i.e. only surface radiation), (ii) assuming the left hand side of Eq. (11) to be zero (i.e. steady state heat transfer, and decoupled conduction and radiation within the air gap), and (iii) assuming constant air gap properties. As shown in Figure 4, the present model predicts skin burn injuries to take place earlier than that predicted by the simplified model. For second-degree burn predictions, the difference between the two models increases as the air gap width decreases, i.e. the maximum difference is about %10 for air gap

width of 1 mm. In contrast, the difference in the prediction for third-degree burn increases as the air gap width increases, i.e. the maximum difference is about %16 for air gap with of 6 mm. since second-degree burns take place during the exposure period while third-degree burns take place during the cool down period, the difference in prediction for skin burn injuries reflects the role of the air gap in the energy transfer from the fabric to the skin.

The influence of the air gap in the present model compared to the simpler model is to absorb and emit thermal radiation. Absorbing the thermal radiation increases the energy stored in the air and also the air temperature, while emitting radiation to the fabric reduces the energy loss by radiation from the fabric. Both effects cause a significant increase in the conduction heat transfer through the air gap compared to the simple model. This increase in turn leads to predicted time to skin burn injury which is less than for the simple model. Note that the influence of the conduction heat transfer decreases as the air gap width increases due to the increase in the thermal resistance. This explains the reduction in the difference between the two model predictions as the air gap increases. During the cool down period, as the energy transfer is significantly reduced, the energy stored in the air gap causes the conduction heat transfer to gradually decrease. This explains the increase in the difference between the two model predictions during the cool down period as the air gap width increases due to the increase in its thermal resistance.

The predicted temperature distribution within the protective clothing system is shown in Figure 5. During the exposure, there is a significant temperature gradient within the fabric. However, during the cool down period, the temperatures on both sides of the fabric are almost equal as shown in Figure 5(a). The temperature difference (about $50^{o}C$) across the fabric at the end of exposure diminished to zero almost immediately once the exposure ends. The insulating

effect of the air gap is shown by the large temperature difference between the backside of the fabric and the skin surface. This large temperature difference, which is established across the 6.35 mm (1/4 in.) air gap width in only 10 s, illustrates the critical role of the air gap and the importance of the air gap model. Figure 5(b) shows the predicted skin temperature distribution. Recall that the base of the subcutaneous layer is assumed to remain at 37^{o}C, the body core temperature, throughout the simulation. Basal layer temperatures are high enough during the exposure period that first and second degree urn injuries will occur. The simulation indicates that for the above mentioned exposure conditions, first-degree burn is predicted to occur after 5.4 s and second-degree burn after 5.6 s of exposure. While, the dermal base temperature is relatively low during the exposure, it continues to increase during the cool down period causing predicted third-degree burn injury 25.6 s after the end of exposure. The time delay in the energy transfer through the dermis and subcutaneous layers is attributed to the high thermal capacity of these layers compared to the epidermis layer.

Figure 6 illustrates the spatial temperature distribution in the air gap at different times during the exposure and the cool down periods. The curvature in the temperature distribution shows the influence of the present air gap model compared to the straight lines predicted by the simpler models with an approximate air gap analysis that only included steady state conduction. This curvature in the temperature distribution increases towards the skin during the exposure period while it diminishes during the cool down period.

Figure 7 depicts the variation in the thermal properties of the air gap, which illustrates the need for considering the variation in the air properties with temperature. In this figure, front and back refer to the air layer immediately next to the fabric and the skin, respectively. The extreme temperature variation within the air gap causes a rapid change in its thermal properties.

For example, during the exposure period, the thermal conductivity of the air layer adjacent to the fabric is almost double that adjacent to the skin, while the volumetric heat capacity, ρc_P, of the air layer adjacent to the fabric is almost one-half that adjacent to the skin. This variation in the air gap properties diminished to almost zero by the end of the cool down period. It is noted that the change in the volumetric heat capacity, ρc_P, is mostly due to the change in the air density. In order to satisfy conservation of mass within the air gap, an outflow of air would be required to account for the rapid decrease in the air gap density during the exposure. The 1-D nature of the model did not account for this mass flux, which represents an inherent limitation of 1-D analyses of protective clothing systems. However, a more accurate treatment of the mass balance for the air gap would not change the physics of the heat transfer process in protective clothing.

Figure 8 shows the variation in the fabric apparent heat capacity during the simulation. According to the apparent heat capacity model developed by Torvi [1], the higher peaks represent the evaporation of the fabric initial water content while the lower peaks represent the fabric thermal degradation. The figure implies that the evaporation of initial water content of the fabric takes place within the first second of exposure, while the degradation of the fabric starts after the third second of exposure and lasts until the end of exposure (10 s). The figure gives a prediction for tracking the propagation of moisture evaporation and thermochemical reactions in the fabric during the exposure that can supplement the contributions made by Chitrphiromsri [17] and Zhu et al. [9].

Further insight can be gained by exploring the energy balance of the system. Figure 9(a) shows the energy balance for the fabric. A total heat flux of about 83 kW/m^2 is transferred to the system at the beginning of exposure as a combination of both convection (q''_{cnv_fl}) and radiation (q''_{rad_fl}) heat flux from the hot gases to the fabric. As the fabric temperature increases, the

convection heat transfer from the hot gases to the fabric decreases. The radiation losses from the fabric exposed surface ($q''_{rad\ fab-amb}$) steadily increase until they exceed the radiant heat transfer from the flame (q''_{rad_fl}). The difference between the energy input and loss is stored in the fabric ($q''_{strg\ fab}$) causing its thermal decomposition and increasing its temperature. During the cool down period, most of the energy loss occurs during the first 10 s after the exposure ends. The cool down of the fabric mainly occurs through the loss of its stored energy by radiation on both sides of the fabric to the ambient and the skin. The convection heat transfer from the fabric to the ambient ($q''_{cnv\ fab-amb}$) is shown to be relatively insignificant during the cool down of the fabric.

The radiation heat transfer through the air gap from the fabric to the skin is the dominant heat transfer mode within the air gap, Figure 9(b). The radiation heat transfer from the backside of the fabric to the skin is increasing throughout the exposure as the fabric temperature is increasing and the backside of the fabric is charring. The energy stored in the air gap ($q''_{strg\ air}$), in terms of elevating its temperature, represents only a small portion of the total energy transport within the air gap. The air gap reaches its maximum capacity to store energy after the first 5 s of exposure. The heat fluxes at the air-epidermis interface are included in Figure 9(c). However, a detailed distribution of the heat fluxes within the air gap is shown in Figure 10.

The energy balance for the skin is illustrated in Figure 9(c). Almost 80% of the energy transfer to the skin takes place by radiation ($q''_{rad\ air-ep}$), while the rest is transferred by conduction ($q''_{cnd\ air-ep}$). A small portion of the total energy transferred to the skin is stored in the epidermis layer ($q''_{strg\ ep}$), while the majority of this energy is stored in the dermis layer ($q''_{strg\ ds}$). That is due to the extremely small mass of the epidermis layer compared to the dermis layer. The blood perfusion in the dermis($q''_{perf\ ds}$) and subcutaneous($q''_{perf\ sc}$) layers has an

insignificant effect on the energy content of the skin due to the limited blood perfusion rate. During the cool down period, the energies stored in the epidermis and dermis layers are released by conduction to the subcutaneous layer.

Figure 10(a) illustrates the conduction heat flux through the air gap from the fabric to the skin. It indicates that the conduction heat transfer rate through the air gap increases with time during the exposure as the fabric backside temperature increases. Recalling that the air gap model in the literature assumed steady state conduction heat transfer through the air gap, the deviation in the heat flux lines from constant values is attributed to the present air gap model. Figure 10(b) shows the variation in the radiation heat flux as it passes through the air gap from the fabric to the skin. The curvature in the heat flux lines represents the effect of the air gap on absorbing and emitting radiation heat transfer versus a constant heat flux for the assumption of fabric-skin surface radiation. As mentioned before, the radiation from the fabric to the skin is found to be the main source of energy transfer to the skin. The effect of the air gap on thermal radiation depends on the absorption coefficient of the air gap, which in this case is estimated to be 5 m^{-1}.

The influence of the air gap absorption coefficient on the model prediction was investigated in terms of skin burn predictions. As shown in Figure 11, it was found that increasing the air gap absorption coefficient causes only a negligible increase in the expected time to receive a second-degree burn, but it increases the expected time to receive a third-degree burn injury by about 21% as the absorption coefficient increases from 0 to 15 m^{-1}. One of the possible reasons for the increase in the air gap absorption coefficient is the formation of soot as a combustion product of the fabric. It should be noted that the actual value of the air gap absorption coefficient depends on the composition of the exhaust gases filling the gap between

the fabric and the skin. Determining this coefficient more precisely would require a detailed study of the combustion of the fabric and the resultant concentration of the exhaust gases in the gap, which changes with time during the exposure.

5. CONCLUSIONS

A numerical model for the transient heat transfer in a protective clothing system is developed. The model used a more complex and realistic analysis for the air gap between the fabric and the skin compared to other models in the literature. The model is employed to explore the transient temperature distribution and the predicted time to receive skin burn injuries. The paper carefully explores the transient energy content of the system, which in turn provides insight into the physics of heat transfer in protective clothing systems. The air gap model itself also contributes to the study of heat transfer in enclosures with high temperatures and heat fluxes boundary conditions. The paper illustrates the dependency of skin burn predictions on the model assumptions, i.e. the use of transient conduction-radiation model for the air gap resulted in prediction of times for skin burn that were less than those of the simpler model. The paper identified an inherent limitation of the 1-D analysis of protective clothing systems related to including density changes in the air gap without any associated convection to ensure conservation of mass. The model will be used in the future to investigate a wider range of exposure conditions, as well as to assess the feasibility of new protection strategies.

REFERENCES

1. D. A. Torvi, Heat Transfer in Thin Fibrous Materials under High Heat Flux Conditions, Ph.D. Thesis, University of Alberta, Edmonton, Alberta, 1997.
2. A.M. Stoll, and M.A. Chianta, Method and Rating System for Evaluation of Thermal Protection, Aerospace Medicine, vol. 40, pp. 1232-1238, 1969.

3. American Society for Testing Materials, ASTM F 1939-99 a Standard Test Method for Radiant Protective Performance of Flame Resistant Clothing Materials, West Conshohocken, PA, 1999.
4. American Society for Testing Materials, ASTM D 4108-87 Standard Test Method for Thermal Protective Performance of Materials and Clothing by open-Flame Method, West Conshohocken, PA, 1987.
5. National Fire Protection Association, NFPA 1971, Standard on Protective Ensemble for Structural Fire Fighting, Quincy, MA, 2007.
6. American Society for Testing Materials, ASTM F 1930-00 Standard Test Method for Evaluation of Flame Resistant Clothing for Protection Against Flash Fire Simulations Using an Instrumented Thermal Manikin, West Conshohocken, PA, 2000.
7. F.C. Henriques, Jr., A.R. Moritz, Studies of thermal injuries I: The conduction of heat to and through skin and the temperatures attained therein. A theoretical and experimental investigation, American J. Pathology, vol. 23, pp. 531–549, 1947.
8. D.A. Torvi, and J.D. Dale, Heat Transfer in Thin Fibrous Materials under High Heat Flux, Fire Technology, vol. 35, pp. 210-231, 1999.
9. F. Zhu, and W. Zhang, Modeling Heat Transfer for Heat-resistant Fabrics Considering Pyrolysis Effect under an External Heat Flux, J. Fire Sciences, vol. 27, pp. 81-96, 2009.
10. G. Song, R.L. Barker, H. Hamouda, A.V. Kuznetsov, P. Chitrphiromsri, and R.V. Grimes, Modeling the Thermal Protective Performance of Heat Resistant Garments in Flash Fire Exposures, Textile Research J., vol. 74, pp. 1033-1040, 2004.

11. F. Zhu, and W. Zhang, Evaluation of Thermal Performance of Flame-resistant Fabrics Considering Thermal Wave Influence in Human Skin Model, J. Fire Sciences, vol. 24, pp. 465-485, 2006.

12. H.H. Pennes, Analysis of tissue and arterial blood temperatures in resting human forearm, J. Applied Physiology, vol. 1, pp. 93–122, 1948.

13. Y. Li, and Q. Zhu, A Model of Coupled Liquid Moisture and Heat Transfer in Porous Textiles with Consideration of Gravity, Numerical Heat Transfer A, vol. 43, pp. 510–523, 2003.

14. L. Fengzhi, L. Yi, L. Yingxi, and L. Zhongxuan, Numerical Simulation of Coupled Heat and Mass Transfer in Hygroscopic Porous Materials Considering the Influence of Atmospheric Pressure, Numerical Heat Transfer B, vol. 45, pp. 249–262, 2004.

15. M. Aihua, and L. Yi, Numerical Heat Transfer Coupled with Multidimensional Liquid Moisture Diffusion in Porous Textiles with a Measurable-Parameterized Model, Numerical Heat Transfer A, vol. 56, pp. 246–268, 2009.

16. P. Chitrphiromsri, and A.V. Kuznetsov, Modeling Heat and Moisture Transport in Firefighter Protective Clothing during Flash Fire Exposure, Heat Mass Transfer, vol. 41, pp. 206-215, 2005.

17. P. Chitrphiromsri, Modeling of Thermal Performance of Firefighter Protective Clothing during the Intense Heat Exposure, Ph.D. Thesis, North Carolina State University, Raleigh, North Carolina, 2004.

18. G. Song, P. Chitrphiromsri, D. Ding, Numerical Simulation of Heat and Moisture Transport in Thermal Protective Clothing Under Flash Fire Conditions, Int. J. Occupational Safety and Ergonomics, vol. 14(1), pp. 89-106, 2008.

19. D.A. Torvi, J.D. Dale, and B. Faulkner, Influence of Air Gaps on Bench Top Test Results of Flame Resistant Fabrics, J. Fire Protection Engineering, vol. 10, pp. 1-12, 1999.

20. D.A. Torvi, and T.G. Threlfall, Heat Transfer Model of Flame Resistant Fabrics During Cooling After Exposure to Fire, J. Fire Technology, vol. 42, pp. 27-48, 2006.

21. J.P. Holman, Heat Transfer, 8th ed., pp. 354-359, McGraw-Hill, New York, 1997.

22. M.F. Modest, Radiative Heat Transfer, 2nd ed., pp. 264-281, Academic Press, New York, 2003.

23. F.P. Incropera, and D.P. DeWitt, Fundamentals of Heat and Mass Transfer, 5th ed., pp. 821-826, Wiley, New York, 2002.

24. J.A. Weaver, and A.M. Stoll, Mathematical Model of Skin Exposed to Thermal Radiation, Aerospace Medicine, vol. 40, pp. 24-30, 1969.

25. A.N. Takata, J. Rouse, and T. Stanley, Thermal Analysis Program, I.I.T. Research Institute Report IITRI-J6286, Chicago, 1973.

26. J.C. Chai, and S. V. Patankar, Finite-Volume Method for Radiation Heat Transfer, Advances, in W. J. Minkowycz, and E. M. Sparrow (eds.), Numerical Heat Transfer, vol. 2, chap. 4, Taylor & Francis, 2000.

27. J.C. Chai, One-Dimensional Transient Radiation Heat Transfer Modeling Using a Finite-Volume Method, Numerical Heat Transfer B, vol. 44, pp. 187–208, 2003.

28. M.Y. Kim, S.W. Beak, and J.H. Park, Unstructured Finite-Volume Method for Radiative Heat Transfer in a Complex Two-Dimensional Geometry with Obstacles, Numerical Heat Transfer B, vol. 39, pp. 617–635, 2001.

29. G.D. Raithby, Discussion of the Finite-Volume Method for Radiation, and its Application using 3D Unstructured Meshes, Numerical Heat Transfer B, vol. 35, pp. 389–405, 1999.

30. S.V. Patankar, Numerical Heat Transfer and Fluid Flow, pp. 42-58, McGraw-Hill, New York, 1980.

Table 1. Kevlar®/PBI and burner parameters

	Property	Value
L_{fab}	Fabric thickness	0.6 mm
W_{fab}	Fabric Width	0.05m (2 in.)
ρ_{fab}	Fabric density	323 kg/m^3
γ_{fab}	Fabric extinction factor	0.01
ε_{fab}	Fabric emissivity	0.9
τ_{fab}	Fabric transmissivity	0.01
T_g	Hot gases temperature	2000 K
ε_g	Hot gases emissivity	0.02
h_{fl}	Flame convective heat transfer coefficient	40 W/m^{2}K

Table 2. Human skin thermophysical properties

Property	Epidermis	Dermis	Subcutaneous	Blood
Thickness (m)	8×10^{-5}	2×10^{-3}	1×10^{-2}	-
Density (Kg/m^3)	1200	1200	1000	1060
Specific Heat (J/Kg^oC)	3598	3222	2760	3770
Thermal Conductivity (W/m^oC)	0.255	0.523	0.167	-
Blood Perfusion Rate $(m^3/s)/m^3$ tissue	-	-	-	1.25×10^{-3}

Table 3. The values of the pre-exponential factor and the ratio of the activation energy to ideal gas constant

	Basal Layer	Dermal Base	
Pre-exponential factor (P)	2.185×10^{124}	4.32×10^{64}	$44 \leq T < 50$ºC
	1.823×10^{51}	9.39×10^{104}	$T \geq 50$ºC
Ratio of activation energy to ideal gas constant $(\Delta E/R)$	93534.9	50000	$44 \leq T < 50$ºC
	39109.8	80000	$T \geq 50$ºC

Figure Captions

Figure 1. The protective clothing system schematic diagram.

Figure 2. Schematic of grids.

Figure 3. Comparison between measured and predicted skin simulant surface temperature.

Figure 4. Influence of the air gap model on skin burn predictions for various air gap widths.

Figure 5. Temporal temperature distribution within the clothing system; (a) fabric and air gap, (b) skin.

Figure 6. The variation in the air gap temperature distribution.

Figure 7. The variation in the air gap thermal conductivity and volumetric heat capacity.

Figure 8. The variation in the fabric apparent heat capacity as an indication of the underlying moisture transfer and thermochemical reactions.

Figure 9. The protective clothing system energy balance; (a) fabric, (b) air gap, (c) skin.

Figure 10. Spatial distribution of the heat transfer fluxes within the air gap: (a) conduction heat transfer flux, (b) radiation heat transfer flux.

Figure 11. Influence of the air gap absorption coefficient on skin burn prediction.

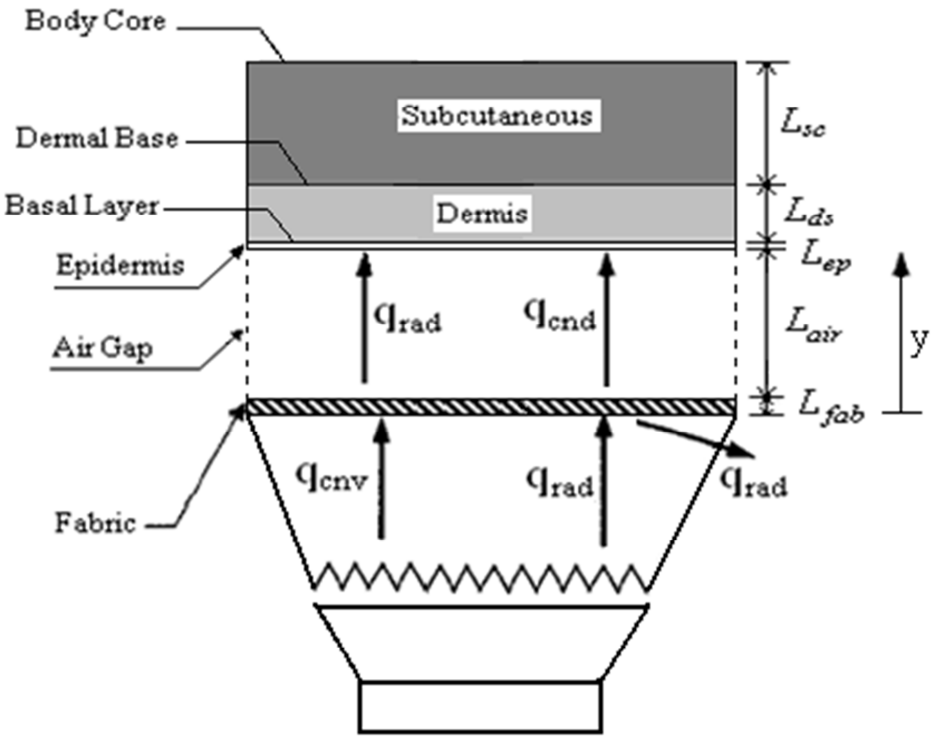

Figure 1. The protective clothing system schematic diagram.

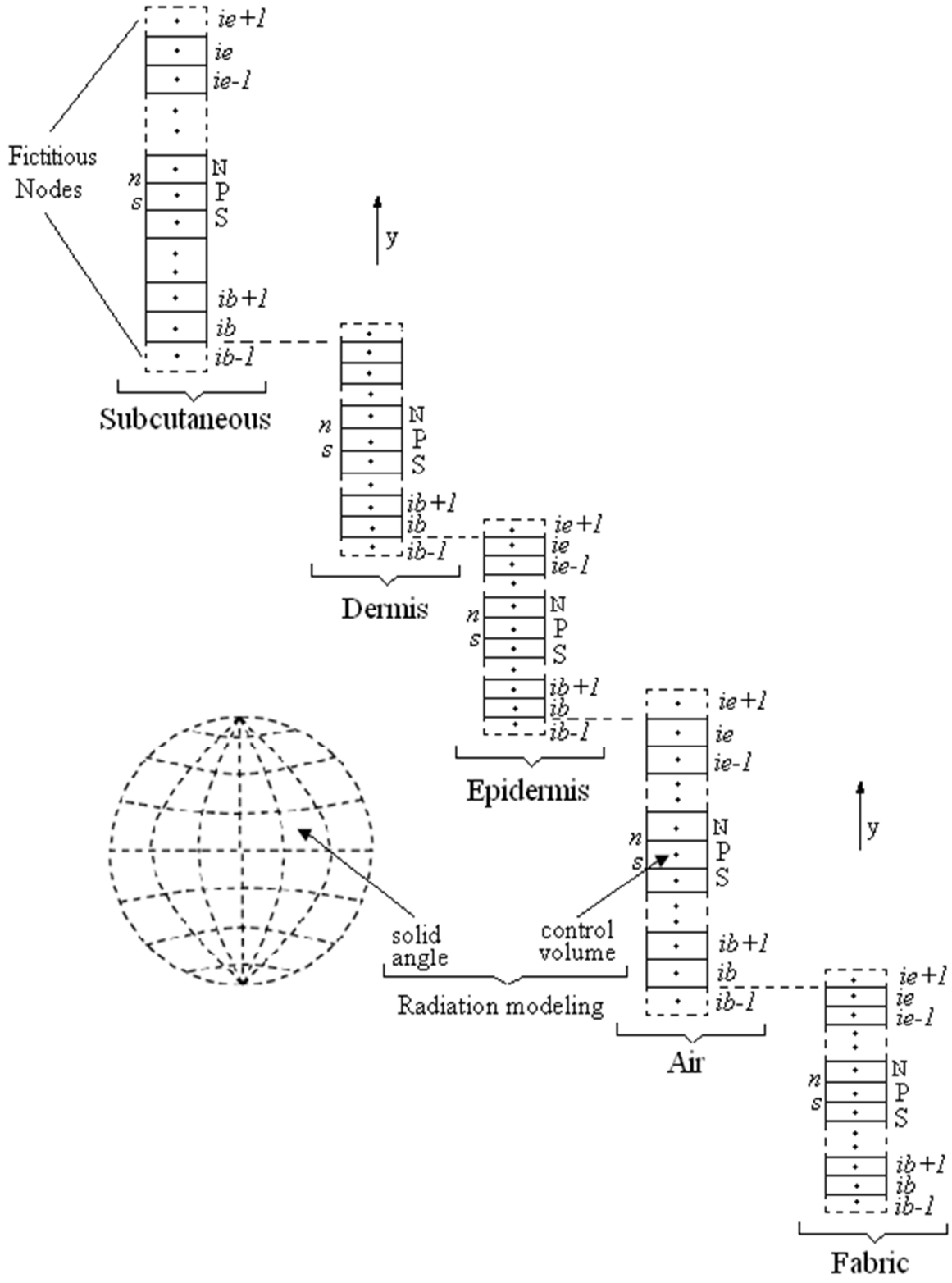

Figure 2. Schematic of grids.

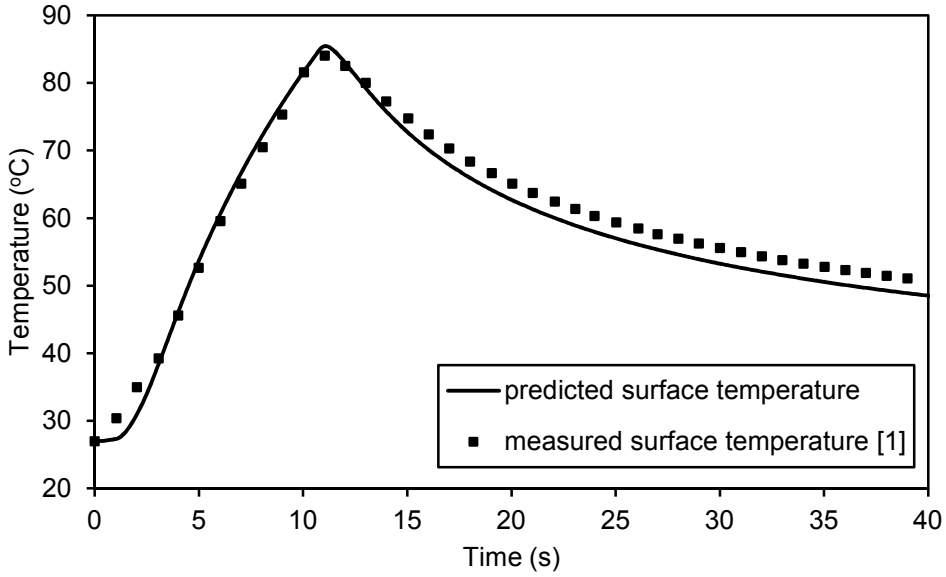

Figure 3. Comparison between measured and predicted skin simulant surface temperature.

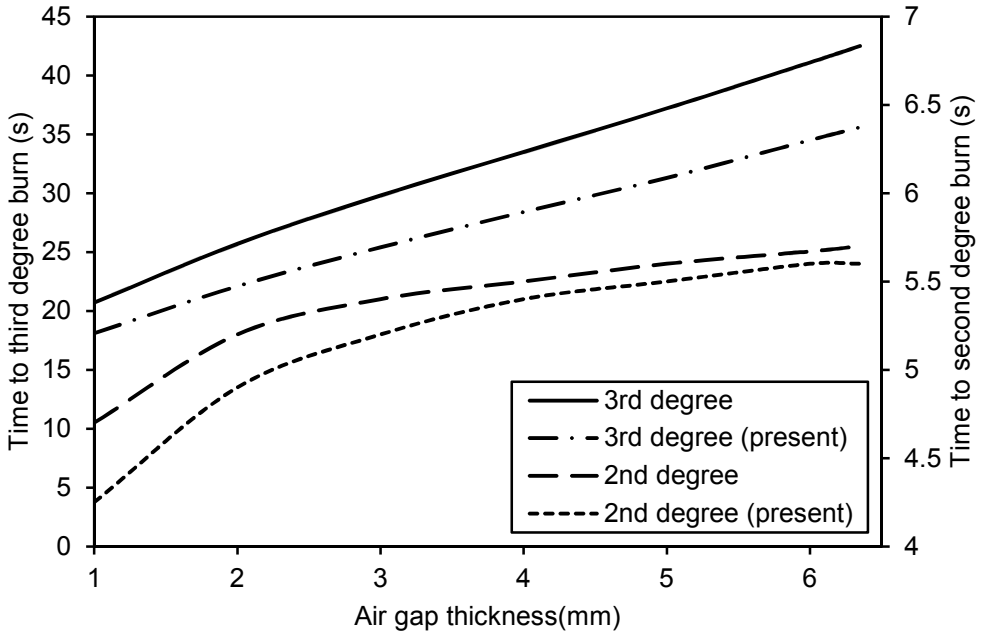

Figure 4. Influence of the air gap model on skin burn predictions for various air gap widths.

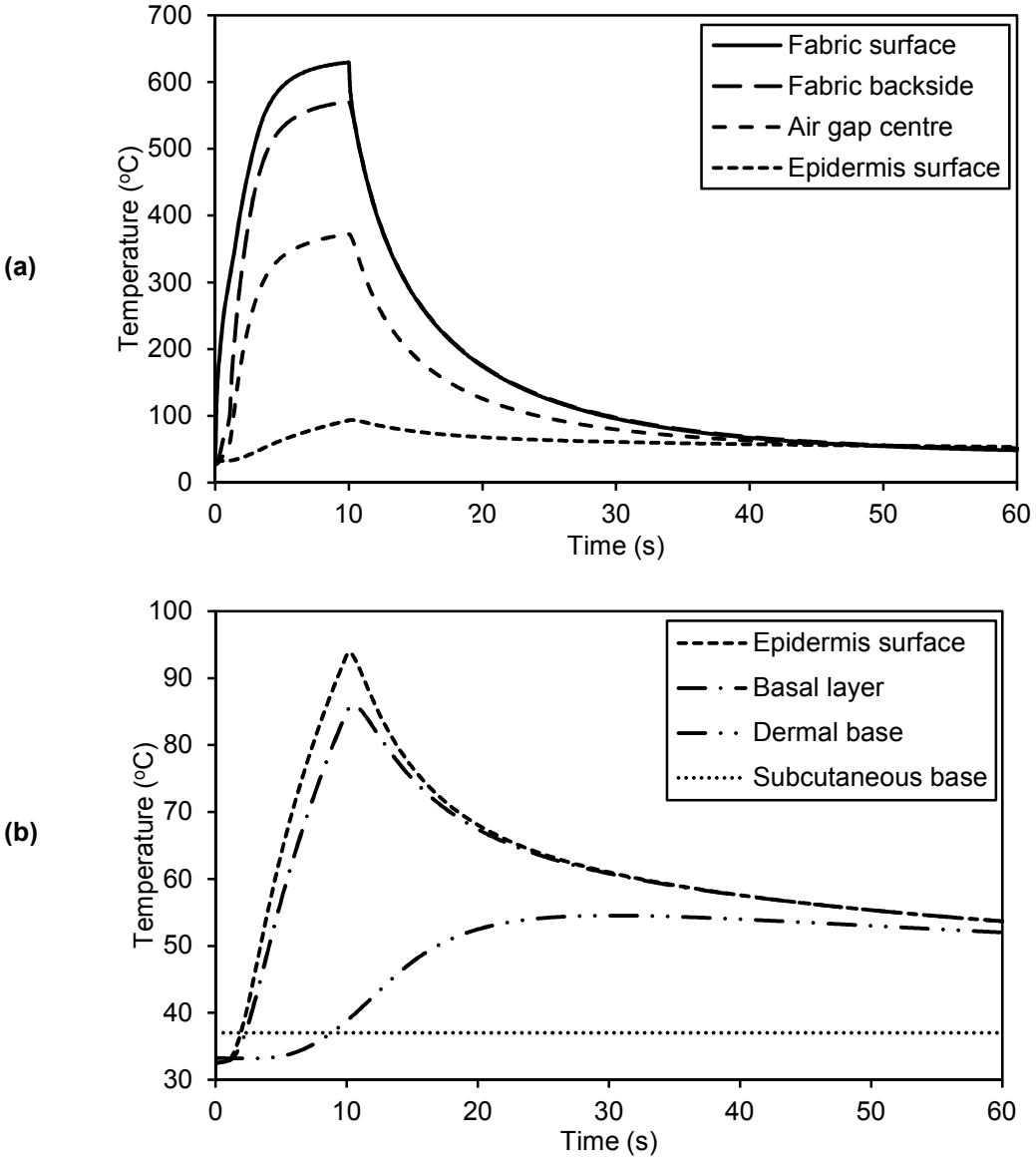

Figure 5. Temporal temperature distribution within the clothing system: (a) fabric and air gap, (b) skin.

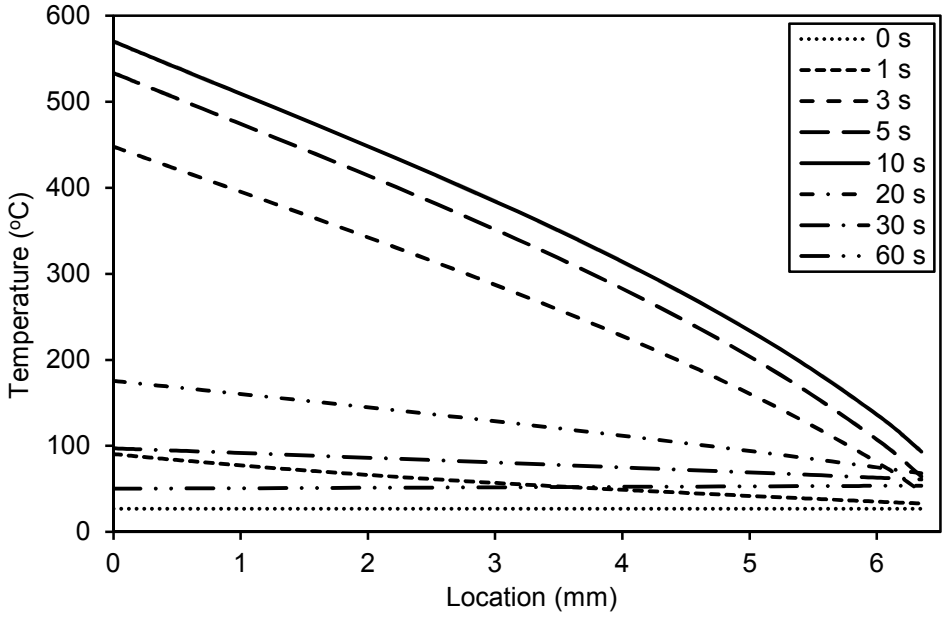

Figure 6. The variation in the air gap temperature distribution.

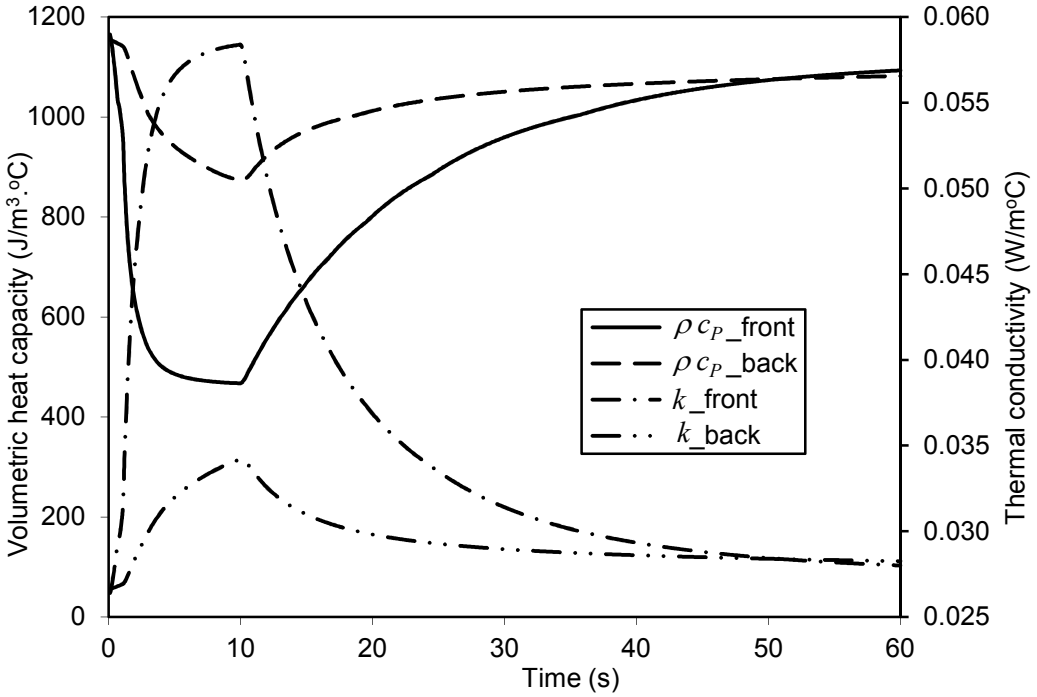

Figure 7. The variation in the air gap thermal conductivity and volumetric heat capacity.

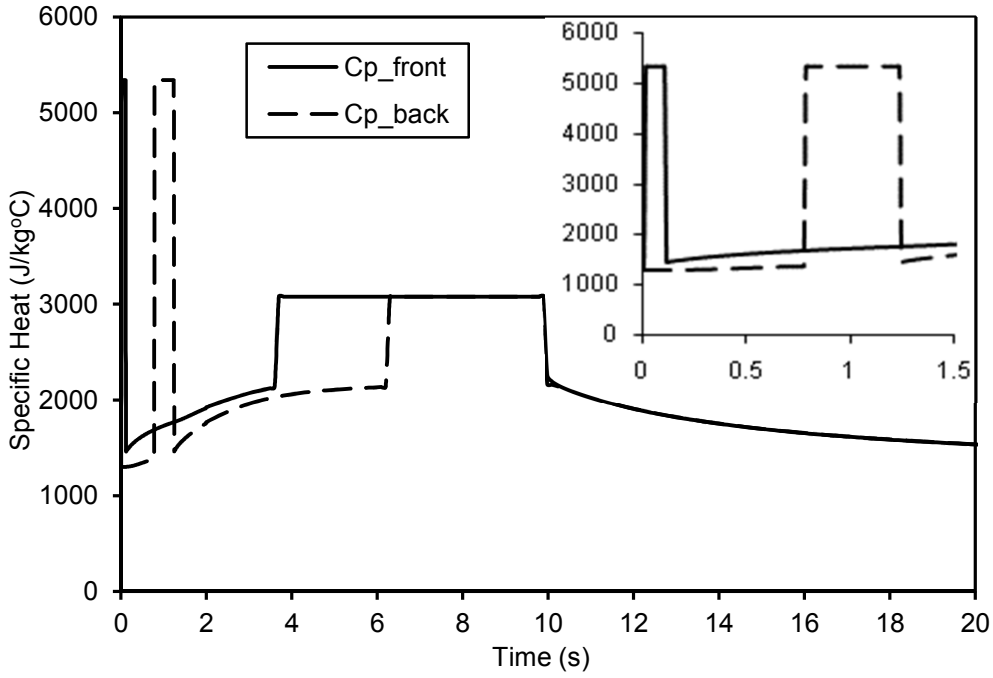

Figure 8. The variation in the fabric apparent heat capacity as an indication of the underlying moisture transfer and thermochemical reactions.

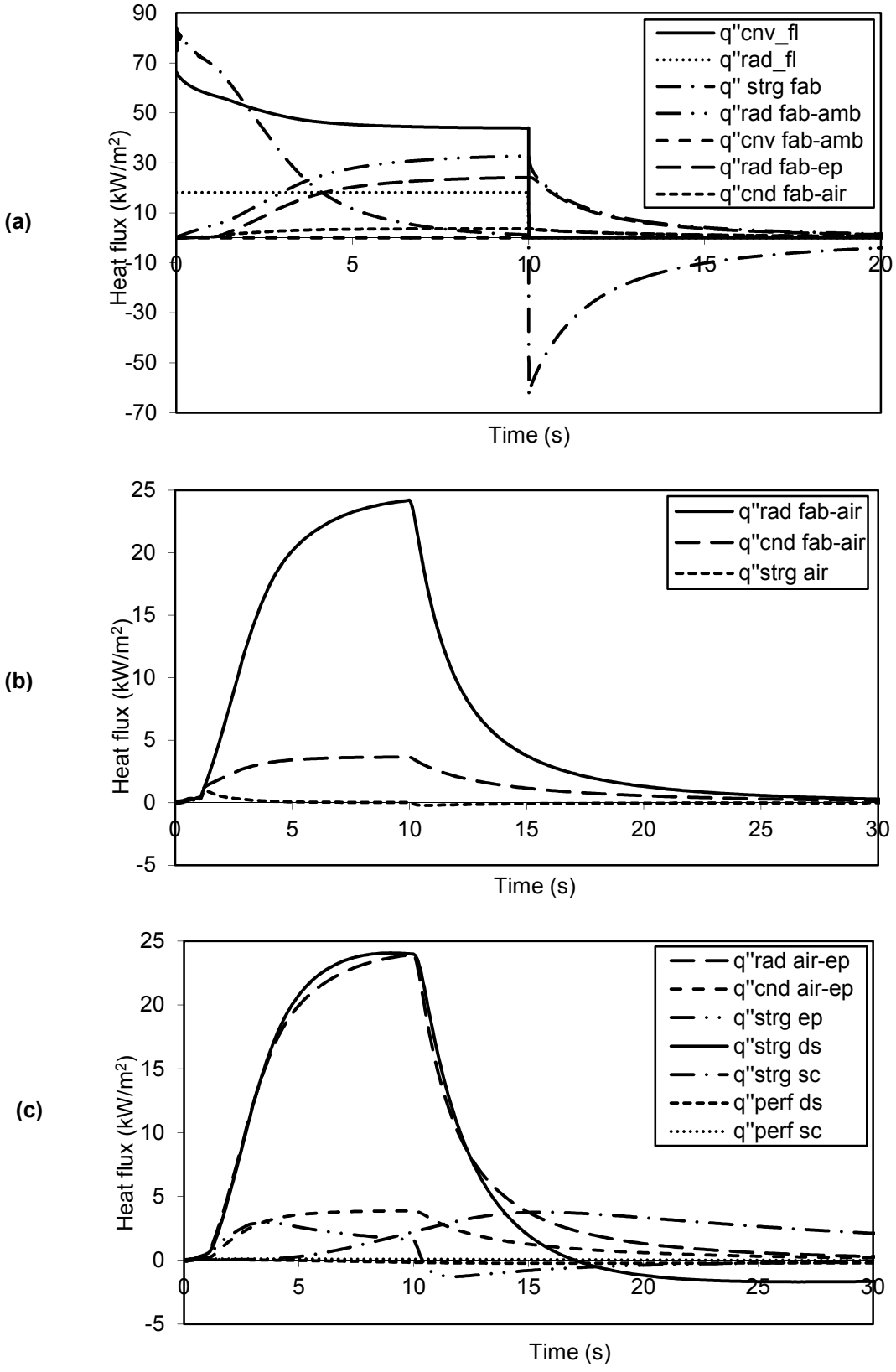

Figure 9. The protective clothing system energy balance: (a) fabric, (b) air gap, (c) skin.

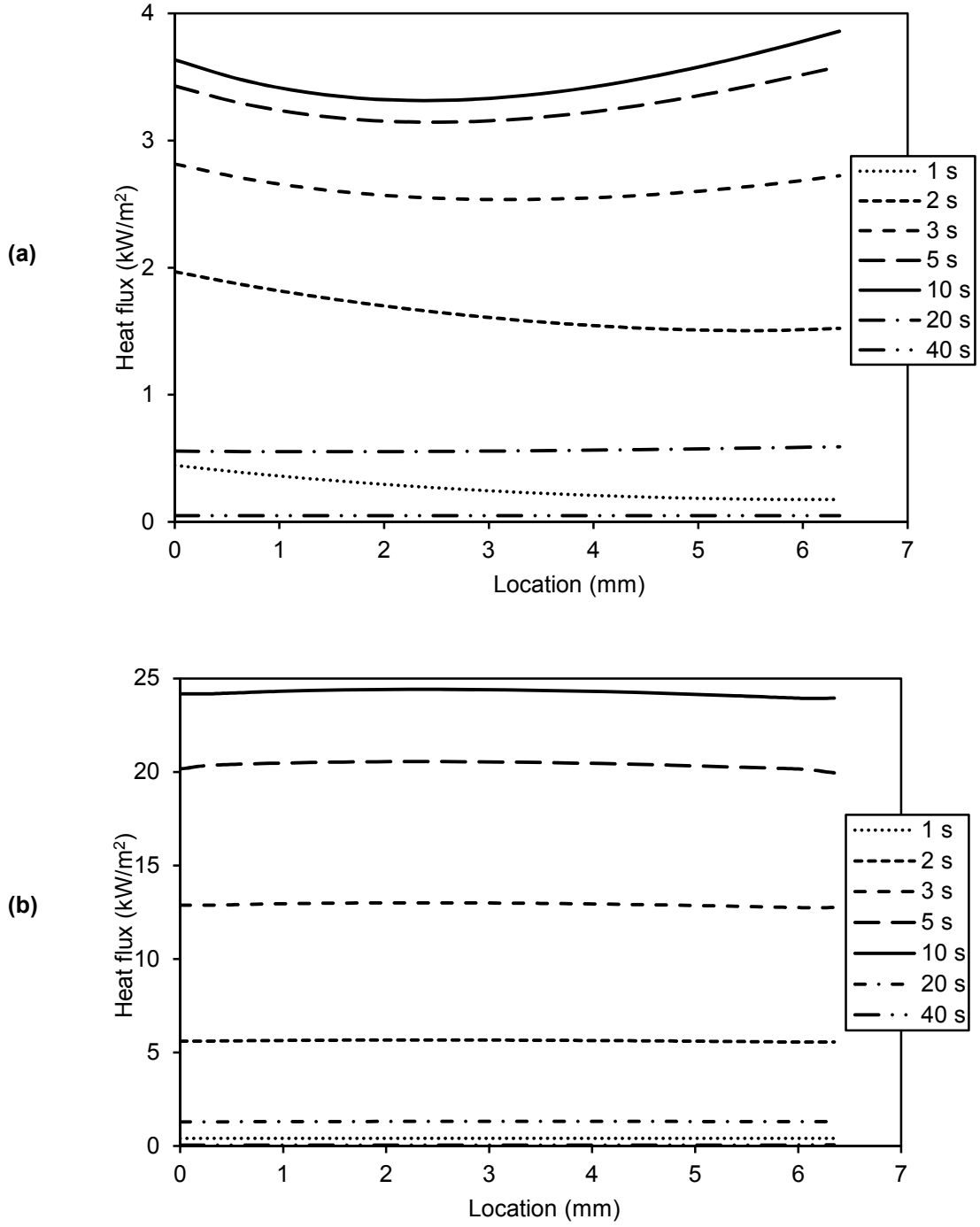

Figure 10. Spatial distribution of the heat transfer fluxes within the air gap:

(a) conduction heat transfer flux, (b) radiation heat transfer flux.

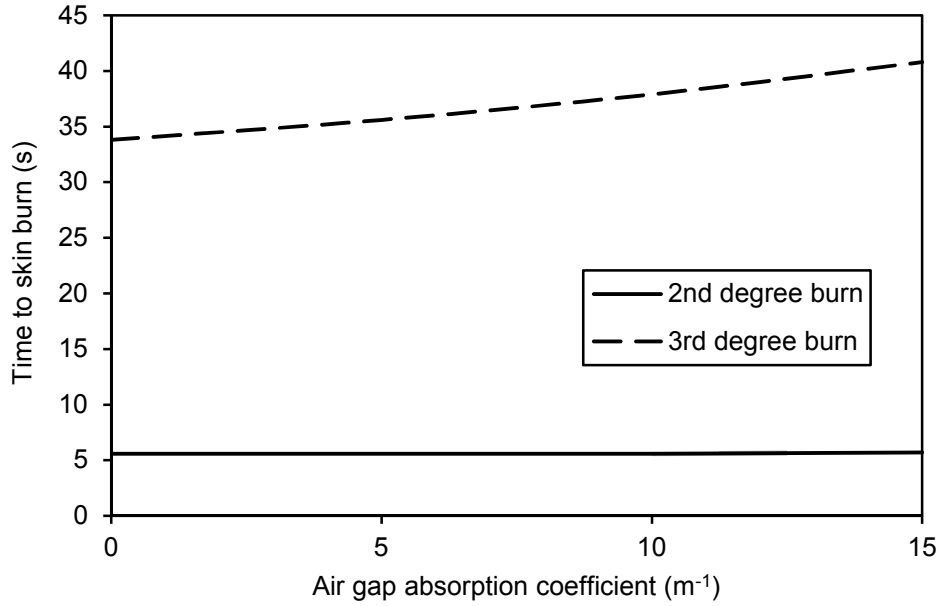

Figure 11. Influence of the air gap absorption coefficient on skin burn prediction.

CHAPTER 3

INFLUENCE OF THE AIR GAP BETWEEN PROTECTIVE CLOTHING AND SKIN ON CLOTHING PERFORMANCE DURING FLASH FIRE EXPOSURE

Published as

A. Ghazy and D.J. Bergstrom, Influence of the Air Gap between Protective Clothing and Skin on Clothing Performance during Flash Fire Exposure, Heat Mass Transfer, 2011, DOI: 10.1007/s00231-011-0791-y.

Contribution of this Chapter to the Thesis

The research work presented in this chapter aims at achieving the second objective of the thesis. More specifically, the chapter introduces a parametric study of the clothing parameters that affect the conduction-radiation heat transfer through the air gap between the clothing and the skin such as the air gap absorption coefficient, air gap width, fabric thickness, and fabric backside emissivity. The influence of each parameter on the conduction and radiation heat fluxes distributions within the air gap as well as on the temperature distribution within the clothing system was investigated. A comparison between the influences of each parameter on the prediction of the clothing performance was made between the present model and the typical model in the literature.

Influence of the Air Gap between Protective Clothing and Skin on Clothing Performance during Flash Fire Exposure

Ahmed Ghazy and Donald J. Bergstrom

Department of Mechanical Engineering, University of Saskatchewan, Saskatoon, Saskatchewan, Canada

Address correspondence to Donald J. Bergstrom, Department of Mechanical Engineering, University of Saskatchewan, 57 Campus Dr., Saskatoon, SK S7N 5A9, Canada. E-mail: Don.Bergstrom@usask.ca

ABSTRACT

A finite volume model was developed to simulate transient heat transfer in protective clothing during flash fire exposure. The model accounts for the combined conduction-radiation heat transfer in the air gap between the fabric and skin. The variation in the fabric and air gap properties with temperature and the thermochemical reactions in the fabric are also considered. This study investigates the influence of the air gap in protective clothing on the energy transfer through the clothing and hence on its performance. Different parameters that affect the conduction-radiation heat transfer through the air gap such as the air gap absorption coefficient and the air gap width were studied. Finally, the paper demonstrates that an innovative and potentially significant way to improve protective clothing performance is to reduce the emissivity on the backside of the fabric.

LIST OF SYMBOLS

A	surface area, m^2
a, b	finite volume discrete equation coefficient, source term

C	heat capacity, J/kg K
c_P	specific heat at constant pressure, J/kg K
D_c^l	directional cosine integrated over $\Delta\Omega^l$
$\hat{e}$	unit vector in coordinate direction
G	incident radiation, W/m^2
h	convective heat transfer coefficient, W/m^{2}K
I	Intensity, W/m^2
k	thermal conductivity, W/m K
L	thickness, m
P	pre-exponential factor, 1/s
q''	heat flux, W/m^2
$\vec{r}$	position vector, m
R	ideal gas constant, J/mol K
$\hat{s}$	unit vector in a given direction
S	source function
s	geometric distance, m
T	temperature, K
t	time, s
W	fabric width, m
y	linear vertical coordinate, m

Greek Symbols

Ω	solid angle, sr
θ	polar angle, rad

φ	quantitative measure of skin damage
ϕ	azimuthal angle, rad
ΔE	activation energy of skin, J/kmol
ΔV	volume of control volume, m^3
$\Delta\Omega^l$	control angle
α	air gap absorptivity
ε	emissivity
γ	extinction coefficient of the fabric, 1/m
κ	air gap absorption coefficient, 1/m
ρ	density, kg/m^3 or surface reflectivity
σ	Stefan-Boltzmann constant, 5.67×10^{-8} W/m^2K^4
τ	transmissivity
ω	blood perfusion rate, $(m^3/s)/m^3$ of human tissue

Subscripts

air	air
amb	ambient conditions
b	human blood / black body
cnv	convection heat transfer
cr	human body core
ep, ds, sc	epidermis , dermis, subcutaneous human skin layers
exp	exposure
fab	fabric
fl	flame

g	hot gases
n, s	north, south control volume faces
P	control volume central node
R , rad	radiation heat transfer
x, y, z	coordinate directions

Superscripts

A	apparent
l	index for direction

1. INTODUCTION

Flash fire is one of the possible hazards for workers in many industries including the petroleum and petrochemical sector. Firefighters also face a variety of high temperature and heat flux exposures including flash fire. Even sports car drivers are subject to flash fire hazard. Exposures to flash fire are usually of short duration (a few seconds) and typically end when the individual escapes from the location of the fire. Exposure to fire can result in skin burn injuries that range from first-degree burn injury to third-degree burn injury depending on the exposure intensity and duration.

A variety of different types of protective clothing made from fire resistant fabrics are widely used in many industrial applications to provide protection against fire exposure. Evaluating the performance of protective clothing usually involves estimating the total energy transfer through the fabric that causes burn injury to the human skin on the other side of the fabric. Bench top tests are employed to evaluate the performance of protective clothing using fabric specimens. A variety of different types and levels of exposure are used in these tests to examine the fabric. For example, according to ASTM D 4108 [1], the fabric specimen is exposed

to flame contact with a Meker burner. This type of flame represents a combination of convective and radiant exposures with a nominal heat flux of approximately 80 kW/m^2. ASTM F 1939 [2] employs a different type of exposure where a set of quartz tubes are used to produce a purely radiant exposure. In addition, NFPA 1971 [3] use a Meker burner and quartz tubes to produce both convective and radiant exposures. In these bench top tests, the extent of skin burn injuries is predicted using the criterion developed by Stoll and Chianta [4]. In contrast to bench top tests, manikin tests, according to ASTM F 1930 [5], can be used to evaluate the performance of the entire garment rather than only a specimen of the fabric. Henriques' burn integral [6] is employed in this test to predict skin burn injuries at different locations on the body using heat flux measurements made by skin simulant gauges installed on different parts of the manikin's body.

The air gap between protective clothing and the human skin plays an important role in the protective performance of the clothing since burn injuries are caused by the energy transferred from the hot fabric to the skin through this gap. Moreover, the width of the air gap can determine the mechanism of energy transfer between the fabric and the skin. For example, Torvi et al. [7, 8] found that energy is transferred by conduction and radiation from the fabric to the skin for air gaps of 6.4 mm (1/4 in.) or less, while convection heat transfer takes place for larger gaps. However, the air gap width between the fabric and skin depends on the garment size and the location on the body [9].

The influence of the air gap on protective clothing performance in terms of skin burn predictions has been addressed in the literature by many researchers. Torvi et al. [7, 8] investigated the influence of the air gap width on the protective performance of a single layer fire-resistant fabric during a contact flame bench top test. Song et al. [9] measured the air gap

widths between a single layer garment and the manikin's body (PyroMan®) for different types and sizes of protective garments using a three-dimensional body scanning technique. They then used these air gap widths in their 1-D model to simulate heat transfer in a single layer protective garment worn by PyroMan® and exposed to a laboratory flash fire. Chitrphiromsri et al. [10, 11] used these air gap values again in their 1-D model to simulate the coupled heat and moisture transfer in firefighters' clothing during flash fire exposure.

Despite wide recognition of the influence of the air gap on protective clothing performance, most studies reported in the literature use a relatively simple model for the air gap. For example, they often decouple the conduction and radiation heat transfer through the air gap, and instead assume steady state conduction and only surface radiation heat transfer through the air gap. A more careful analysis and model for the heat transfer through the air gap would contribute to a more accurate prediction of the clothing performance. Given this motivation, Ghazy and Bergstrom [12] introduced a more sophisticated model for the heat transfer through the air gap between the protective clothing and human skin during flash fire exposure. The new air gap model was shown to significantly affect the predictions for time to skin burn injury.

Recognising the important role of the air gap in the performance of protective clothing, then a better understanding of the heat transfer within the air gap should suggest ways to improve the clothing performance. This paper introduces a further investigation of the combined conduction-radiation heat transfer through the air gap in protective clothing during flash fire exposure. In addition to the model improvements described in reference [12], more realistic boundary conditions have been implemented for the radiation heat transfer through the air gap where the non-reflecting boundary assumption was replaced by the reflecting one. This paper is a completion of the study introduced in [12] rather than just a modification of its model. The main

objective of the present paper is to investigate the influence of different parameters that affect the combined conduction-radiation heat transfer in the air gap, as a radiation participating medium, and their subsequent influence on the performance of protective clothing. In this context, the study documents a novel approach to reduce energy transfer through the air gap and hence improving the clothing performance by reducing the emissivity of the backside of the fabric.

2. PROBLEM FORMULATION

Figure 1 shows a typical protective clothing system that consists of a single layer of Kevlar®/PBI fire-resistant fabric, the human skin, and an air gap between the fabric and the skin. The fabric is exposed to flame contact with a nominal heat flux of 83 kW/m^2. The human skin consists of epidermis, dermis, and subcutaneous layers where blood perfusion takes place in the latter two layers. Skin burn injuries may occur as a result of the intense energy transfer from the fabric to the skin through the air gap.

For air gap widths equal to that of the standard Thermal Protective Performance (TPP) test [1] (6.35 mm (1/4 in.)) or less, the 1-D transient conduction-radiation heat transfer in the air gap is expressed as

$$\rho(T)c_P(T)\frac{\partial T}{\partial t} = \frac{\partial}{\partial y}\left(k(T)\frac{\partial T}{\partial y}\right) - \frac{\partial q_R^{"}}{\partial y} \tag{1}$$

where ρ, c_P, and k are the air density, specific heat, and thermal conductivity, respectively, and $q_R^{"}$ is the radiative heat flux through the air gap, which can be obtained by solving the Radiative Transfer Equation (RTE) for the air gap as described below.

Consider the air gap as a gray, absorbing, and emitting medium; the change in intensity along a radiation ray path is written [13] as

$$\frac{dI(\vec{r},\hat{s})}{ds} = -\kappa(\vec{r})I(\vec{r},\hat{s}) + \kappa(\vec{r})I_b(\vec{r}) \tag{2}$$

where I is the radiation intensity, which varies with the spatial position $\vec{r}$ and the angular direction $\hat{s}$, κ is the air gap absorption coefficient, s is the geometric distance, and I_b is the black body intensity. The unit direction $\hat{s}$ is defined as

$$\hat{s} = (sin\theta\ cos\phi)\hat{e}_x + (sin\theta\ sin\phi)\hat{e}_y + (cos\theta)\hat{e}_z \tag{3}$$

where $\hat{e}_x$, $\hat{e}_y$, and $\hat{e}_z$ are unit vectors in the x, y, and z directions, θ is the polar angle measured from $\hat{e}_z$, and ϕ is the azimuthal angle measured from $\hat{e}_x$. The black body intensity is defined as

$$I_b = \frac{\sigma T^4}{\pi} \tag{4}$$

where σ is the Stephan-Boltzmann constant, and T is the medium temperature. The absorption coefficient of the air gap, κ, is estimated to be 5 m^{-1} based on a calculation for the absorptivity of the hot gases in the gap, α, using Hottel's method [14] i.e.

$$\alpha = 1 - exp(-\kappa L_{air}) \tag{5}$$

where L_{air} is the air gap width.

The divergence of radiative heat flux in Eq. (1) is obtained from the relation

$$\frac{\partial q_R^{"}}{\partial y} = \kappa\left(4\pi I_b(\vec{r}) - G(\vec{r})\right) \tag{6}$$

where $G(\vec{r})$ is incident radiation, which is defined as

$$G(\vec{r}) = \int_{4\pi} I(\vec{r},\hat{s})d\,\Omega \tag{7}$$

where $d\Omega$ is the control angle containing the radiation ray $I(\vec{r},\hat{s})$. The radiation intensity distribution within the air is estimated by solving the RTE (Eq. (2)) numerically along with its boundary conditions.

Assuming both the fabric backside and the skin surface to behave as opaque gray diffusive surfaces, the boundary conditions for the air gap RTE are written [13] as

$$I_{fab}(\vec{r},\hat{s}) = \varepsilon_{fab2}(\vec{r})I_{b,fab}(\vec{r}) + \frac{\rho_{fab2}(\vec{r})}{\pi}\int_{\hat{s}'\cdot\hat{n}<0} I(\vec{r},\hat{s}')|\hat{s}'\cdot\hat{n}|d\,\Omega' \quad at\ y = L_{fab} \tag{8}$$

$$I_{ep}(\vec{r},\hat{s}) = \varepsilon_{ep}(\vec{r})I_{b,ep}(\vec{r}) + \frac{\rho_{ep}(\vec{r})}{\pi}\int_{\hat{s}'\cdot\hat{n}<0} I(\vec{r},\hat{s}')|\hat{s}'\cdot\hat{n}|d\,\Omega' \quad at\ y = L_{fab} + L_{air} \tag{9}$$

where ε_{fab2} , and ρ_{fab2} are the fabric backside emissivity and reflectivity, ε_{ep} and ρ_{ep} are the epidermis surface emissivity and reflectivity, $\hat{s}'$ is the reflected ray unit direction, $\hat{n}$ is the unit normal to the surface, dΩ' is the solid angle containing the reflected ray, and L_{fab} is the fabric thickness. The left hand side of Eq. (8) is the total radiation intensity emitted from the backside surface of the fabric. The first term on the right hand side of Eq. (8) is the radiation intensity emitted from the backside surface of the fabric as a gray body. The second term on the right hand side of Eq. (8) is the radiation intensity reflected on the backside surface of the fabric. The corresponding terms in Eq. (9) have similar meanings.

The boundary conditions for Eq. (1) are obtained from the continuity of temperature between the air gap and both the fabric and the skin, i.e.

$$T_{air}|_{y=L_{fab}} = T_{fab}\big|_{y=L_{fab}} \qquad t > 0 \tag{10}$$

$$T_{air}|_{y=L_{fab}+L_{air}} = T_{ep}\big|_{y=L_{fab}+L_{air}} \qquad t > 0 \tag{11}$$

where T_{fab} is the fabric temperature and T_{ep} is the epidermis layer temperature. Both temperatures can be obtained by solving the energy equations for the fabric and the epidermis layer, respectively. The air gap initial condition is

$$T_{air}(y, t = 0) = T_{amb} \tag{12}$$

where T_{amb} is the ambient temperature, which is taken as 300 K. The properties of dry air [14] were used to account for the variation in the thermal properties of the hot gases in the gap with temperature.

The energy equation for the fabric is expressed [15, 16] as

$$\rho C^A(T)\frac{\partial T}{\partial t} = \frac{\partial}{\partial y}\left(k(T)\frac{\partial T}{\partial y}\right) - \frac{\partial}{\partial y}q^{"}_{rad}(y) \qquad 0 < t \le t_{exp} \qquad (13a)$$

$$\rho c_P(T)\frac{\partial T}{\partial t} = \frac{\partial}{\partial y}\left(k(T)\frac{\partial T}{\partial y}\right) \qquad t > t_{exp} \qquad (13b)$$

where ρ, c_P, and k are the fabric density, specific heat, and thermal conductivity, respectively, $q^{"}_{rad}(y)$ is the transmitted portion of the radiant heat flux from the flame to the fabric, C^A is the fabric apparent heat capacity [8, 15], and t_{exp} is the exposure duration. Beer's law [17] was used [8, 15] to account for the absorption of the incident thermal radiation as it penetrates the pores of the fabric, i.e.

$$q^{"}_{rad}(y) = q^{"}_{rad\_fl}\, exp(-\gamma y) \qquad (14)$$

The term $q^{"}_{rad\_fl}$, which represents the radiant portion of exposure, is written as

$$q^{"}_{rad\_fl} = \sigma \varepsilon_g T_g^4 \qquad (15)$$

where σ is the Stefan-Boltzmann constant, ε_g is the hot gases emissivity, and T_g is the hot gases temperature (K). The extinction coefficient of the fabric γ is given [8, 15] by

$$\gamma = \frac{-ln(\tau)}{L_{fab}} \qquad (16)$$

where τ is the fabric transmissivity.

The boundary conditions for the fabric energy equation are as follows.

$$-k_{fab}(T)\frac{\partial T_{fab}}{\partial y}\bigg|_{y=0} = h_{fl}\left(T_g - T_{fab(y=0)}\right) - \sigma\varepsilon_{fab1}\left(1-\varepsilon_g\right)\left(T^4_{fab(y=0)} - T^4_{amb}\right) \qquad (17a)$$

$$0 < t \le t_{exp}$$

$$k_{fab}(T)\frac{\partial T_{fab}}{\partial y}\bigg|_{y=0} = h_{cnv}\left(T_{fab(y=0)} - T_{amb}\right) + \sigma\varepsilon_{fab1}\left(T^4_{fab(y=0)} - T^4_{amb}\right) \tag{17b}$$

$$t > t_{exp}$$

$$-k_{fab}(T)\frac{\partial T_{fab}}{\partial y}\bigg|_{y=L_{fab}} = q''_y(\vec{r})\big|_{y=L_{fab}} - k_{air}(T)\frac{\partial T_{air}}{\partial y}\bigg|_{y=L_{fab}} \qquad t > 0 \tag{18}$$

Where h_{fl} is the convective heat transfer coefficient from the flame to the fabric, ε_{fab1} is the fabric exposed surface emissivity, and h_{cnv} is the convective heat transfer coefficient from the fabric to the ambient during the cool down period. The latter is estimated from an empirical correlation for natural convection heat transfer from a horizontal heated plate facing downwards to air at atmospheric pressure [17] as

$$h_{cnv} = 0.59\left(\frac{T_{fab(y=0)} - T_{amb}}{W_{fab}}\right)^{1/4} \tag{19}$$

The first term on the right hand side of Eq. (17a) is the convection portion of the exposure from the hot gases to the fabric, while the second term is the radiant losses from the fabric to the ambient during the exposure. The first term on the right hand side of Eq. (17b) represents the convection losses from the fabric to the ambient, while the second term represents the radiant losses to the ambient during the cool down of the fabric. The right hand side of Eq. (18) is the combined conduction-radiation heat transfer in the air gap at the fabric-air interface.

The emitted radiation from the fabric backside surface is estimated as

$$q''_y(\vec{r})\big|_{y=L_{fab}} = \int_{4\pi} I(\vec{r},\hat{s})(\hat{s}\cdot\hat{e}_y)d\,\Omega\Big|_{y=L_{fab}} \tag{20}$$

The fabric initial condition is

$$T_{fab}(y, t = 0) = T_{amb} \tag{21}$$

The bioheat equation developed by Pennes [18] was employed to model heat transfer in the skin tissues. The energy equations for the three layers of skin are written as

$$(\rho c_P)_{ep} \frac{\partial T}{\partial t} = \frac{\partial}{\partial y}\left(k_{ep} \frac{\partial T}{\partial y}\right) \tag{22}$$

$$(\rho c_P)_{ds} \frac{\partial T}{\partial t} = \frac{\partial}{\partial y}\left(k_{ds} \frac{\partial T}{\partial y}\right) + (\rho c_P)_b \omega_b (T_{cr} - T) \tag{23}$$

$$(\rho c_P)_{sc} \frac{\partial T}{\partial t} = \frac{\partial}{\partial y}\left(k_{sc} \frac{\partial T}{\partial y}\right) + (\rho c_P)_b \omega_b (T_{cr} - T) \tag{24}$$

where ω_b is the blood perfusion rate within the dermis and subcutaneous layers, T_{cr} is the human core body temperature, and ρ, c_P, and k have their conventional meaning.

The continuity of temperature and heat flux represents the inner boundary conditions between the skin layers as follows.

$$T_{ep}\big|_{y=L_{fab}+L_{air}+L_{ep}} = T_{ds}\big|_{y=L_{fab}+L_{air}+L_{ep}} \qquad t > 0 \tag{25}$$

$$k_{ep} \frac{\partial T_{ep}}{\partial y}\bigg|_{y=L_{fab}+L_{air}+L_{ep}} = k_{ds} \frac{\partial T_{ds}}{\partial y}\bigg|_{y=L_{fab}+L_{air}+L_{ep}} \qquad t > 0 \tag{26}$$

$$T_{ds}\big|_{y=L_{fab}+L_{air}+L_{ep}+L_{ds}} = T_{sc}\big|_{y=L_{fab}+L_{air}+L_{ep}+L_{ds}} \qquad t > 0 \tag{27}$$

$$k_{ds} \frac{\partial T_{ds}}{\partial y}\bigg|_{y=L_{fab}+L_{air}+L_{ep}+L_{ds}} = k_{sc} \frac{\partial T_{sc}}{\partial y}\bigg|_{y=L_{fab}+L_{air}+L_{ep}+L_{ds}} \qquad t > 0 \tag{28}$$

where L_{ep}, L_{ds}, L_{sc} are the epidermis, dermis, and subcutaneous layers thickness, respectively.

The skin boundary conditions are

$$-k_{ep} \frac{\partial T_{ep}}{\partial y}\bigg|_{y=L_{fab}+L_{air}} = q_y^{"}(\vec{r})\big|_{y=L_{fab}+L_{air}} - k_{air}(T) \frac{\partial T_{air}}{\partial y}\bigg|_{y=L_{fab}+L_{air}} \qquad t > 0 \tag{29}$$

$$T_{sc}\big|_{y=L_{fab}+L_{air}+L_{ep}+L_{ds}+L_{sc}} = T_{cr} \qquad t > 0 \tag{30}$$

where the radiation heat flux received by the epidermis surface is calculated as

$$q_y^{"}(\vec{r})\big|_{y=L_{fab}+L_{air}} = \int_{4\pi} I(\vec{r},\hat{s})(\hat{s}\cdot\hat{e}_y)d\,\Omega\Big|_{y=L_{fab}+L_{air}} \tag{31}$$

The skin initial condition is expressed as a linear temperature distribution between 32.5ºC at the epidermis surface and 37ºC at the subcutaneous base (core body temperature).

As the temperature at the interface between the epidermis and the dermis layers (basal layer) reaches 44^{o}C, Henriques' integral [6] is employed to predict times to receive skin burn injuries as follows.

$$\varphi = \int_0^t P\ exp\left(-\frac{\Delta E}{RT}\right)dt \tag{32}$$

where the basal layer temperature is used in the integral to predict first and second degree burn injuries. A first-degree burn occurs when the value of φ reaches 0.53, and a second-degree burn occurs when the value of φ reaches 1. To predict third-degree burn injury, the temperature at the interface between the dermis and the subcutaneous (dermal base) is used in the integral. A third degree burn takes place when the value of φ reaches 1. The values for the pre-exponential factor P, and the activation energy ΔE of the skin were determined by Weaver and Stoll [19] for second-degree burn injury. The corresponding values for third-degree burn injury were determined by Takata [20].

3. NUMERICAL SOLUTION

The numerical discretization of the RTE (Eq. (2)) was performed by the finite volume method [21] where the step scheme was employed to relate the face intensity to the nodal intensity as follows.

$$a_P^l I_P^l = a_N^l I_N^l + a_S^l I_S^l + b^l \tag{33}$$

where $I^l \equiv I(\vec{r}, \hat{s})$ and

$$a_N^l = max(-A_n D_{cn}^l, 0) \tag{34}$$

$$a_S^l = max(-A_s D_{cs}^l, 0) \tag{35}$$

$$a_P^l = ma\,x(A_n D_{cn}^l, 0) + ma\,x(A_s D_{cs}^l, 0) + \kappa_P \Delta V_P \Delta\Omega^l \tag{36}$$

$$b^l = S_P^l \Delta V_P \Delta\Omega^l \tag{37}$$

where

$$D_{cs}^l = -D_{cn}^l \tag{38}$$

$$D_{cn}^l = \int_{\Delta\Omega^l} \left(\hat{s}^l \cdot \hat{e}_y\right) d\Omega \tag{39}$$

$$\Delta\Omega^l = \int_{\Delta\Omega^l} d\Omega \tag{40}$$

$$A_n = A_s = \Delta x \tag{41}$$

$$\Delta V_P = \Delta x\, \Delta y \tag{42}$$

$$S_P^l = \kappa_P I_{b,P} \tag{43}$$

The discretization of the energy equation for the air gap and the energy equations for both the fabric and the skin (epidermis, dermis, and subcutaneous) was also performed by the finite volume method [22]. A fully implicit scheme was employed for the temporal discretization. The boundary conditions were applied using fictitious nodes. A Gauss-Seidel point-by-point iterative scheme was used to solve the discrete energy equations due to the nonlinearity that comes from the conduction-radiation coupling within the air gap, the radiation boundary condition, and the variation in the thermal properties of both the fabric and the air gap with temperature. The solution marches in time as follows. For each time step, temperatures from the previous time step are used as initial values for the iteration loop. The air gap, fabric

backside, and epidermis surface temperatures are used to estimate the radiation intensity distribution within the air gap. Then the divergence of the radiative heat flux within the air gap and the radiation heat flux at both sides of the air gap are calculated to be employed in the air gap energy equation and the boundary condition equations of the fabric and the skin. Next, new temperatures are calculated by visiting each grid starting from the fabric surface to the subcutaneous base. The thermal properties for the fabric and the air gap, the temperature values in the source term, and the divergence of radiative heat flux are updated based on the current temperature distribution within the iteration loop. The iterative solver continues until the non-dimensional change in the temperature field becomes less than 10^{-5}. The influence of the grid size and time step were studied in order to ensure negligible influence on the solution fields. After the system temperature distribution at a given time step is obtained, the basal layer and the dermal base temperatures are employed in the Henriques' integral (equation (32)) to predict times to receive skin burn injuries. The numerical solution of the developed model was solved using an in-house computational code developed by the first author (Ahmed Ghazy) where it takes approximately two hours to obtain typical simulation results.

Note that the energy equations of the model are dependent on a scalar quantity that is the temperature, while the RTE is dependent on a vector quantity that is the radiation intensity. The Finite Volume Method (FVM) used to solve the RTE is a modification of that used for solving the energy equations, where the RTE is discretized over a control volume and a control angle versus the discretization of the energy equation solely over the spatial control volume. There are many other methods to solve the RTE including the Monte Carlo method, the discrete-ordinates method, the lattice Boltzmann method, etc., but we selected the FVM partly due to its conservative properties.

4. RESULTS AND DISCUSSION

In order to validate the model, a simulation of the open flame bench top test done by Torvi [8] using skin simulant material was performed. The operating data are the same for both the simulation and the test and the thermophysical properties of the skin stimulant material were accounted for in the simulation. Figure 2 shows a comparison between the predicted and measured skin simulant surface temperature during both the exposure and the cool down periods. The model was able to successfully predict the sharp rise in the skin simulant surface temperature during the exposure period. For example, the percentage error between the model predictions and the measurements is equal to 0.2% at time equal to 5 seconds while it is equal to 4.8% at time equal to 25 seconds. The small discrepancy between the prediction and measurements during the exposure and the cool down periods can be attributed to factors not considered in the model. For example, a reduction in the fabric thickness due to pyrolysis and a reduction in the air gap width due to fabric shrinkage would change the test geometry (These two factors will be discussed later in this section). Without more extensive experimental data, it is not possible to definitively identify the source of the small deviations observed in Figure 2.

The fabric and hot gas parameters used in the simulation are listed in Table 1, while the human skin thermophysical properties are listed in Table 2. The study assumes an exposure to flash fire with nominal heat flux of about 83 kW/m^2 for 10 s followed by 90 s of cool down. Simulations were carried out for a variation in the air gap absorption coefficient, air gap width, fabric backside emissivity and fabric thickness.

Figure 3 illustrates the effect of the variation in the air gap absorption coefficient on the conduction-radiation heat transfer through the air gap. Figure 3(a) indicates that the emitted radiation from the backside of the fabric decreases during the exposure period as the air gap

absorption coefficient increases. In contrast, the influence of the air gap absorption coefficient on the emitted radiation from the backside of the fabric becomes insignificant during the cool down period. Figure 3(b) compares the radiation heat flux distribution through the air gap for different absorption coefficients. The figure shows a significant deviation in the radiation heat flux from the case of only surface radiation (absorption coefficient is equal to zero) that is used by most previous models in the literature. Moreover, this deviation increases with the increase of the absorption coefficient and the radiation intensity. The conduction heat transfer through the air gap behaves opposite to the radiation heat transfer. Figure 3(c) shows that the conduction heat flux at the fabric-air interface increases as the air gap absorption coefficient increases. However, this increase in the conduction heat flux is about one-third the reduction in the radiation heat flux. Figure 3(d) illustrates the variation in the conduction heat flux across the air gap for different values of the air gap absorption coefficient. Comparing Figure 3(d) to Figure 3(b) illustrates that the variation in the conduction heat flux through the air gap is less than that of the radiation heat flux. The conduction and radiation heat flux have opposing extrema in the air gap, i.e. maximum conduction heat flux values take place where the minimum radiation heat flux values exist and vice versa.

Despite the influence of the air gap absorption coefficient on the heat transfer fluxes through the air gap, the overall effect on the temperature distribution within the air gap is minimal. The influence of the air gap absorption coefficient on the protective clothing performance in terms of skin burn predictions is summarised in Figure 4. There is an insignificant increase in the time to receive second-degree burn as the value of the air gap absorption coefficient increases from 0 to 15 m^{-1}. On the other hand, the time to receive third degree burn during the cool down period increases by about 30% as the air gap absorption

coefficient increases from 0 to 15 m^{-1}. The actual value of the air gap absorption coefficient would depend on the concentration of the hot gases in the gap, which in turn depends on the fabric type, exposure duration, and diffusion of the hot gases through the clothing system.

The width of the air gap between the protective clothing and human skin varies from one location to another on a worker's body. In addition, a reduction in the air gap size might take place due to thermal shrinkage of the fabric due to flame exposure. The effect of varying the air gap width on the conduction-radiation heat transfer through the air gap is shown in Figure 5. A decrease in the air gap width from 6 mm to 1 mm causes a significant reduction in the emitted radiation from the backside of the fabric, Figure 5(a), and a corresponding increase in the conduction heat flux at the fabric-air interface, Figure 5(b). The increase in the conduction heat flux is greater than the corresponding decrease in the radiation heat flux during both the exposure and the cool down periods. Note that the influence of the reduction in the gap width on the heat transfer across the air gap increases significantly as the fabric moves closer to the skin. The variation in both the radiation and conduction heat fluxes across the air gap is shown in Figure 5 (c) and (d), respectively.

Figure 6 shows the influence of the air gap width on the temperature at three locations in the gap. The reduction in the gap width reduces the temperature of the fabric backside, Figure 6(a), and at the centre of the gap, Figure 6(b), while it increases the epidermis surface temperature, Figure 6(c). This behavior can be attributed to the increase in the conductive heat transfer rate from the fabric to the skin across the air gap as the fabric moves closer to the skin. It is evident that the influence of the air gap width becomes more significant as the fabric moves closer to the skin.

As an assessment of the present air gap model, the skin burn predictions for different air gap widths using the present air gap model are compared to those produced using a simpler air gap model in Figure 7. The present model was simplified to match the typical model found in the literature by: (i) using an air gap absorption coefficient value of zero (i.e. only surface radiation), (ii) assuming the left hand side of Eq. (1) to be zero (i.e. steady state conduction, and decoupled conduction and radiation within the air gap), and (iii) assuming constant air gap properties. In general, the present air gap model predicted skin burn injuries to occur earlier than did the simpler model. The reduction in the air gap width causes only a small reduction in the time to receive second-degree burn, while it causes a significant decrease in the time to receive third-degree burn injuries. The fact that the simple model will over-predict the time to skin burn injury indicates the significance of adopting a more sophisticated model for the air gap.

A general conclusion based on the model results and consistent with other studies is that radiation heat transfer through the air gap from the fabric backside to the skin is the dominant mode of heat transfer through the gap and the major cause for skin burn injuries. Any reduction in the radiation heat transfer through the air gap would be expected to significantly improve the protective clothing performance. One conceptual approach to reduce the emitted radiation from the backside of the fabric is to reduce the fabric surface emissivity. Due to fire exposure, the charred fabric surface with an emissivity of 0.9 causes a large emitted radiation from the fabric backside to the skin. Reducing the fabric backside surface emissivity could potentially be accomplished by coating the fabric backside surface with a brightly colored fire resistant paint.

The potential reduction in the emitted radiation from the fabric backside due to reducing the fabric surface emissivity is explored in Figure 8. Reducing the fabric backside emissivity decreases the emitted radiation from the fabric to the skin during both the exposure and the cool

down period. Moreover, the reduction in the radiation heat transfer emitted from the fabric backside increases as the fabric emissivity decreases. Figure 8(b) shows that the conduction heat transfer through the air gap increases during the exposure and the cool down periods as the fabric emissivity decreases. However, this increase in the conduction flux is small compared to the reduction in the radiation flux. The variation in the radiation and conduction heat flux distribution through the air gap due to the variation in the fabric backside emissivity is illustrated in Figures 8(c) and 8(d), respectively.

Figure 9 illustrates the influence of the fabric backside emissivity on the transient temperature field at three locations in the air gap. An increase in the fabric backside temperature is expected as the fabric backside emissivity is decreased, Figure 9(a). This can be attributed to the decrease in the fabric capability to lose energy by radiation to the skin during both the exposure and the cool down periods. Figure 9(b) shows an increase in the air gap centre temperature as the fabric emissivity decreases. The reduction in the emitted radiation from the fabric to the skin appears in the form of a significant reduction in the epidermis surface temperature as shown in Figure 9(c). Moreover, similar to the trend for the emitted radiation from the fabric, the reduction in the epidermis surface temperature increases as the fabric backside emissivity decreases.

The influence of the reduction in the fabric backside emissivity on skin burn predictions using the present air gap model is compared to that using the simple model in Table 3. Similar to previous results, the present air gap model predicts skin burn injuries to take place earlier than the simple model. Note that Table 3 indicates that, for the above-mentioned simulation parameters, reducing the fabric backside emissivity to 0.8 or less would prevent receiving third-degree burn injury. Further, reducing the fabric backside emissivity to 0.1 would prevent

receiving second-degree burn and postpone first-degree burn to the cool down period. On a theoretical basis, reducing the fabric backside emissivity is a promising approach to improve the clothing performance.

Multiple layers of protective clothing are used [11, 23, 24] to increase the clothing thermal resistance and hence to improve the clothing protective performance. In this study, we also investigated the influence of increasing the thickness of a single layer garment rather than having multiple layers. It is shown in Figure 10(a) that increasing the fabric thickness reduces the fabric backside temperature during the exposure period. This is due to increasing the fabric capacity to store energy and hence reducing the fabric energy loss during the exposure. This also leads to a corresponding increase in the fabric backside temperature during the cool down period. The temperature at the centre of the air gap follows the trend of the fabric backside during both the exposure and the cool down periods as shown in Figure 10(b). A significant reduction in the epidermis surface temperature occurs during the exposure period as the fabric thickness increases, Figure 10(c). However, this reduction diminishes during the cool down period despite the increase in the air gap temperature, which can be attributed to the discharge of the thermal energy stored in the epidermis layer into both the dermis and subcutaneous layers.

The influence of increasing the fabric thickness on the conduction-radiation heat transfer through the air gap is illustrated in Figure 11. The emitted radiation, Figure 11(a), and the conduction heat flux, Figure 11(b), from the fabric backside follow the behavior of the fabric backside temperature shown in Figure 10(a) during both the exposure and the cool down periods. A significant reduction in the emitted radiation from the fabric backside surface is evident in Figure 11(a) as the fabric thickness increases. A corresponding reduction in the conduction heat flux from the fabric is shown in Figure 11(b). However, the reduction in the conduction heat flux

is much smaller than for the radiation heat flux. In addition, a delay in emitting radiation from the fabric backside as the fabric thickness increases is noted during the exposure period compared to the more rapid increase in the conduction heat flux. The spatial variation in the radiation and conduction heat flux through the air gap at different times is illustrated in Figures 11(c) and 11(d), respectively.

The effect of a variation in the fabric thickness on skin burn predictions compared to that predicted by the simple model is investigated in Figure 12. The present air gap model predicts skin burn injuries to take place earlier than does the simple model, which is consistent with previous findings. The present air gap model indicates that increasing the fabric thickness to 0.7 mm would prevent third-degree burn injuries. In contrast, even if the fabric thickness was increased to triple its original thickness (1.8 mm) both first and second-degree burns could not be prevented. Instead, these burn injuries would be delayed until the cool down period. Finally, the simulation results indicate that reducing the fabric backside emissivity is more promising in terms of improving the clothing performance than increasing the fabric thickness, and thus warrants further investigation.

5. CONCLUSIONS

A more sophisticated model for transient heat transfer in the air gap between the fabric and the skin in protective clothing has been developed and implemented in a numerical code. The model was employed to investigate the influence of different parameters on the combined conduction-radiation heat transfer through the gap and on the corresponding protective performance of the clothing. The air gap absorption coefficient had a relatively minimal influence on the temperature distribution within the air gap. On the other hand, it significantly affects times to receive skin burn injuries, especially third-degree burn. Any reduction in the air

gap width below the standard air gap width of 1/4 in. (6.4 mm) causes a significant effect on the heat transfer through the air gap and hence on the clothing performance. In addition, the closer the fabric is to the skin, the more influential the reduction in the air gap width. The study investigated an innovative approach to improve the clothing performance, which is to reduce the fabric backside emissivity using a fire resistant coating. In theory, this approach was found to be much more effective than increasing the fabric thermal resistance by increasing the fabric thickness or using multiple layers. The results demonstrate the importance of the air gap analysis for predicting clothing performance, which then motivates use of a more sophisticated model such as adopted in this study. In a more general context, this study contributes to the knowledge of transient conduction-radiation heat transfer in enclosures with high temperature and heat flux boundary conditions.

REFERENCES

1. American Society for Testing Materials, ASTM D 4108-87 Standard Test Method for Thermal Protective Performance of Materials and Clothing by open-Flame Method, West Conshohocken, PA, 1987.
2. American Society for Testing Materials, ASTM F 1939-99 a Standard Test Method for Radiant Protective Performance of Flame Resistant Clothing Materials, West Conshohocken, PA, 1999.
3. National Fire Protection Association, NFPA 1971, Standard on Protective Ensemble for Structural Fire Fighting, Quincy, MA, 2007.
4. A.M. Stoll, and M.A. Chianta, Method and Rating System for Evaluation of Thermal Protection, Aerospace Medicine, vol. 40, pp. 1232-1238, 1969.

5. American Society for Testing Materials, ASTM F 1930-00 Standard Test Method for Evaluation of Flame Resistant Clothing for Protection Against Flash Fire Simulations Using an Instrumented Thermal Manikin, West Conshohocken, PA, 2000

6. F.C. Henriques, Jr., A.R. Moritz, Studies of thermal injuries I: The conduction of heat to and through skin and the temperatures attained therein. A theoretical and experimental investigation, American J. Pathology, vol. 23, pp. 531–549, 1947.

7. D.A. Torvi, J.D. Dale, and B. Faulkner, Influence of Air Gaps on Bench Top Test Results of Flame Resistant Fabrics, J. Fire Protection Engineering, vol. 10, pp. 1-12, 1999.

8. D. A. Torvi, Heat Transfer in Thin Fibrous Materials under High Heat Flux Conditions, Ph.D. Thesis, University of Alberta, Edmonton, Alberta, 1997.

9. G. Song, R.L. Barker, H. Hamouda, A.V. Kuznetsov, P. Chitrphiromsri, and R.V. Grimes, Modeling the Thermal Protective Performance of Heat Resistant Garments in Flash Fire Exposures, Textile Research J., vol. 74, pp. 1033-1040, 2004.

10. P. Chitrphiromsri, and A.V. Kuznetsov, Modeling Heat and Moisture Transport in Firefighter Protective Clothing during Flash Fire Exposure, Heat Mass Transfer, vol. 41, pp. 206-215, 2005.

11. P. Chitrphiromsri, Modeling of Thermal Performance of Firefighter Protective Clothing during the Intense Heat Exposure, Ph.D. Thesis, North Carolina State University, Raleigh, North Carolina, 2004.

12. A. Ghazy, D.J. Bergstrom, Numerical Simulation of Transient Heat Transfer in a Protective Clothing System during a Flash Fire Exposure, Numerical Heat Transfer A, vol. 58(9), pp. 702-724, 2010.

13. M.F. Modest, Radiative Heat Transfer, 2nd edition, Academic Press, New York, 2003.

14. F.P. Incropera, and D.P. DeWitt, Fundamentals of Heat and Mass Transfer, 5th edition, John Wiley & Sons, Inc., New York, 2002.

15. D.A. Torvi, and J.D. Dale, Heat Transfer in Thin Fibrous Materials under High Heat Flux, Fire Technology, vol. 35, pp. 210-231, 1999.

16. D.A. Torvi, and T.G. Threlfall, Heat Transfer Model of Flame Resistant Fabrics During Cooling After Exposure to Fire, Fire Technology, vol. 42, pp. 27-48, 2006.

17. J.P. Holman, Heat Transfer, 8th edition, McGraw-Hill Co., 1997.

18. H.H. Pennes, Analysis of tissue and arterial blood temperatures in resting human forearm, J. Applied Physiology, vol. 1, pp. 93–122, 1948.

19. J.A. Weaver, and A.M. Stoll, Mathematical Model of Skin Exposed to Thermal Radiation, Aerospace Medicine, vol. 40, pp. 24-30, 1969.

20. A.N. Takata, J. Rouse, and T. Stanley, Thermal Analysis Program, I.I.T. Research Institute Report IITRI-J6286, Chicago, 1973.

21. J. C. Chai and S. V. Patankar, Finite-Volume Method for Radiation Heat Transfer, Advances in Numerical Heat Transfer, editors; W. J. Minkowycz, and E. M. Sparrow, vol. 2, Ch. 4, Taylor & Francis, pp. 109-141, 2000.

22. S.V. Patankar, Numerical Heat Transfer and Fluid Flow, Taylor & Francis, Washington, DC, 1980.

23. W.E. Mell, J.R. Lawson, A Heat Transfer Model for Firefighters' Protective Clothing, J. Fire Technology, vol. 36, pp. 39-68, 2000.

24. R.L. Vettori, W.H. Twilley, D.W. Stroup, Measurement Techniques for Low Heat Flux Exposures to Fire Fighters Protective Clothing, NISTIR 6750, National Institute of Standards and Technology, Gaithersburg, MD, 2001.

Table 1. Kevlar®/PBI and hot gases parameters

	Property	Value
L_{fab}	Fabric thickness	0.6 mm
W_{fab}	Fabric Width	0.05 m (2 in.)
ρ_{fab}	Fabric density	323 kg/m^3
γ_{fab}	Fabric extinction factor	0.01
ε_{fab}	Fabric emissivity	0.9
τ_{fab}	Fabric transmissivity	0.01
T_g	Hot gases temperature	2000 K
ε_g	Hot gases emissivity	0.02
h_{fl}	Flame convective heat transfer coefficient	40 W/m^{2}K

Table 2. Human skin thermophysical properties

Property	Epidermis	Dermis	Subcutaneous	Blood
Thickness (m)	8×10^{-5}	2×10^{-3}	1×10^{-2}	-
Density (Kg/m^3)	1200	1200	1000	1060
Specific Heat (J/Kg^oC)	3598	3222	2760	3770
Thermal Conductivity (W/m^oC)	0.255	0.523	0.167	-
Blood Perfusion Rate $(m^3/s)/m^3$ tissue	-	-	-	1.25×10^{-3}

Table 3. Influence of fabric backside emissivity on skin burn prediction

Fabric backside emissivity	Time to receive skin burn (s)					
	Present model			Simple model		
	1st degree	2nd degree	3rd degree	1st degree	2nd degree	3rd degree
0.1	14.7	-	-	-	-	-
0.15	10.7	12.1	-	-	-	-
0.2	9.7	10.3	-	11.6	15	-
0.3	8.3	8.8	-	9.2	9.7	-
0.4	7.4	7.9	-	8.5	9	-
0.5	6.8	7.2	-	8	8.4	-
0.6	6.3	6.7	-	7.2	7.6	-
0.7	6	6.3	-	6.6	7	-
0.8	5.7	6	-	6.2	6.5	-
0.85	5.6	5.9	68.8	5.7	6	-
0.9	5.5	5.7	42.3	5.6	5.8	79.4

Figure Captions

Figure 1. The protective clothing system schematic diagram.

Figure 2. Comparison between measured and predicted skin simulant surface temperature.

Figure 3. The influence of the air gap absorption coefficient on the energy transfer within the air gap (a) the emitted radiation from the fabric (b) radiation heat flux within the air gap (c) the conduction heat transfer at air-fabric interface (d) conduction heat flux within the air gap.

Figure 4. Influence of the air gap absorption coefficient on skin burn predictions.

Figure 5. The influence of the air gap width on the energy transfer within the air gap (a) the emitted radiation from the fabric (b) the conduction heat transfer at air-fabric interface (c) radiation heat flux within the air gap (d) conduction heat flux within the air gap.

Figure 6. Influence of the air gap width on the temperature at three locations in the air gap (a) fabric backside (b) temperature at the air gap centre (c) epidermis surface.

Figure 7. Influence of the air gap width on skin burn predictions.

Figure 8. The influence of the fabric backside emissivity on the energy transfer within the air gap (a) the emitted radiation from the fabric, (b) the conduction heat transfer at air-fabric interface, (c) radiation heat flux within the air gap, (d) conduction heat flux within the air gap.

Figure 9. Influence of the fabric backside emissivity on the temperature at three locations in the air gap (a) fabric backside (b) air gap centre temperature (c) epidermis surface.

Figure 10. Influence of the fabric thickness on the temperature at three locations in the air gap (a) fabric backside (b) temperature at the air gap centre (c) epidermis surface.

Figure 11. The influence of the fabric thickness on the energy transfer within the air gap (a) the emitted radiation from the fabric (b) the conduction heat transfer at air-fabric interface (c) radiation heat flux within the air gap (d) conduction heat flux within the air gap.

Figure 12. Influence of the fabric thickness on skin burn predictions.

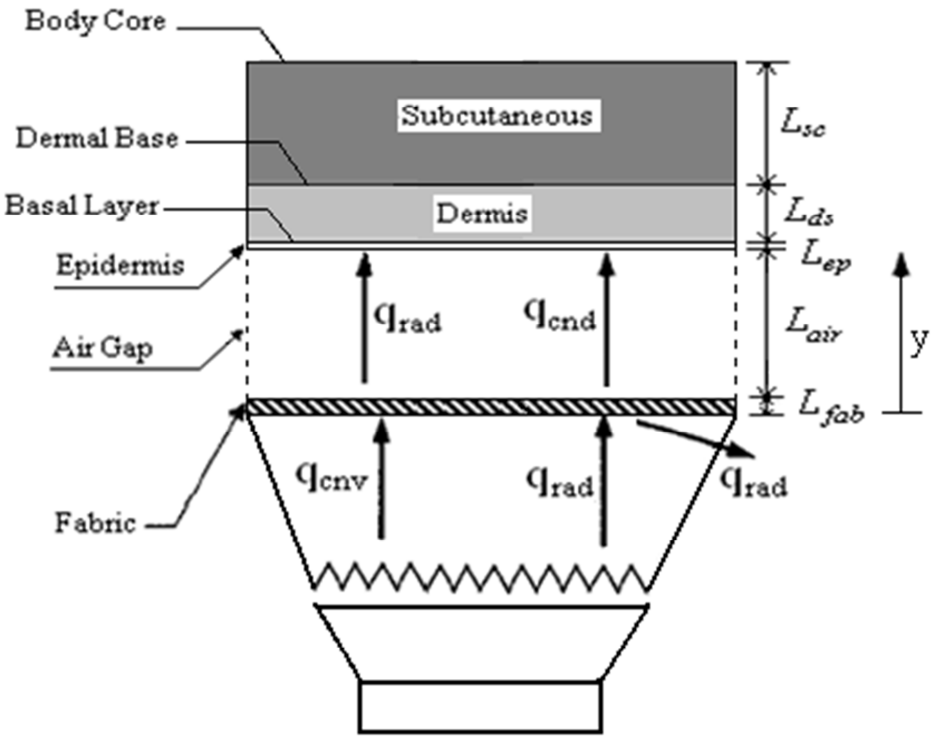

Figure 1. The protective clothing system schematic diagram.

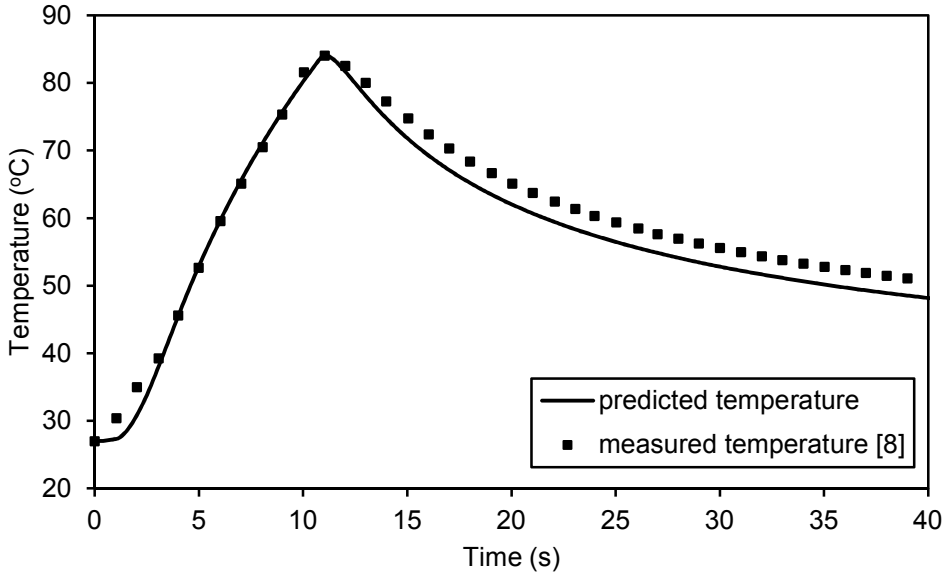

Figure 2. Comparison between measured and predicted skin simulant surface temperature.

(a)

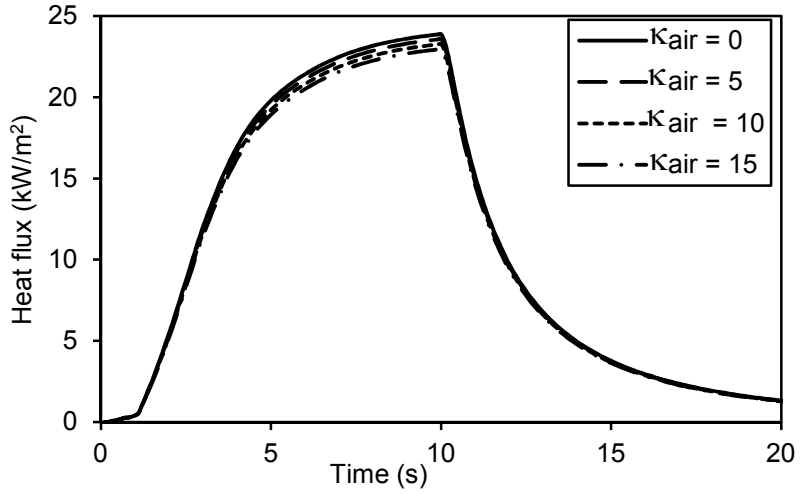
Heat flux (kW/m²)
Time (s)
κair = 0
κair = 5
κair = 10
κair = 15

(b)

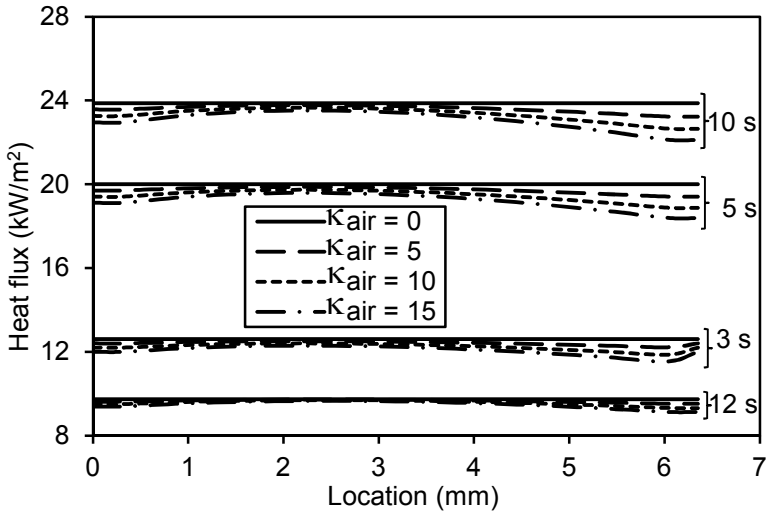
Heat flux (kW/m²)
Location (mm)
10 s
5 s
3 s
12 s
κair = 0
κair = 5
κair = 10
κair = 15

(c)

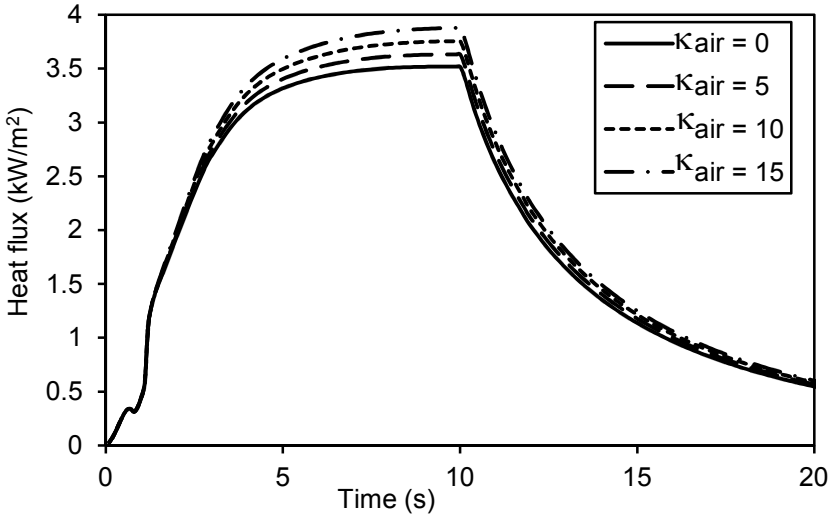
Heat flux (kW/m²)
Time (s)
κair = 0
κair = 5
κair = 10
κair = 15

(d)

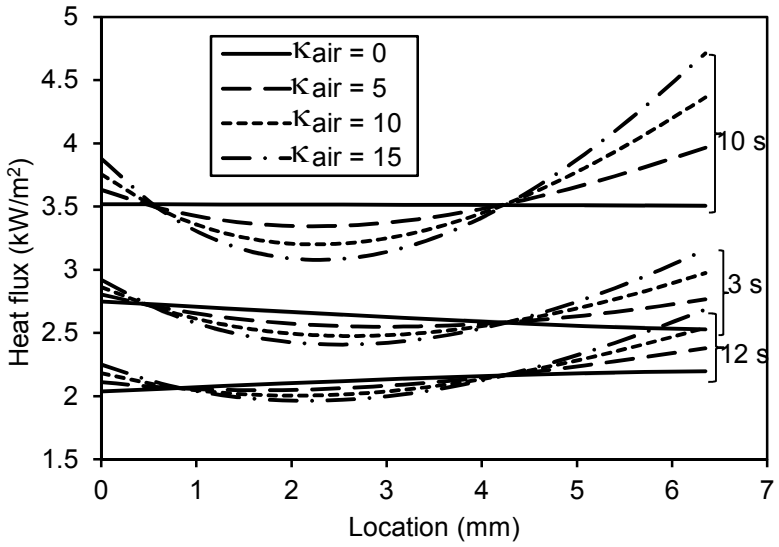

Figure 3. The influence of the air gap absorption coefficient on the energy transfer within the air gap: (a) the emitted radiation from the fabric, (b) radiation heat flux within the air gap, (c) the conduction heat transfer at air-fabric interface, (d) conduction heat flux within the air gap.

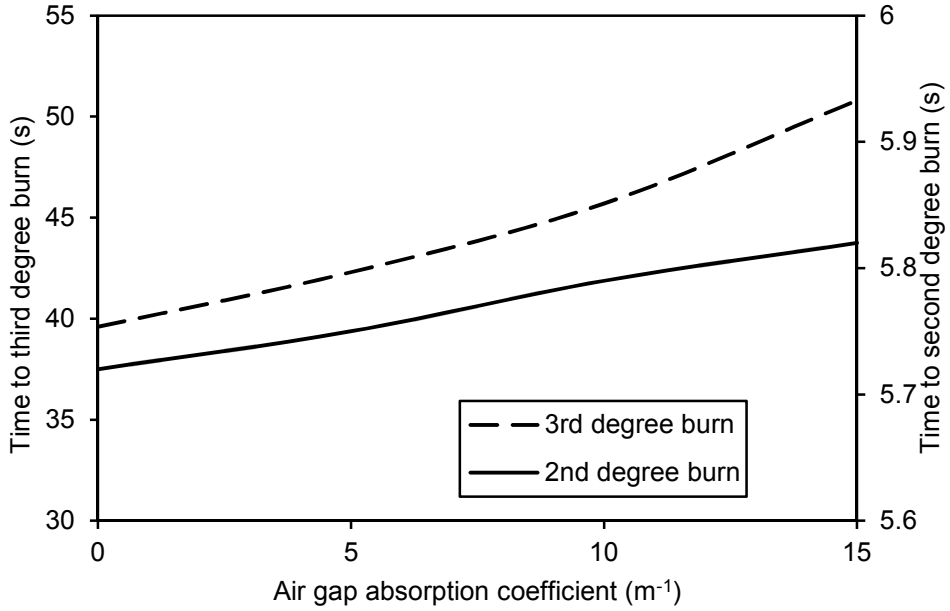

Figure 4. Influence of the air gap absorption coefficient on skin burn predictions.

(a)

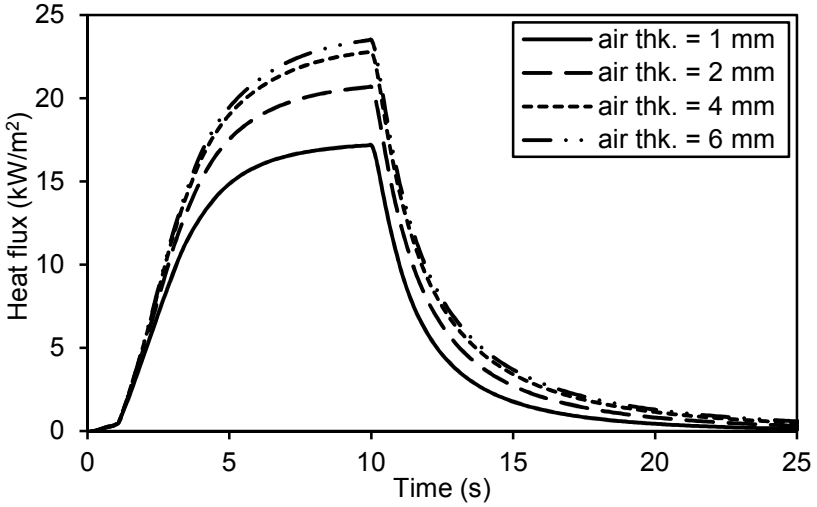
air thk. = 1 mm
air thk. = 2 mm
air thk. = 4 mm
air thk. = 6 mm
Heat flux (kW/m²)
Time (s)
0
5
10
15
20
25

(b)

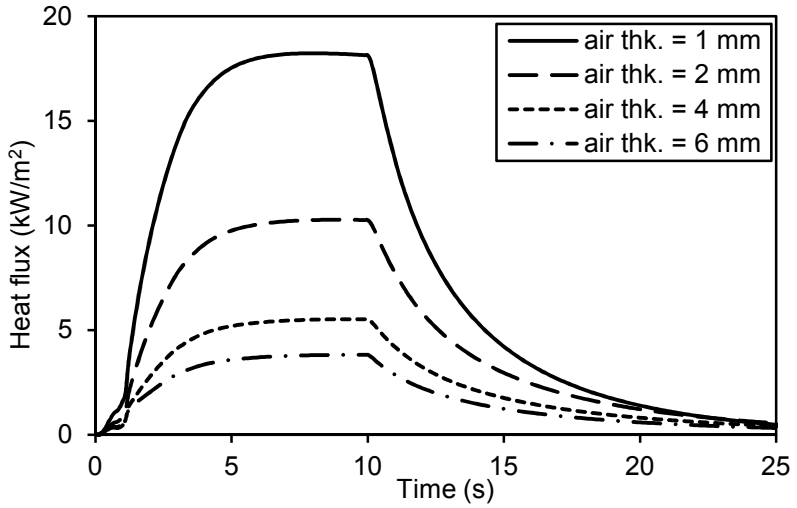
air thk. = 1 mm
air thk. = 2 mm
air thk. = 4 mm
air thk. = 6 mm
Heat flux (kW/m²)
Time (s)
0
5
10
15
20
25

(c)

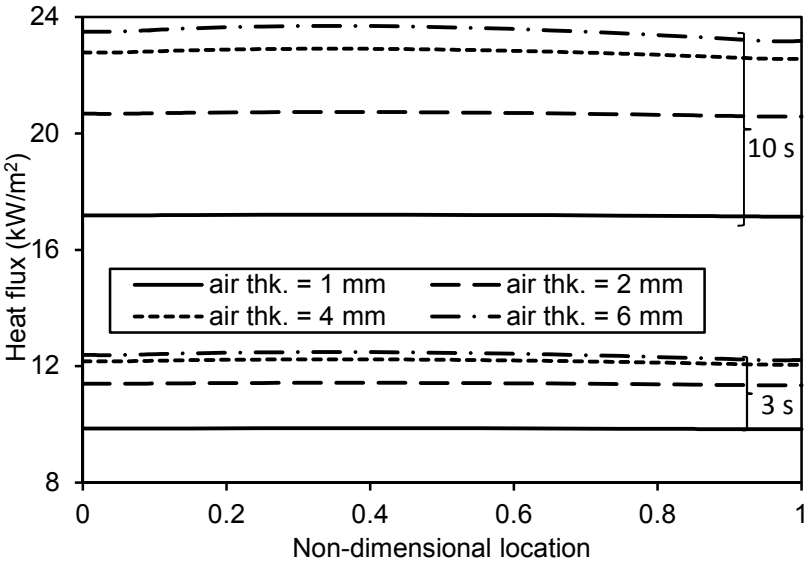
air thk. = 1 mm
air thk. = 2 mm
air thk. = 4 mm
air thk. = 6 mm
10 s
3 s
Heat flux (kW/m²)
Non-dimensional location
8
12
16
20
24
0
0.2
0.4
0.6
0.8
1

(d)

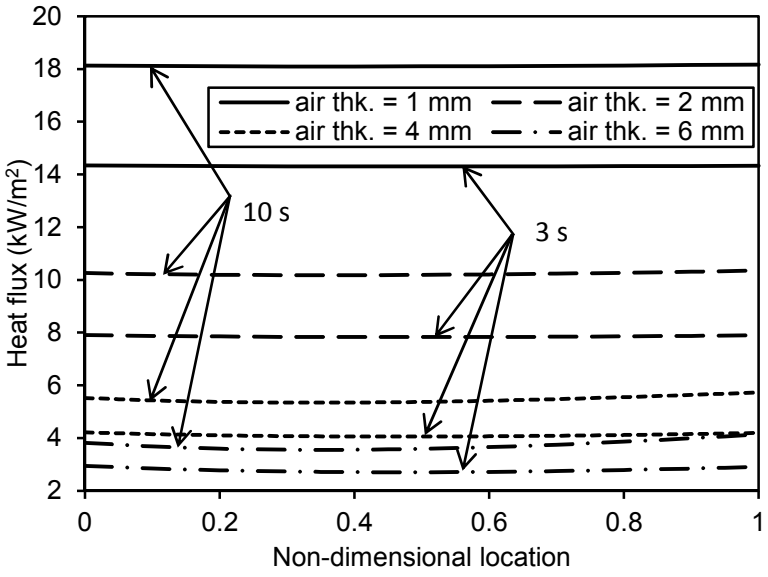

Figure 5. The influence of the air gap width on the energy transfer within the air gap: (a) the emitted radiation from the fabric, (b) the conduction heat transfer at air-fabric interface, (c) radiation heat flux within the air gap, (d) conduction heat flux within the air gap.

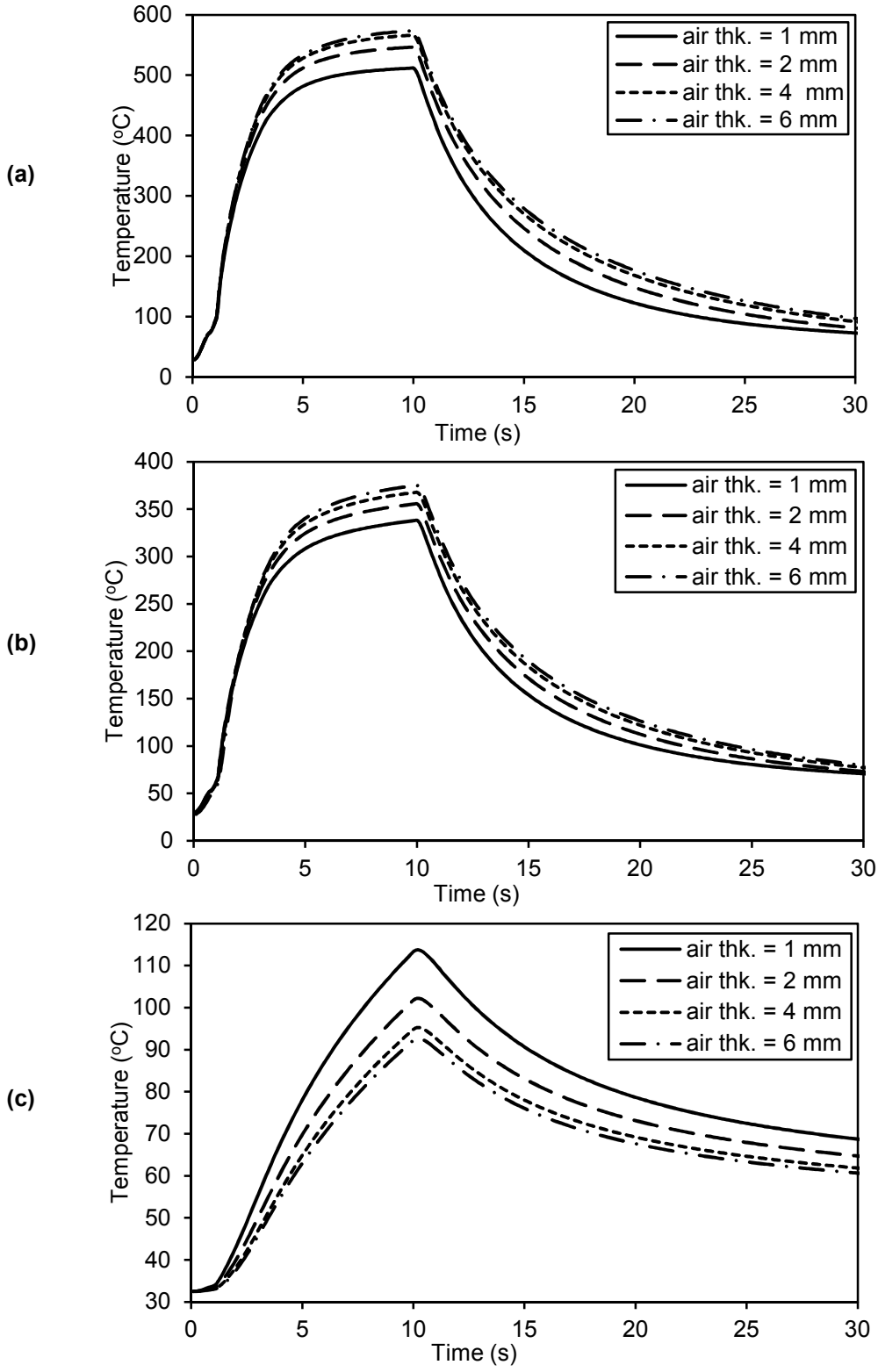

Figure 6. Influence of the air gap width on the temperature at three locations in the air gap: (a) fabric backside, (b) temperature at the air gap centre, (c) epidermis surface.

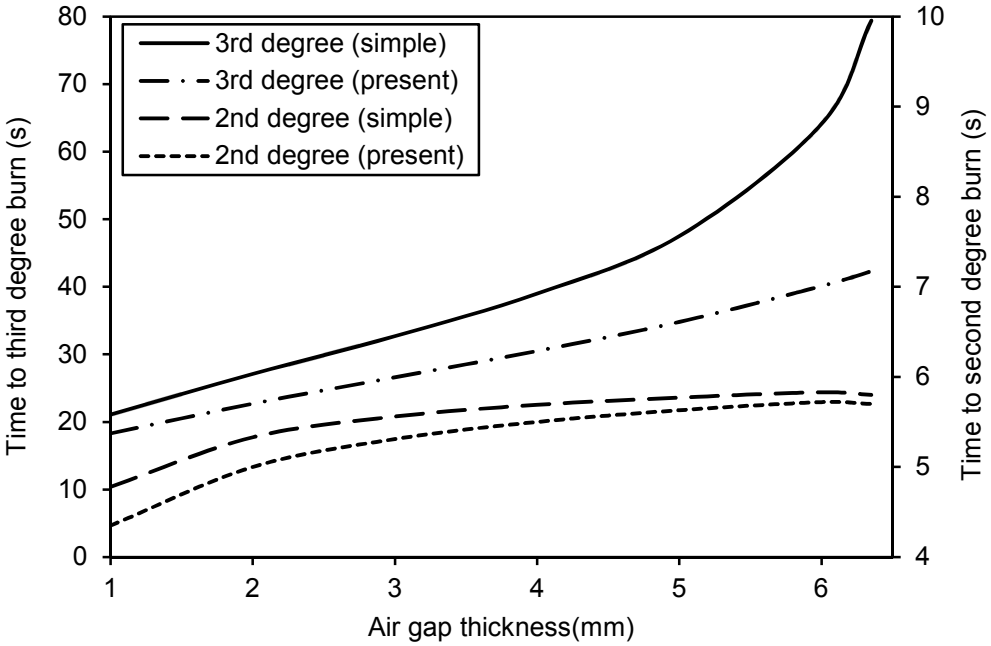

Figure 7. Influence of the air gap width on skin burn predictions.

(a)

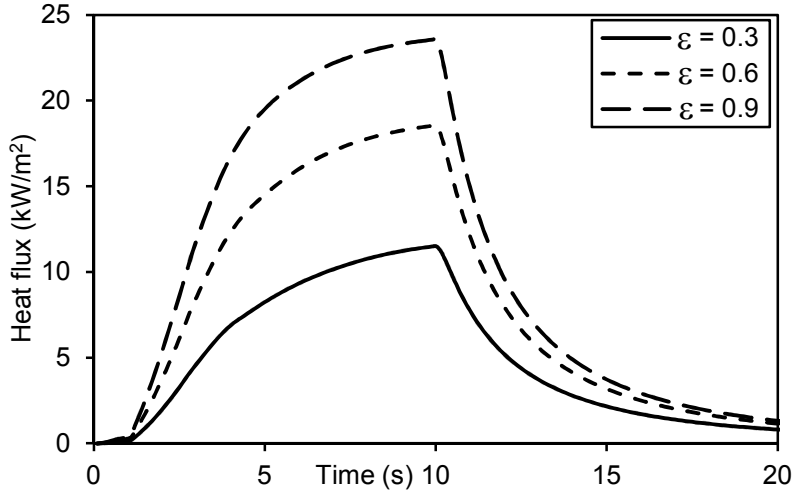
ε = 0.3
ε = 0.6
ε = 0.9
Heat flux (kW/m²)
Time (s)
0
5
10
15
20
25

(b)

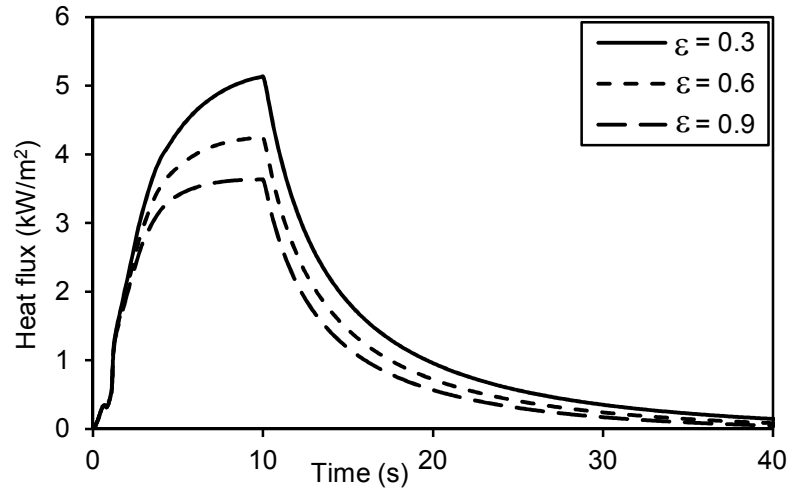
ε = 0.3
ε = 0.6
ε = 0.9
Heat flux (kW/m²)
Time (s)
0
10
20
30
40
1
2
3
4
5
6

(c)

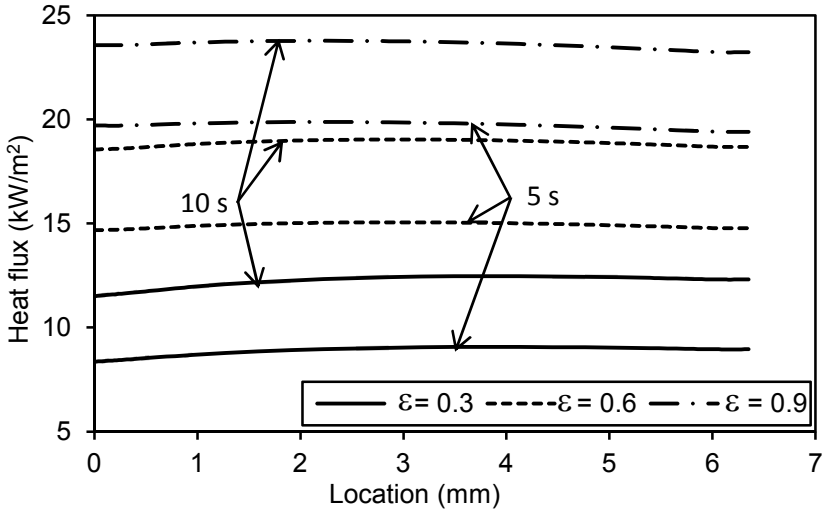
10 s
5 s
ε= 0.3
ε = 0.6
ε = 0.9
Heat flux (kW/m²)
Location (mm)
0
1
2
3
4
5
6
7
5
10
15
20
25

(d)

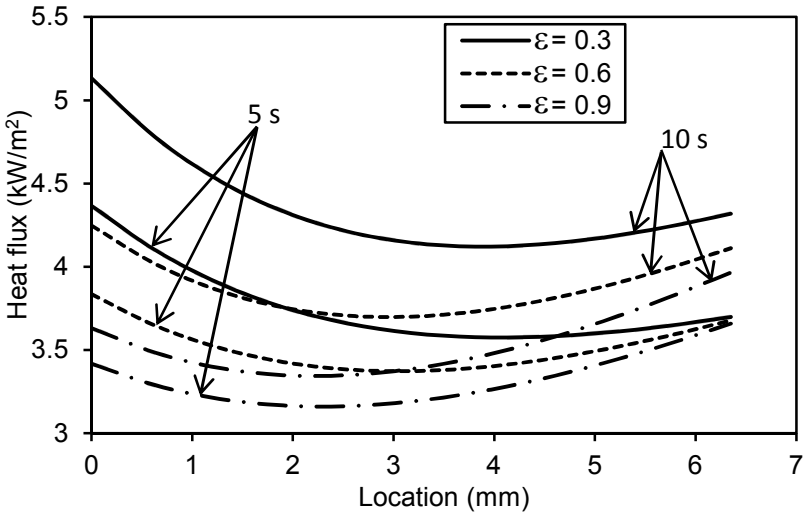

Figure 8. The influence of the fabric backside emissivity on the energy transfer within the air gap: (a) the emitted radiation from the fabric, (b) the conduction heat transfer at air-fabric interface, (c) radiation heat flux within the air gap, (d) conduction heat flux within the air gap.

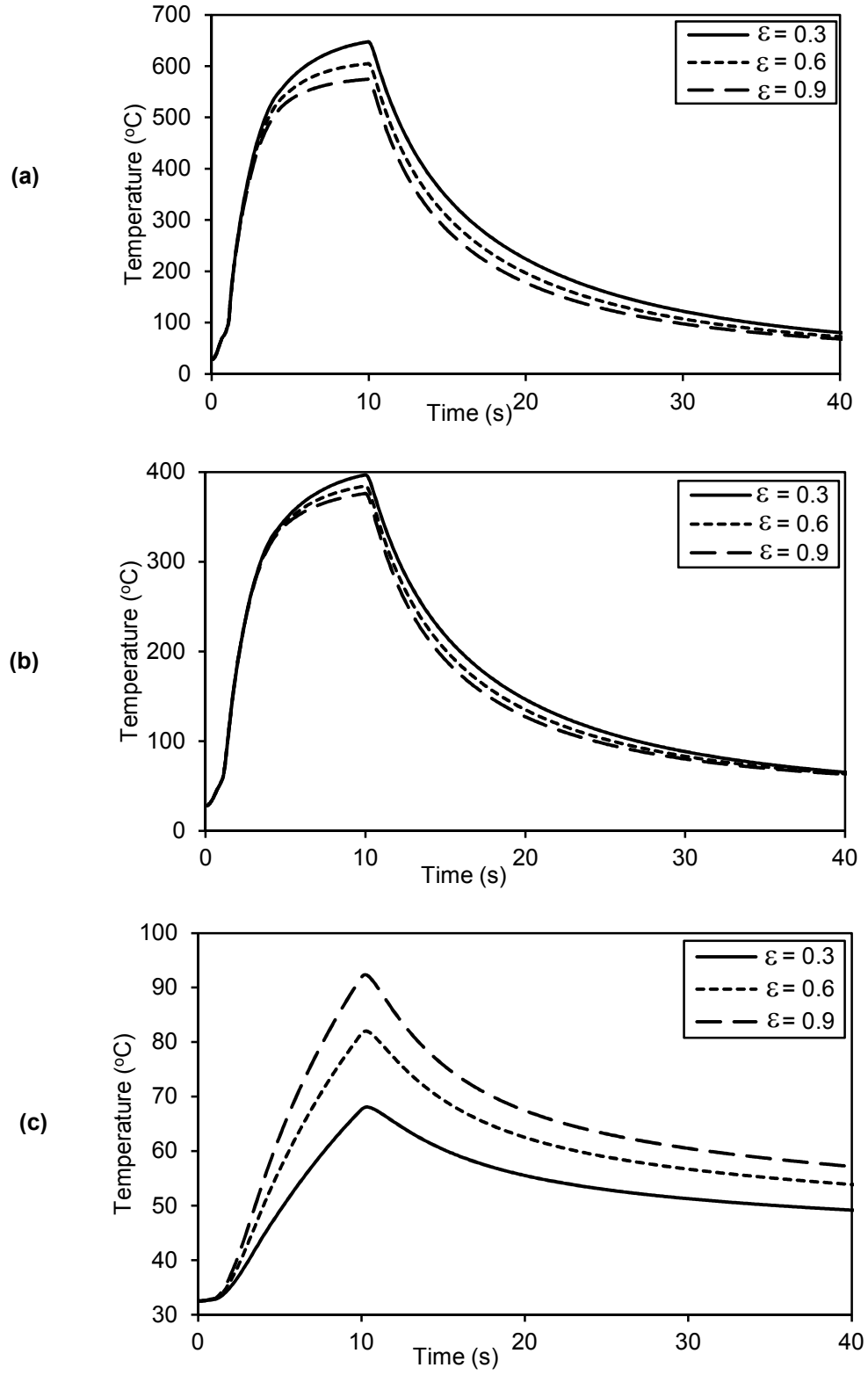

Figure 9. Influence of the fabric backside emissivity on the temperature at three locations in the air gap: (a) fabric backside, (b) air gap centre temperature, (c) epidermis surface.

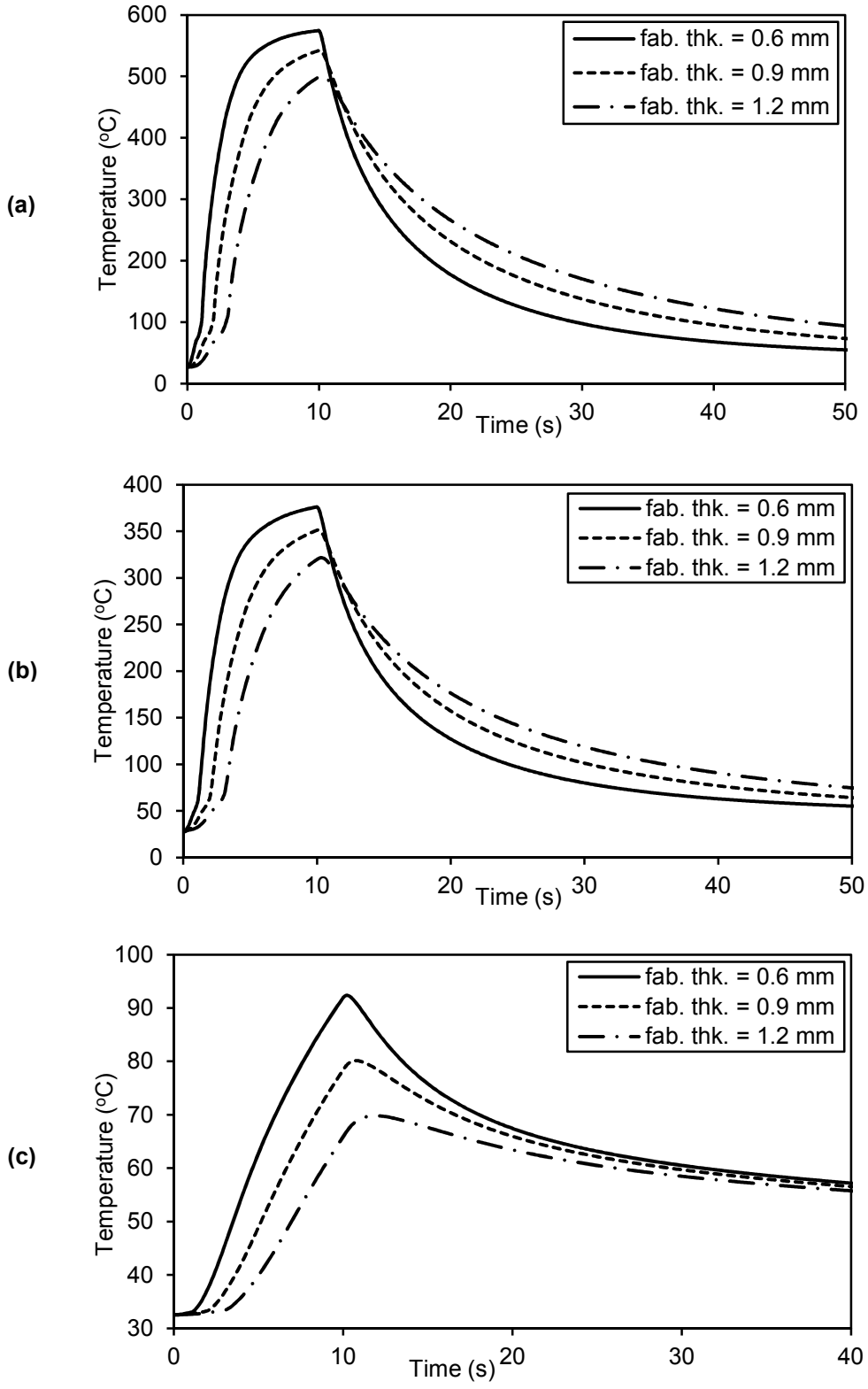

Figure 10. Influence of the fabric thickness on the temperature at three locations in the air gap: (a) fabric backside, (b) temperature at the air gap centre, (c) epidermis surface.

(a)

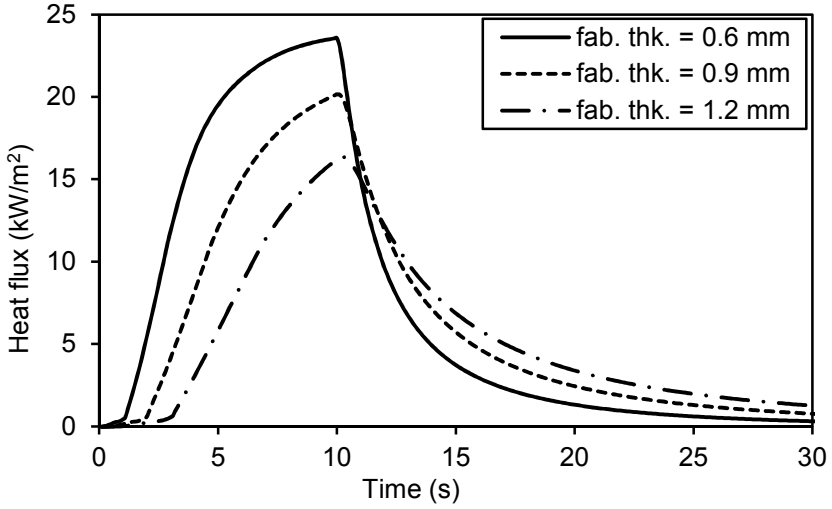
fab. thk. = 0.6 mm
fab. thk. = 0.9 mm
fab. thk. = 1.2 mm
Heat flux (kW/m2)
Time (s)
0
5
10
15
20
25
30

(b)

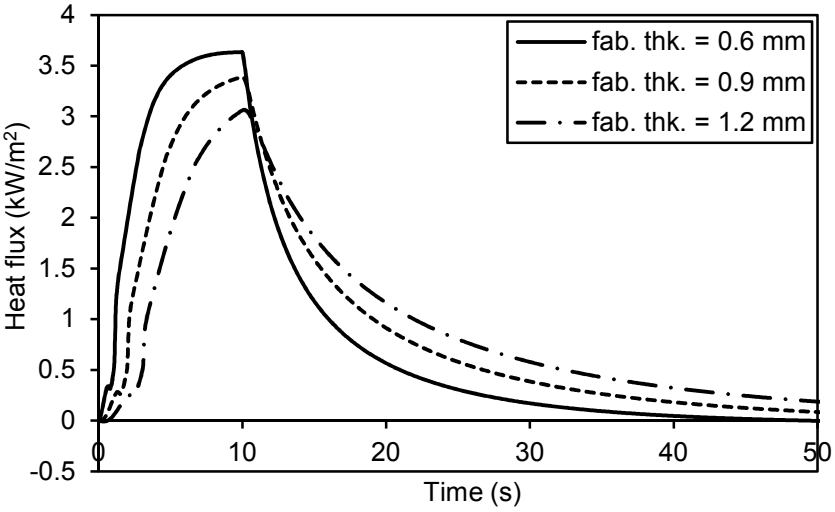
fab. thk. = 0.6 mm
fab. thk. = 0.9 mm
fab. thk. = 1.2 mm
Heat flux (kW/m2)
Time (s)
-0.5
0
0.5
1
1.5
2
2.5
3
3.5
4
10
20
30
40
50

(c)

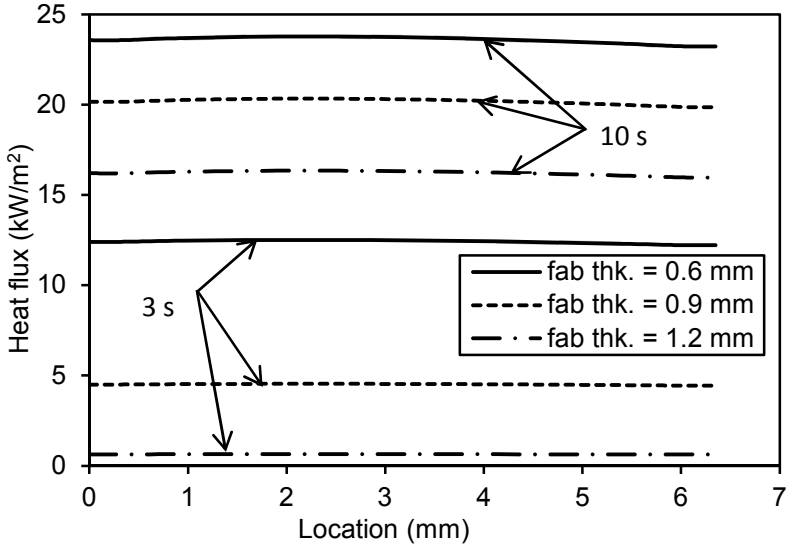
10 s
3 s
fab thk. = 0.6 mm
fab thk. = 0.9 mm
fab thk. = 1.2 mm
Heat flux (kW/m2)
Location (mm)
0
5
10
15
20
25
1
2
3
4
6
7

(d)

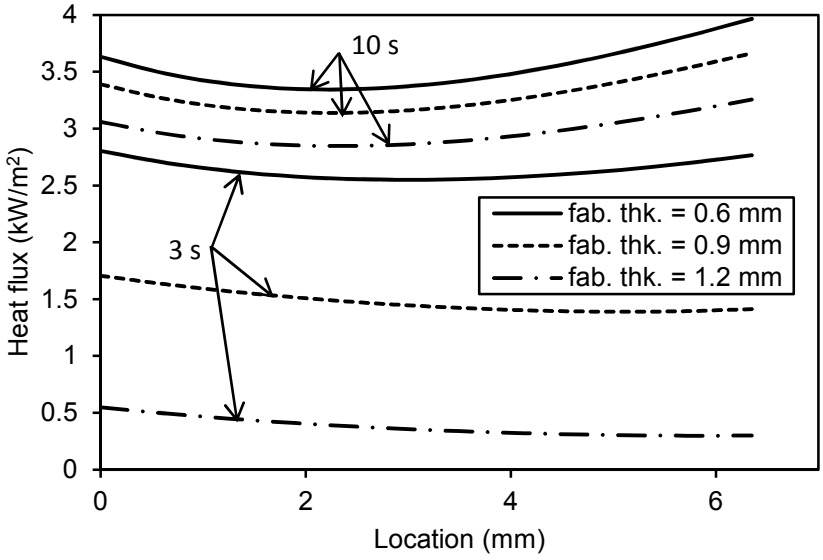

Figure 11. The influence of the fabric thickness on the energy transfer within the air gap: (a) the emitted radiation from the fabric, (b) the conduction heat transfer at air-fabric interface, (c) radiation heat flux within the air gap, (d) conduction heat flux within the air gap.

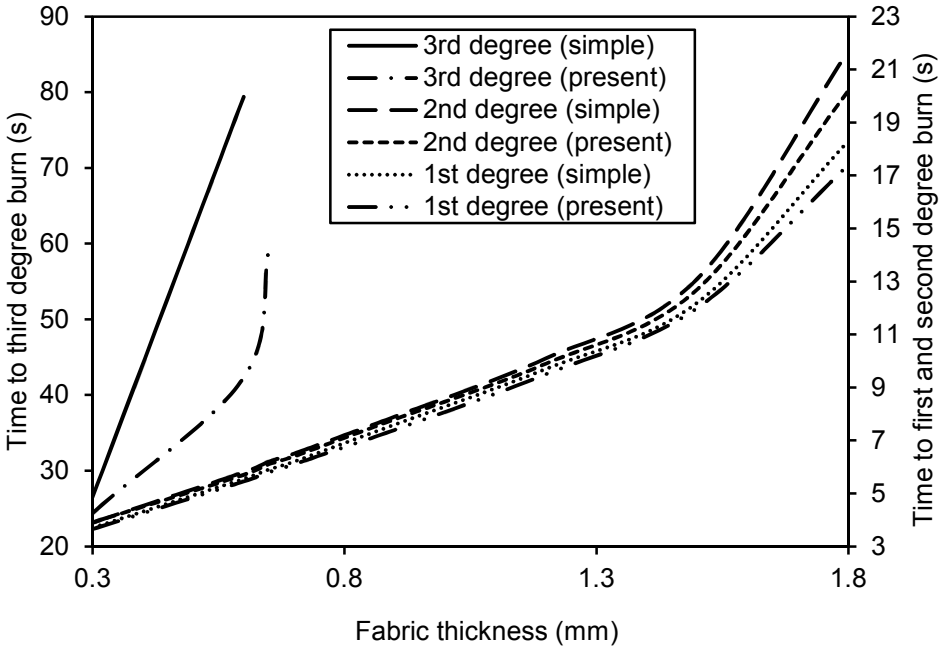

Figure 12. Influence of the fabric thickness on skin burn predictions.

CHAPTER 4

NUMERICAL SIMULATION OF THE INFLUENCE OF FABRIC'S MOTION ON PROTECTIVE CLOTHING PERFORMANCE DURING FIRE EXPOSURE

Submitted as

A. Ghazy and D.J. Bergstrom, Numerical Simulation of the Influence of Fabric's Motion on Protective Clothing Performance during Fire Exposure, Int. J. Heat Mass Transfer, 2011.

Contribution of this Chapter to the Thesis

The research work presented in this chapter aims at achieving the third objective of the thesis. More specifically, the chapter addresses the influence of the periodic variation in the air gap width and content due to the motion of the person wearing the clothing on the heat transfer in the protective clothing system. The influence of the variation in the frequency and amplitude of the fabric periodic movement on the performance of the clothing was also investigated.

Numerical Simulation of the Influence of Fabric's Motion on Protective Clothing Performance during Fire Exposure

Ahmed Ghazy and Donald J. Bergstrom

Department of Mechanical Engineering, University of Saskatchewan, Saskatoon, Saskatchewan, Canada

Address correspondence to Donald J. Bergstrom, Department of Mechanical Engineering, University of Saskatchewan, 57 Campus Dr., Saskatoon, SK S7N 5A9, Canada. E-mail: Don.Bergstrom@usask.ca

ABSTRACT

The motion of a person wearing protective clothing induces the clothing to move periodically towards the skin causing a cyclic variation in the air gap between the fabric and the skin. At the same time, the clothing movement causes cooling air to periodically flow into the air gap between the fabric and the skin. This paper uses a finite volume model to investigate these two effects and the resultant effect of the protective clothing movement on its performance during flash fire exposure. Special attention is drawn to the air gap model since it responds directly to the clothing movement. A parametric study is carried out to investigate the influence of a wider range of clothing movement. Specifically, the effect of the variation in the periodic movement frequency and amplitude on the clothing performance was investigated. The results show that increasing the movement frequency improves the clothing protective performance, while increasing the movement amplitude worsens the clothing performance.

Keywords: conduction-radiation, finite volume method, protective clothing.

NOMENCLATURE

A	surface area, m^2
a, b	finite volume discrete equation coefficient, source term
C	heat capacity, J/kg K
c_P	specific heat at constant pressure, J/kg K
c_v	specific heat at constant volume, J/kg K
D_c^l	directional cosine integrated over $\Delta\Omega^l$
$\hat{e}$	unit vector in coordinate direction
f	frequency
G	incident radiation, W/m^2
h	convective heat transfer coefficient, W/m^2K
I	intensity, W/m^2
k	thermal conductivity, W/mK
L	thickness, m
P	pre-exponential factor, 1/s
q''	heat flux, W/m^2
$\vec{r}$	position vector, m
R	ideal gas constant, J/mol K
rps	revolutions per second
$\hat{s}$	unit vector in a given direction
S	source function
s	geometric distance, m
T	temperature, K

t	time, s
W	fabric width, m
y	linear vertical coordinate, m

Greek Symbols

Ω	solid angle, sr
θ	polar angle, rad
φ	quantitative measure of skin damage
ϕ	azimuthal angle, rad
ΔE	activation energy of skin, J/kmol
ΔV	volume of control volume, m^3
$\Delta\Omega^l$	control angle
α	air gap absorptivity
ε	emissivity
γ	extinction coefficient of the fabric, 1/m
κ	air gap absorption coefficient, 1/m
ρ	density, kg/m^3 or surface reflectivity
σ	Stefan-Boltzmann constant, 5.67×10^{-8} W/m^2K^4
τ	transmissivity
ω	blood perfusion rate, $(m^3/s)/m^3$ of human tissue

Subscripts

air	air
amb	ambient conditions

b	human blood / black body
cnv	convection heat transfer
cr	human body core
ep, ds, sc	epidermis , dermis, subcutaneous human skin layers
exp	exposure
fab	fabric
fbr	fabric fiber
fl	flame
g	hot gases
mix	mixture
n, s	north, south control volume faces
P	control volume central node
R , rad	radiation heat transfer
x, y, z	coordinate directions

Superscript

A	apparent
l	index for direction

1. INTRODUCTION

Protective clothing is widely used in many industries and applications to provide protection against fire exposure. Exposure to fire can result in skin burn injuries that range from first-degree to third-degree burn injury depending on the exposure intensity and duration. The type of protective clothing varies according to the type of fire hazard encountered, which differs for firefighting, petroleum and petrochemical industries, or sports car driving. Flash fire is one of

the possible fire hazards for workers in these industries and applications. Exposure to flash fire is usually of short duration (a few seconds) until the worker runs away from the fire location.

The typical protective clothing system consists of a fire resistant fabric, the human skin, and an air gap between the fabric and skin. Evaluating the thermal protective performance (TPP) of the clothing is typically done by estimating the total energy transfer through the fabric that causes burn injury to the human skin on the other side of the fabric. For example, Bench top tests [1-4] are used in evaluating the TPP of fabric specimens using the criterion developed by Stoll and Chianta [5]. In contrast, manikin tests [6] can be used to evaluate the TPP of the whole garment at different locations of the body using Henriques' burn integral [7].

Modeling the performance of protective clothing has been extensively reported in the literature and various innovations have been added to this growing body of research work. Torvi et al. [8, 9] modeled heat transfer in a single layer of fire-resistant fabric exposed to a heat flux of about 80 kW/m^2 during a contact flame bench top test. Mell et al. [10] modeled heat transfer in clothing consisting of three layers with 1 mm air gaps between layers during a radiant exposure of 2.5 kW/m^2. Song et al. [11] combined heat transfer in protective fabric and human skin to simulate heat transfer in a single layer protective garment worn by an instrumented manikin (PyroMan®) that was exposed to a laboratory flash fire. By adopting Gibson's model [12] for multiphase transport in porous media, Chitrphiromsri et al. [13, 14] simulated the coupled heat and moisture transfer in multiple layer firefighters' clothing during flash fire exposure. Chitrphiromsri et al. [15] also investigated numerically the feasibility of developing a firefighters' garment that includes a water injection system. Song et al. [16] modeled heat and moisture transfer in multiple layer firefighters' clothing during the contact flame TPP test. Zhu et al. [17] considered the fabric thermal degradation at high temperature in a one-dimensional

model to simulate heat transfer in heat-resistant fabrics during radiant exposure. In almost all the models in the literature used to evaluate the performance of protective clothing, Pennes's model [18] was used to model heat transfer in the human skin. However, Zhu et al. [19] applied a more realistic model for heat transfer in the human skin, which allows for a finite speed of heat transfer in the skin, to evaluate the thermal performance of flame-resistant fabrics during radiant exposure.

Many researchers have identified the important role that the air gap between the fabric and the skin plays in the clothing protective performance. Torvi et al. [8, 20] investigated the influence of the air gap width on the protective performance of a single layer fire-resistant fabric during a contact flame bench top test. Song et al. [11] used a three-dimensional body scanning technique to measure the air gap between the garment and the manikin body at different locations on the body (e.g. leg, arm, shoulder, etc.). Sawcyn and Torvi [21] considered a quasi-multi-dimensional approach in order to improve the heat transfer modeling of the air gap in bench top tests of protective fabrics. However, most studies reported in the literature have used a relatively simple and approximate air gap model. Given this context, Ghazy and Bergstrom [22] introduced a more sophisticated model for the heat transfer through the air gap between the protective clothing and human skin during flash fire exposure.

One complexity not yet considered in modeling protective clothing performance is the motion of the person wearing the clothing. The person's motion during the act of extinguishing the fire or escaping from the fire location will induce the clothing to move in a manner, which can be identified as periodically inwards and outwards with respect to the skin. This periodic movement of the clothing can be considered to cause two contradictory actions. The first is to change the air gap width in a periodic fashion. Decreasing the air gap width will concentrate the

exposure on the skin and thus decrease the clothing protective performance. In contrast, increasing the air gap width will reduce the energy transfer through the air gap and hence improve the clothing performance. The second action is the periodic cooling of the air gap due to a convective inflow. The fabric movement towards the skin displaces a portion of the hot gases in the gap to another location next to the skin or to the ambient through the fabric pores. The fabric movement away from the skin draws fresh air into the gap. This fresh air mixes with the hot air inside the gap and reduces the overall temperature of the air mixture within the gap. This periodic cooling of the air gap would be expected to improve the clothing protective performance.

This paper investigates the influence of the motion of the person wearing the clothing on the transient heat transfer through the clothing and its protective performance. The model assumes a periodic variation in the air gap width due to the fabric movement. The variation in the air gap properties due to the periodic cooling is also considered. A parametric study was carried out to investigate different motion scenarios.

2. PROBLEM FORMULATION

The typical protective clothing system shown in Figure 1 consists of a single layer of Kevlar®/PBI fire-resistant fabric, human skin, and an air gap between the fabric and the skin. The fabric is exposed to flame contact with a nominal heat flux of about 83 kW/m^2. In order to simulate the wearer's motion, the fabric is assumed to move periodically towards and then away from the skin, causing a periodic variation in the air gap width as well as a periodic cooling of the air within the gap.

The analysis of the protective clothing system can be divided into three elements: the fabric, air gap, and human skin. The energy equations for the three elements are solved

simultaneously. The continuity of temperature and heat flux represents the inner boundary conditions between these elements.

2.1. Heat Transfer in the Fabric

The energy equation of the fabric during the exposure and cool down periods is expressed [9, 23] as

$$\rho C^{A}(T)\frac{\partial T}{\partial t} = \frac{\partial}{\partial y}\left(k(T)\frac{\partial T}{\partial y}\right) - \frac{\partial}{\partial y}q^{"}_{rad}(y) \qquad 0 < t \leq t_{exp} \qquad (1a)$$

$$\rho c_{P}(T)\frac{\partial T}{\partial t} = \frac{\partial}{\partial y}\left(k(T)\frac{\partial T}{\partial y}\right) \qquad t > t_{exp} \qquad (1b)$$

where ρ, c_P, and k are the fabric density, specific heat, and thermal conductivity, respectively. t_{exp} is the exposure duration. C^A is the fabric apparent heat capacity [8, 9] that accounts for the evaporation of the moisture enclosed in the fabric's pores and the energy consumed by thromochemical reactions in the fabric such as fabric pyrolysis. In Eq. (1a), $q^{"}_{rad}(y)$is the transmitted portion of the radiant heat flux from the flame to the fabric. Beer's law [24] was employed [8, 9] to account for the absorption of the incident thermal radiation as it penetrates the pores of the fabric, i.e.

$$q^{"}_{rad}(y) = q^{"}_{rad\,fl}\,exp(-\gamma y) \qquad (2)$$

where the extinction coefficient of the fabric γ is given [8, 9] by

$$\gamma = \frac{-ln(\tau)}{L_{fab}} \qquad (3)$$

where τ is the fabric transmissivity and L_{fab} is the fabric thickness.

The radiant portion of exposure, $q^{"}_{rad\,fl}$, is written as

$$q^{"}_{rad\,fl} = \sigma\varepsilon_{g}T_{g}^{4} \qquad (4)$$

where σ is the Stefan-Boltzmann constant, ε_g is the hot gas emissivity, and T_g is the hot gas temperature (K). The Kevlar®/PBI thermal conductivity was determined from the fiber to air fraction in the fabric [8, 9] as follows.

$$k_{fab}(T) = 0.8\, k_{air}(T) + 0.2\, k_{fbr}(T) \tag{5}$$

where k_{fbr} and k_{air} are the fiber thermal conductivity and the thermal conductivity of the air contained in the fabric's pores, respectively.

The boundary conditions for the fabric energy equation are as follows.

$$-k(T)\left.\frac{\partial T}{\partial y}\right|_{y=0} = h_{fl}\left(T_g - T_{fab(y=0)}\right) - \sigma\varepsilon_{fab1}\left(1-\varepsilon_g\right)\left(T^4_{fab(y=0)} - T^4_{amb}\right) \qquad 0 < t \le t_{exp} \tag{6a}$$

$$k(T)\left.\frac{\partial T}{\partial y}\right|_{y=0} = h_{cnv}\left(T_{fab(y=0)} - T_{amb}\right) + \sigma\varepsilon_{fab1}\left(T^4_{fab(y=0)} - T^4_{amb}\right) \qquad t > t_{exp} \tag{6b}$$

$$-k(T)\left.\frac{\partial T}{\partial y}\right|_{y=L_{fab}} = q''_y(\vec{r})\big|_{y=L_{fab}} - k_{air}(T)\left.\frac{\partial T_{air}}{\partial y}\right|_{y=L_{fab}} \qquad t > 0 \tag{7}$$

where h_{fl} is the convective heat transfer coefficient from the flame to the fabric, ε_{fab1} is the fabric exposed surface emissivity, T_{amb} is the ambient temperature (300 K), and h_{cnv} is the convective heat transfer coefficient from the fabric to the ambient during the cool down period. The latter is estimated from an empirical correlation for natural convection heat transfer from a horizontal heated plate facing downwards to air at atmospheric pressure [24] as

$$h_{cnv} = 0.59\left(\frac{T_{fab(y=0)} - T_{amb}}{W_{fab}}\right)^{1/4} \tag{8}$$

where W_{fab} is the fabric width. Finally, $q''_y(\vec{r})\big|_{y=L_{fab}}$ is the emitted radiation from the fabric backside surface, which will be discussed later in this section.

The fabric initial condition is

$$T_{fab}(x, t = 0) = T_{amb} \tag{9}$$

2.2. Heat Transfer in the Air Gap

For air gap widths equal to that of the standard TPP [2] (1/4 in. (6.35 mm)) or less, the 1-D transient conduction-radiation heat transfer in the air gap is expressed as

$$\rho(T)c_P(T)\frac{\partial T}{\partial t} = \frac{\partial}{\partial y}\left(k(T)\frac{\partial T}{\partial y}\right) - \frac{\partial q_R^{"}}{\partial y} \tag{10}$$

where ρ , c_P, and k are the air density, specific heat, and thermal conductivity, respectively. In order to estimate the divergence of the radiative heat flux through the air gap, $\frac{\partial q_R^{"}}{\partial y}$, the Radiative Transfer Equation (RTE) of the air gap should be solved as it will be discussed later in this section.

Due to the wearer's motion, the air gap width between the fabric and the skin is assumed to vary periodically according to the equation

$$y = y_o + \Delta y \sin(2\pi f t) \tag{11}$$

where y is the air gap width at any time t, Δy is the fabric movement amplitude, f is the fabric movement frequency, and y_o is the average air gap width, as shown in Figure 1. As the fabric moves outwards away from the skin, air inflow at ambient conditions is assumed to fill the extra space created within the gap. This ambient air mixes with the hot gases inside the gap. Assuming a constant volume process, the instantaneous mixture properties can be calculated by

$$\rho_{mix} = \frac{\rho_{air}\, y_o + \rho_{amb}\, \Delta y}{y_o + \Delta y} \tag{12}$$

$$c_{v,mix}\, T_{mix} = \frac{\rho_{air}\, c_{v,air}\, T_{air}\, y_o + \rho_{amb}\, c_{v,amb}\, T_{amb}\, \Delta y}{\rho_{mix}\, (y_o + \Delta y)} \tag{13}$$

where ρ_{mix} is the mixture density, ρ_{air} is the air gap density, ρ_{amb} is the ambient density, $c_{v,mix}$ is the mixture specific heat, T_{mix} is the mixture temperature, $c_{v,air}$ is the air gap specific heat, T_{air} is the air gap temperature, and $c_{v,amb}$ is the ambient specific heat.

The boundary conditions for the air gap energy equation are obtained from the continuity of temperature between the air gap and both the fabric and the skin (epidermis) surface as follows.

$$T_{air}|_{y=L_{fab}} = T_{fab}\big|_{y=L_{fab}} \qquad t > 0 \tag{14}$$

$$T_{air}|_{y=L_{fab}+L_{air}} = T_{ep}\big|_{y=L_{fab}+L_{air}} \qquad t > 0 \tag{15}$$

where T_{ep} is the epidermis surface temperature and L_{air} is the air gap width.

The air gap initial condition is

$$T_{air}(y, t = 0) = T_{amb} \tag{16}$$

The properties of dry air [25] are used to account for the variation in the thermal properties of the hot gases in the gap with temperature.

2.3. Heat Transfer in the Human Skin

The human skin consists of epidermis, dermis, and subcutaneous layers where blood perfusion takes place in the latter two layers. The bioheat equation developed by Pennes [18] was employed to model heat transfer in the skin tissues. The energy equations for the three layers of the skin are written as

$$(\rho c_P)_{ep} \frac{\partial T}{\partial t} = \frac{\partial}{\partial y}\left(k_{ep} \frac{\partial T}{\partial y}\right) \tag{17}$$

$$(\rho c_P)_{ds} \frac{\partial T}{\partial t} = \frac{\partial}{\partial y}\left(k_{ds} \frac{\partial T}{\partial y}\right) + (\rho c_P)_b \omega_b (T_{cr} - T) \tag{18}$$

$$(\rho c_P)_{sc}\frac{\partial T}{\partial t} = \frac{\partial}{\partial y}\left(k_{sc}\frac{\partial T}{\partial y}\right) + (\rho c_P)_b \omega_b (T_{cr} - T) \tag{19}$$

where ω_b is the blood perfusion rate within the dermis and subcutaneous layers, T_{cr} is the human core body temperature, and ρ , c_P, and k have their conventional meaning.

The skin boundary conditions are

$$-k_{ep}\frac{\partial T_{ep}}{\partial y}\Big|_{y=L_{fab}+L_{air}} = q_y^{"}(\vec{r})\Big|_{y=L_{fab}+L_{air}} - k_{air}(T)\frac{\partial T_{air}}{\partial y}\Big|_{y=L_{fab}+L_{air}} \qquad t > 0 \tag{20}$$

$$T_{sc}|_{y=L_{fab}+L_{air}+L_{ep}+L_{ds}+L_{sc}} = T_{cr} \qquad t > 0 \tag{21}$$

where L_{ep}, L_{ds}, L_{sc} are the widths of the epidermis, dermis, and subcutaneous layers, respectively. The continuity of temperature and heat flux represents the inner boundary conditions between the skin layers. The radiation heat flux at the fabric-skin interface, $q_y^{"}(\vec{r})\big|_{y=L_{fab}+L_{air}}$, will be discussed later in this section.

A linear temperature distribution between 32.5ºC at the epidermis surface and 37ºC at the subcutaneous base (core body temperature) is assumed as the skin initial condition. When the basal layer (interface between the epidermis and the dermis layers) temperature reaches 44^{o}C, skin burn injury takes place. Henriques integral [7] is employed to predict times to receive skin burn as follows.

$$\varphi = \int_0^t P\, exp\left(-\frac{\Delta E}{RT}\right) dt \tag{22}$$

where the values for the pre-exponential factor P and the activation energy ΔE of the skin were determined by Weaver and Stoll [26] for second degree burn injury. However, the corresponding values for third degree burn injury were determined by Takata [27]. In order to calculate times for first and second degree burns, the basal layer temperature is used in the above integral. The

dermal base (the interface between the dermis and the subcutaneous) temperature is used in the integral to calculate times to third degree burn.

2.4. Radiation Heat Transfer in the Air Gap

Assuming that the air gap behaves as a gray, absorbing, and emitting medium, the change in the intensity along a radiation ray path is written [28] as

$$\frac{dI(\vec{r},\hat{s})}{ds} = -\kappa(\vec{r})I(\vec{r},\hat{s}) + \kappa(\vec{r})I_b(\vec{r}) \tag{23}$$

where I is the radiation intensity, which varies with the spatial position $\vec{r}$ and the angular direction $\hat{s}$, κ is the air gap absorption coefficient, s is the geometric distance, and I_b is the black body intensity that is defined as

$$I_b = \frac{\sigma T^4}{\pi} \tag{24}$$

where σ is the Stephan-Boltzmann constant and T is the medium temperature.

The unit direction $\hat{s}$ is defined as

$$\hat{s} = (sin\theta\ cos\phi)\hat{e}_x + (sin\theta\ sin\phi)\hat{e}_y + (cos\theta)\hat{e}_z \tag{25}$$

where $\hat{e}_x$, $\hat{e}_y$, and $\hat{e}_z$ are unit vectors in x, y, and z directions, θ is polar angle measured from $\hat{e}_z$, and ϕ is azimuthal angle measured from $\hat{e}_x$.

Assuming both the fabric backside and the skin (epidermis) surface to behave as opaque gray surfaces, the boundary conditions for the air gap RTE (Eq. 23) are written as

$$I_{fab}(\vec{r},\hat{s}) = \varepsilon_{fab2}(\vec{r})I_{b,fab}(\vec{r}) + \frac{\rho_{fab2}(\vec{r})}{\pi}\int_{\hat{s}'\cdot\hat{n}<0} I(\vec{r},\hat{s}')|\hat{s}'\cdot\hat{n}|d\,\Omega' \quad at\ y = L_{fab} \tag{26}$$

$$I_{ep}(\vec{r},\hat{s}) = \varepsilon_{ep}(\vec{r})I_{b,ep}(\vec{r}) + \frac{\rho_{ep}(\vec{r})}{\pi}\int_{\hat{s}'\cdot\hat{n}<0} I(\vec{r},\hat{s}')|\hat{s}'\cdot\hat{n}|d\,\Omega' \quad at\ y = L_{fab} + L_{air} \tag{27}$$

where ε_{fab2} and ρ_{fab2} are the fabric backside emissivity and reflectivity, ε_{ep} and ρ_{ep} are the epidermis surface emissivity and reflectivity, $\hat{s}'$ is the reflected ray unit direction, $\hat{n}$ is the unit normal to the surface, and $d\Omega'$ is the solid angle containing the reflected ray.

The RTE (Eq. 23) was solved along with its boundary conditions using the Finite Volume method [29]. Integrating the RTE over a control volume and control angle, the 1-D discrete equation using the step scheme is written as

$$a_P^l I_P^l = a_N^l I_N^l + a_S^l I_S^l + b^l \tag{28}$$

where

$$a_N^l = max(-A_n D_{cn}^l, 0), a_S^l = max(-A_s D_{cs}^l, 0) \tag{29}$$

$$a_P^l = max(A_n D_{cn}^l, 0) + max(A_s D_{cs}^l, 0) + \kappa_P \Delta V_P \Delta\Omega^l \tag{30}$$

$$b^l = S_P^l \Delta V_P \Delta\Omega^l \tag{31}$$

$$D_{cn}^l = \int_{\Delta\Omega^l} \left(\hat{s}^l \cdot \hat{e}_y\right) d\Omega, D_{cs}^l = -D_{cn}^l \tag{32}$$

$$\Delta\Omega^l = \int_{\Delta\Omega^l} d\Omega \tag{33}$$

$$S_P^l = \kappa_P I_{b,P} \tag{34}$$

The divergence of radiative heat flux in Eq. (10) is obtained from the relation

$$\frac{\partial q_R^{"}}{\partial y} = \kappa\left(4\pi I_b(\vec{r}) - G(\vec{r})\right) \tag{35}$$

where $G(\vec{r})$ is incident radiation, which is defined as

$$G(\vec{r}) = \int_{4\pi} I(\vec{r}, \hat{s}) d\,\Omega \tag{36}$$

The radiation heat flux at both sides of the air gap can be estimated as

$$q_y^{"}(\vec{r})\big|_{y=L_{fab}} = \int_{4\pi} I(\vec{r},\hat{s})(\hat{s}\cdot\hat{e}_y)d\,\Omega\Big|_{y=L_{fab}} \tag{37}$$

$$q_y^{"}(\vec{r})\big|_{y=L_{fab}+L_{air}} = \int_{4\pi} I(\vec{r},\hat{s})(\hat{s}\cdot\hat{e}_y)d\,\Omega\Big|_{y=L_{fab}+L_{air}} \tag{38}$$

3. NUMERICAL SOLUTION

The finite volume method [30] was employed in the discretization of the energy equations for the fabric, air gap, and the skin (epidermis, dermis, and subcutaneous) along with their boundary conditions. A fully implicit scheme was used for the temporal discretization. The Gauss-Seidel point by point iterative scheme was used to solve the discrete energy equations. The solution marches as follows. For each time step, temperatures from the previous time step are used as initial values for the iteration loop. The air gap width is updated according to the sine function. When the air gap width decreases, an uniform reduction in the air gap control volumes sizes is assumed and the air properties in each control volume do not change. As the air gap width increases, an uniform increase in the control volumes sizes is assumed. In addition, the mixing between the air properties in each control and ambient air properties is performed according to Eqs. (12) and (13) which results in a change in the air properties in each control volume. The air gap, fabric backside, and epidermis surface temperatures are used to solve the RTE through the air gap. Next, the divergence of radiative heat flux within the air gap and the radiation heat flux at both sides of the air gap is estimated to be employed in the air gap energy equation and the boundary condition equations of the fabric and the skin. Then new temperatures are calculated by visiting each control volume starting from the fabric surface to the subcutaneous base. The thermal properties for the fabric and the air gap, the temperature values

in the source terms, and the divergence of radiative heat flux are updated based on the current temperature within the iteration loop. The iterative solver continues until the non-dimensional change in the temperature field becomes less than 10^{-5}. Then both the basal layer and the dermal base temperatures are used in the Henriques integral (Eq. (22)) to predict times to receive skin burn injuries.

4. RESULTS AND DISCUSSION

The model validation has been performed by simulating the open flame bench top test done by Torvi [8] using skin simulant material and a constant air gap width of 6.4 mm (1/4 in.). Figure 2 shows a comparison between the predicted and measured skin simulant surface temperature during both the exposure and the cool down periods. The model was able to successfully predict the sharp rise in the skin simulant surface temperature during the exposure period. However, other factors that are not considered in the model such as the reduction in the fabric thickness due to pyrolysis might be the source of the small deviation between the prediction and measurements. Without more extensive experimental data, it is not possible to definitively identify the source of the small discrepancy observed in Figure 2.

The fabric and the hot gas parameters used in the simulation are listed in Table 1 while the human skin thermophysical properties are listed in Table 2. The simulation assumed an exposure of 10 s followed by 60 s of cool down. A sine wave with an average value of 3 mm, an amplitude of 1.5 mm, and a frequency of 0.5 rps was employed to account for the periodic variation in the air gap width. We will refer to this case as the baseline case. The simulation was first carried out to investigate the influence of the fabric periodic movement (baseline case) on the heat transfer within the protective clothing and its performance compared to that for a constant air gap width of 3 mm. Next, a parametric study was performed to capture the entire

effect of the fabric movement. The influence of the variation in the periodic movement frequency from 0 rps to 6 rps was investigated in order to cover a wide range of fabric motion speed. In addition, the influence of a variation in the periodic movement amplitude from 0 mm to 2.5 mm was studied. It should be mentioned here that the air gap width values used in this study were chosen in such way to ensure that the air gap width at any time (due to the fabric movement) does not exceed 6.35 mm (1/4 in.), which is the critical width for convection heat transfer within the air gap [8, 20].

Figure 3 illustrates the temporal variation in the clothing system temperature due to the fabric periodic movement (baseline case) compared to that of a constant air gap width of 3 mm. The notation (m) is used in the figures to indicate the fabric movement in order to distinguish between the baseline case and the case of constant air gap width. It is shown in Figure 3(a) that the periodic movement of the fabric has a minimal effect on the fabric temperature during both the exposure and the cool down periods. However, the periodic cooling of the air gap by the entering air causes a fluctuating reduction in the air gap temperature during both the exposure and the cool down periods compared to that for a constant air gap width. This fluctuating reduction is clearly evident close to the fabric and in the middle of the air gap where temperatures were initially high. However, the fluctuation almost vanishes close to the skin because of the relatively low initial temperature of the air gap there. Figure 3(b) shows a small increase in the epidermis surface and the basal layer temperatures compared to that for a constant air gap width. This increase in the skin temperature indicates that the influence of the reduction in the air gap width due to the fabric periodic movement dominates the opposing effect of the cooling air entering the gap. However, the temperature of the dermal base layer does not significantly change with the periodic movement of the fabric.

The cooling effect of the air entering the air gap is illustrated in Figure 4 which gives the temporal variation in the air gap centre temperature. The saw-like parts of the profile represent the periods of an increase in the air gap width due to the fabric movement when both air heating and inflow air mixing take place. Each time step through these intervals is shown by two lines: a vertical line that represents the drop in the air gap temperature due to mixing with the inflow ambient air, and an inclined line that represents the subsequent heating of the air gap as a result of the energy transfer within the system. Ideally, the two processes (mixing and heating) would be simultaneous. A resultant reduction in the air gap temperature is evident during the increase in the air gap width, which reflects the cooling effect of the entering air. The continuous parts of the profile represent the intervals when the air gap width decreases due to the fabric movement.

The corresponding variation in the air gap volumetric heat capacity and thermal conductivity are illustrated in Figure 5 at the interfaces with both the fabric (called the front) and the skin (called the back). A slight fluctuation in the air gap volumetric heat capacity and thermal conductivity is evident during the exposure and cool down periods. However, the overall trend of these thermophysical properties is still the same as that for a constant air gap width [22].

Figure 6 illustrates the variation in the protective clothing system energy balance as a result of the fabric periodic movement (baseline case) compared to that for a constant air gap width of 3 mm. A more complete discussion of the protective clothing energy balance can be found in Ghazy and Bergstrom [22]. The small fluctuating reduction in the fabric temperature (see Figure 3a) caused a related fluctuating reduction in the radiation losses from the fabric to both the ambient ($q''_{rad\ fab\text{-}amb}$) and the air gap ($q''_{rad\ fab\text{-}air}$), Figure 6(a), compared to that for a constant air gap width. The reduction in the radiation heat transfer from the fabric backside to the

air is attributed to the reduction in the fabric backside temperature associated with an increase in the skin surface temperature. The fluctuating conduction heat transfer at the interface between the fabric and the air ($q''_{cnd\ fab\text{-}air}$) tends to increase its value compared to that for a constant air gap width. This is attributed to the combination of the reduction in the air gap width and reduction in the air gap temperature due to the cooler inflow air. Note that, the maximum values of conduction heat transfer take place when the fabric moves closer to the skin so that the conductive resistant of the air gap reaches its minimum value.

The cooling effect of the inflow air causes a significant fluctuation in the energy transfer through the air gap, Figure 6(b). This periodic cooling causes a small increase in the air capacity to store energy ($q_{\ strg\ air}$) compared to that for a constant air gap width. The conduction heat transfer at the air-skin interface ($q''_{cnd\ air\text{-}ep}$) is significantly increased compared to that for a constant air gap width, as well. This result is consistent with the increase in the energy transfer by conduction at the fabric-air interface ($q''_{cnd\ fab\text{-}air}$) (see Figure 6a). The increase in the energy transfer by conduction to the skin leads to a similar increase in the skin temperature as shown previously in Figure 3(b). The increase in the skin surface temperature in addition to the reduction in the emitted radiation from the fabric backside surface ($q''_{rad\ \ fab\text{-}air}$) leads to a reduction in the radiation energy received by the skin ($q''_{rad\ air\text{-}ep}$).

Figure 6(c) shows an increase in the energy stored in the dermis layer over that for a constant air gap width. In contrast, there is almost no increase in the energy stored in the epidermis layer, which can be attributed to the limited heat capacity of the epidermis layer compared to that of the dermis. The influence of the fabric periodic movement on the energy content of the skin completely vanishes in the subcutaneous layer.

The fluctuation in the energy transferred from the fabric to the skin through the air gap due to the fabric periodic movement is depicted by Figure 7. The exposure period between 8 s and 10 s represents a complete cycle for the variation in the air gap width. The air gap width has a mean value of 3 mm at 8 s, 9 s, and 10 s of exposure while a maximum air gap width of 4.5 mm and a minimum air gap width of 1.5 mm are reached at 8.5 s and 9.5 s, respectively. This cycle of air gap width variation was chosen at the end of the exposure period when energy transfer within the clothing system is very close to steady state. The fluctuation in the conductive and radiative heat flux across the air gap is illustrated by Figures 7(a) and 7(b), respectively. The fluctuation in the conductive heat flux is more significant than the fluctuation in the radiative heat flux. The maximum value for the conductive heat flux across the air gap occurs at 9.5 s of exposure where the air gap width reaches its minimal value. In contrast, the large air gap width and the cooling effect of the inflow air at 8.5 s of exposure leads to a relatively low conductive heat flux across the air gap. The radiative heat flux across the air gap has a similar trend to the conductive one but with much less variation in its value (note the expanded axis scale in Figure 7(b)). Overall, the effect of motion on the total heat flux through the air gap, Figure 7(c), follows that of the conductive heat flux.

Table 3 illustrates the influence of the fabric periodic movement on skin burn predictions. It shows that the periodic movement of the fabric causes third degree burn injuries earlier than the corresponding case of constant air gap width. However, this effect is minimal for the specific scenario of the fabric movement (baseline case) considered. Additional simulations were performed to further explore the effect of the fabric movement on heat transfer within the clothing system and its performance.

A variation in the movement frequency from 0 rps to 6 rps with an average gap width of 3 mm and amplitude of 1.5 mm was studied to cover a range of motions. When the fabric periodically moves with a very low frequency, a small reduction in the time to receive skin burn might be expected due to the dominance of the effect of the variation in the air gap width over that of the cooling inflow air, Figure 8. However, increasing the frequency results in an insignificant increase in the time to receive second-degree burn injury. The influence of the movement frequency is more influential during the cool down period after the exposure ends. Increasing the movement frequency increases the time to receive third degree burn injury during the cool down period. For example, an increase of 8% in the predicted time to receive third degree burn would take place with an increase in movement frequency from 0.5 rpm to 4 rpm. This can be attributed to the cooling effect of the entering air especially with the absence of an energy source during the cool down period.

The variation in the fabric movement frequency has an insignificant influence on the fabric temperature, which agrees with the results presented earlier in Figure 3. Increasing the movement frequency increases the fluctuation in the air gap centre temperature following the trend of the fabric periodic motion, Figure 9(a). Increasing the movement frequency increases the effect of cooling the air gap both during and after the exposure. Figure 9(b) illustrates the influence of the movement frequency on the epidermis surface temperature. Small movement frequencies increase the epidermis surface temperature since the reduction in the air gap width is dominant over the cooling effect of the inflow air. However, higher values of movement frequencies increase the cooling effect of the entering air and hence reduce the epidermis surface temperature. A similar influence of the movement frequency on the basal layer temperature is

illustrated by Figure 9(c). However, the fluctuation in the dermal base temperature is damped out at high movement frequency.

Since the periodic movement of the fabric is associated with a variation in the air gap width and properties, special attention was given to the transient heat transfer across the air gap. As shown in Figure 10(a), increasing the movement frequency increases the fluctuation in the conduction heat flux through the air gap without a significant change in its mean value. Figure 10(b) shows that increasing the movement frequency reduces the radiation emitted from the fabric to the skin during the periods when the fabric moves closer to the skin.

The influence of the variation in the periodic movement amplitude was also studied. A range of amplitude values from 0 mm to 2.5 mm was considered. Figure 11 illustrates the variation in the air gap temperature as the fabric movement amplitude increases. It is shown in Figure 11(a) that increasing the movement amplitude has a minimal effect on reducing the fabric backside temperature for small values of the amplitude. However, this effect becomes more influential as the amplitude increases and the fabric moves closer to the skin. For example, a temperature reduction of about 40^{o}C is expected after 7.5 s of exposure as the movement amplitude increases from 1 mm to 2.5 mm. A corresponding decrease in the air gap centre temperature is shown in Figure 11(b) as the movement amplitude increases, while the epidermis surface temperature increases as the fabric movement amplitude increases, Figure 11(c). For example, a temperature increase of about 15^{o}C is expected after 9.5 s of exposure as the movement amplitude increases from 1 mm to 2.5 mm.

Figure 12(a) shows an insignificant decrease in the time to receive second-degree burn injury as the movement amplitude increases. In contrast, a reduction of about 18% in the time to receive third-degree burn is expected as the movement amplitude increases from 0.5 mm to 2.5

mm. This result reflects the dominance of the effect of the reduction in the air gap width over that of the cooling inflow air. Figure 12(b) shows the fluctuation in the basal layer temperature which is associated with an increase in its mean value as the movement amplitude increases. Moreover, it illustrates that the influence of the movement amplitude becomes more significant as the fabric approaches closer to the skin during the fabric periodic movement. The fluctuation in the skin temperature diminishes through the dermis layer, Figure 12(c). However, the dermal base temperature increases as the movement amplitude increases.

The variation in the effect of the movement amplitude on the temperature distribution through the air gap can be explained by considering the influence of the movement amplitude on the energy transfer through the air gap, Figure 13. It is shown in Figure 13(a) that increasing the movement amplitude causes a significant increase in the conduction heat transfer through the air gap from the fabric to the skin. The higher the movement amplitude, the higher the conduction heat flux. This large increase in the conduction heat transfer through the air gap explains both the reduction in the fabric backside temperature and the increase in the skin temperature, Figure 12. The discharge of the fabric energy content to the skin increases as the movement amplitude increases. The increase in the conduction heat transfer through the air gap with the movement amplitude leads to a corresponding decrease in the radiation heat transfer through the air gap, Figure 13(b). This reduction in the radiation heat flux can also be attributed to the decrease in the fabric backside temperature, which is associated with an increase in the skin surface temperature. However, the reduction in the radiation heat flux through the air gap is less than the increase in the conduction heat flux as the movement amplitude increases. Finally, although the amount of inflow air to the gap increases as the movement amplitude increases, the effect of the reduction in the air gap width is dominant over that of the entering air.

5. CONCLUSIONS

A finite volume model has been developed to investigate the effect of the wearer's motion on transient heat transfer through protective clothing during flash fire exposure. The clothing movement was shown to have a significant influence on heat transfer in protective clothing especially through the air gap. The influence of the protective clothing movement on its performance is the result of a combination of the periodic reduction in the air gap width and the periodic cooling of the air within the gap. Increasing the fabric movement frequency improves the protection provided by the clothing due to the more frequent inflow of cool air. Increasing the fabric movement amplitude reduces the protection provided by the clothing by concentrating the exposure on the skin as a result of the reduction in the air gap width. The greater the fabric movement amplitude, the greater the influence on the clothing performance.

This paper focused on studying the influence of the protective clothing wearer's motion on its performance for air gap widths that fall below 6.35 mm (1/4 in.), which is the critical width for natural convection within the air gap. The influence of the periodic movement of the fabric on the clothing performance will vary if the air gap width exceeds 6.35 mm (1/4 in.) due to the change in the heat transfer mechanism within the air gap. The study documents the role of the air gap between the fabric and the skin in the heat transfer through protective clothing and hence the clothing performance. In a general context, the paper also contributes to the knowledge of transient conduction-radiation heat transfer in enclosures with high temperature and heat flux boundary conditions and periodically changing widths.

REFERENCES

1. International Organization for Standardization, ISO 9151 Protective Clothing against Heat and Flame – Determination of Heat Transmission on Exposure to Flame, Geneva, Switzerland, 1995.
2. American Society for Testing Materials, ASTM D 4108-87 Standard Test Method for Thermal Protective Performance of Materials and Clothing by open-Flame Method, West Conshohocken, PA, 1987.
3. American Society for Testing Materials, ASTM F 1939-99 a Standard Test Method for Radiant Protective Performance of Flame Resistant Clothing Materials, West Conshohocken, PA, 1999.
4. National Fire Protection Association, NFPA 1971, Standard on Protective Ensemble for Structural Fire Fighting, Quincy, MA, 2007.
5. A.M. Stoll, and M.A. Chianta, Method and Rating System for Evaluation of Thermal Protection, Aerospace Medicine, vol. 40, pp. 1232-1238, 1969.
6. American Society for Testing Materials, ASTM F 1930-00 Standard Test Method for Evaluation of Flame Resistant Clothing for Protection Against Flash Fire Simulations Using an Instrumented Thermal Manikin, West Conshohocken, PA, 2000.
7. F.C. Henriques, Jr., A.R. Moritz, Studies of thermal injuries I: The conduction of heat to and through skin and the temperatures attained therein. A theoretical and experimental investigation, American J. Pathology, vol. 23, pp. 531-549, 1947.
8. D. A. Torvi, Heat Transfer in Thin Fibrous Materials under High Heat Flux Conditions, Ph.D. Thesis, University of Alberta, Edmonton, Alberta, 1997.

9. D.A. Torvi, and J.D. Dale, Heat Transfer in Thin Fibrous Materials under High Heat Flux, Fire Technology, vol. 35, pp. 210-231, 1999.

10. W. E. Mell, and J. R. Lawson, Heat Transfer Model for Fire Fighter's Protective Clothing, Fire Technology, vol. 36, pp. 39-68, 2000.

11. G. Song, R.L. Barker, H. Hamouda, A.V. Kuznetsov, P. Chitrphiromsri, and R.V. Grimes, Modeling the Thermal Protective Performance of Heat Resistant Garments in Flash Fire Exposures, Textile Research Journal, vol. 74, pp. 1033-1040, 2004.

12. P.W. Gibson, Multiphase Heat and Mass Transfer through Hygroscopic Porous Media with Applications to Clothing Materials, Technical report Natick/TR-97/005. U.S. Army Natick Research, Development and Engineering Center, Natick, MA, 2003.

13. P. Chitrphiromsri, and A.V. Kuznetsov, Modeling Heat and Moisture Transport in Firefighter Protective Clothing during Flash Fire Exposure, Heat Mass Transfer, vol. 41, pp. 206-215, 2005.

14. P. Chitrphiromsri, Modeling of Thermal Performance of Firefighter Protective Clothing during the Intense Heat Exposure, Ph.D. thesis, North Carolina State University, Raleigh, North Carolina, 2004.

15. P. Chitrphiromsri, A.V. Kuznetsov, G. Song, R.L. Barker, Investigation of Feasibility of Developing Intelligent Firefighter-Protective Garments Based on the Utilization of a Water-Injection System, Numerical Heat Transfer A, vol. 49, pp. 427–450, 2006.

16. G. Song, P. Chitrphiromsri, D. Ding, Numerical Simulation of Heat and Moisture Transport in Thermal Protective Clothing Under Flash Fire Conditions, Int. J. Occupational Safety and Ergonomics, vol. 14(1), pp. 89-106, 2008.

17. F. Zhu, and W. Zhang, Modeling Heat Transfer for Heat-resistant Fabrics Considering Pyrolysis Effect under an External Heat Flux, J. Fire Sciences, vol. 27, pp. 81-96, 2009.

18. H.H. Pennes, Analysis of tissue and arterial blood temperatures in resting human forearm, J. Applied Physiology vol. 1, pp. 93–122, 1948.

19. F. Zhu, and W. Zhang, Evaluation of Thermal Performance of Flame-resistant Fabrics Considering Thermal Wave Influence in Human Skin Model, J. Fire Sciences, vol. 24, pp. 465-485, 2006.

20. D.A. Torvi, J.D. Dale, and B. Faulkner, Influence of Air Gaps on Bench Top Test Results of Flame Resistant Fabrics, J. Fire Protection Engineering, vol. 10, pp. 1-12, 1999.

21. C.M.J. Sawcyn, D.A. Torvi, Improving Heat Transfer Models of Air Gaps in Bench Top Tests of Thermal Protective Fabrics, Textile Res. J., vol. 79, pp. 632–644, 2009.

22. A. Ghazy, D.J. Bergstrom, Numerical Simulation of Transient Heat Transfer in a Protective Clothing System during a Flash Fire Exposure, Numerical Heat Transfer A, vol. 58(9), pp. 702-724, 2010.

23. D.A. Torvi, and T.G. Threlfall, Heat Transfer Model of Flame Resistant Fabrics During Cooling After Exposure to Fire, J. Fire Technology, vol. 42, pp. 27-48, 2006.

24. J.P. Holman, Heat Transfer, 8th edition, McGraw-Hill Co., 1997.

25. F.P. Incropera, and D.P. DeWitt, Fundamentals of Heat and Mass Transfer, fifth ed., John Wiley & Sons, Inc., New York, 2002.

26. J.A. Weaver, and A.M. Stoll, Mathematical Model of Skin Exposed to Thermal Radiation, Aerospace Medicine, vol. 40, pp. 24-30, 1969.

27. A.N. Takata, J. Rouse, and T. Stanley, Thermal Analysis Program, I.I.T. Research Institute Report IITRI-J6286, Chicago, IL, 1973.

28. M.F. Modest, Radiative Heat Transfer, second ed., Academic Press, New York, 2003.

29. J. C. Chai and S. V. Patankar, Finite-Volume Method for Radiation Heat Transfer, in: W. J. Minkowycz, and E. M. Sparrow (Eds.), Advances in Numerical Heat Transfer 2, Taylor & Francis, pp. 109-141, 2000.

30. S.V. Patankar, Numerical Heat Transfer and Fluid Flow, Taylor & Francis, Washington, DC, 1980.

Table 1. Kevlar®/PBI and burner parameters

	Property	Value
L_{fab}	Fabric thickness	0.6 mm
W_{fab}	Fabric Width	0.05 m (2 in.)
ρ_{fab}	Fabric density	323 kg/m^3
γ_{fab}	Fabric extinction factor	0.01
ε_{fab}	Fabric emissivity	0.9
τ_{fab}	Fabric transmissivity	0.01
T_g	Hot gases temperature	2000 K
ε_g	Hot gases emissivity	0.02
h_{fl}	Flame convective heat transfer coefficient	40 W/m^{2}K

Table 2. Human skin thermophysical properties

Property	Epidermis	Dermis	Subcutaneous	Blood
Thickness (m)	8×10^{-5}	2×10^{-3}	1×10^{-2}	-
Density (Kg/m^3)	1200	1200	1000	1060
Specific Heat (J/Kg^oC)	3598	3222	2760	3770
Thermal Conductivity (W/m^oC)	0.255	0.523	0.167	-
Blood Perfusion Rate $(m^3/s)/m^3$ tissue	-	-	-	1.25×10^{-3}

Table 3. Influence of fabric periodic movement on skin burn prediction

Case	Time to receive skin burn (s)		
	1st degree	2nd degree	3rd degree
constant air gap width	5.0	5.3	26.6
reference case	5.1	5.3	25.7

Figure Captions

Figure 1. The protective clothing schematic diagram considering the fabric periodic movement due to wearer's motion.

Figure 2. Comparison between measured and predicted skin simulant surface temperature for constant air gap width.

Figure 3. Influence of the fabric periodic movement on the temporal temperature distribution within the clothing system: (a) fabric and air gap, (b) skin.

Figure 4. The cooling effect of the entering air on the air gap centre temperature.

Figure 5. The variation in the air gap thermal conductivity and volumetric heat capacity.

Figure 6. Influence of the fabric periodic movement on the protective clothing system energy balance: (a) fabric, (b) air gap, (c) skin.

Figure 7. Influence of the fabric periodic movement on heat transfer across the air gap through one cycle: (a) conductive heat flux, (b) radiative heat flux, (c) total heat flux.

Figure 8. Influence of the fabric movement frequency on skin burn predictions.

Figure 9. The effect of the fabric movement frequency on the protective clothing system temperature: (a) air gap centre, (b) epidermis surface, (c) dermal base.

Figure 10. The effect of the fabric movement frequency on the energy transfer across the air gap: (a) conductive heat flux at fabric-air interface, (b) emitted radiation from the fabric backside.

Figure 11. Influence of the fabric movement amplitude on the air gap temperature: (a) fabric backside, (b) air gap centre, (c) epidermis surface.

Figure 12. Influence of the fabric movement amplitude on skin burn predictions: (a) time to skin burn, (b) Basal layer temperature, (c) Dermal base temperature.

Figure 13. Influence of the movement amplitude on energy transfer across the air gap: (a) conductive heat flux at fabric-air interface, (b) emitted radiation from the fabric backside.

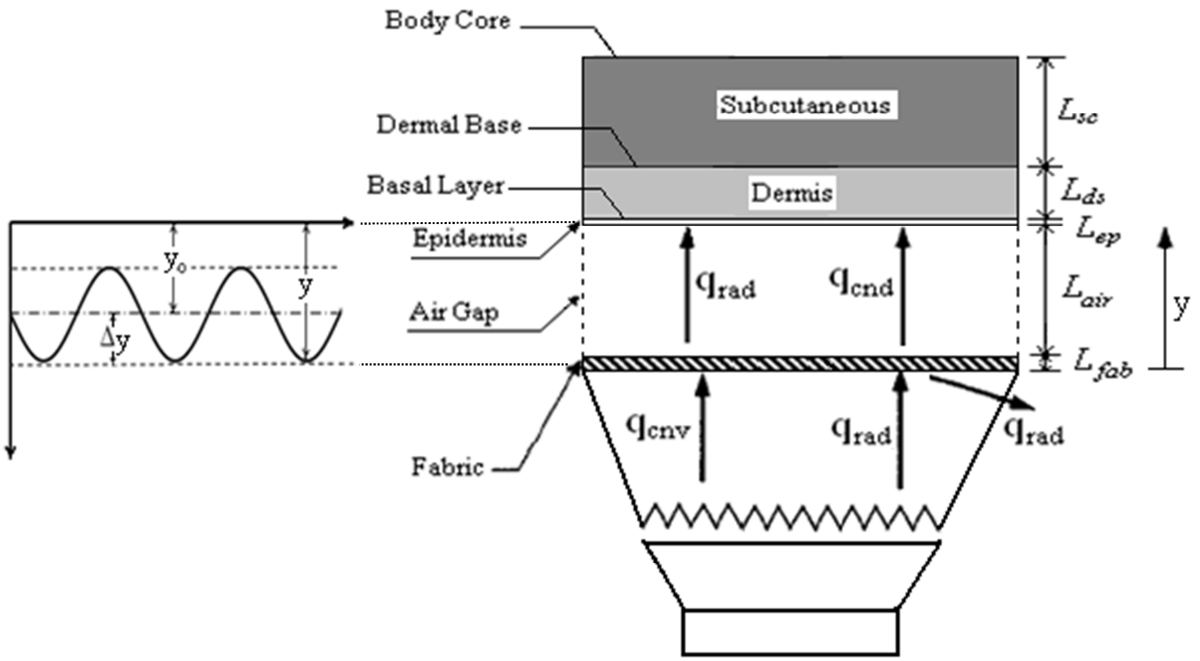

Figure 1. The protective clothing schematic diagram considering the fabric periodic movement due to wearer's motion.

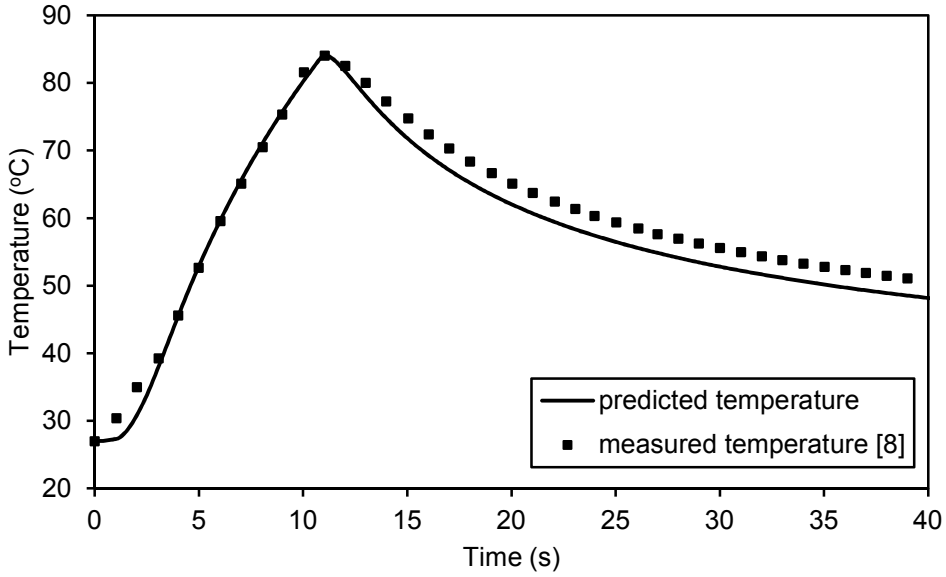

Figure 2. Comparison between measured and predicted skin simulant surface temperature for constant air gap width.

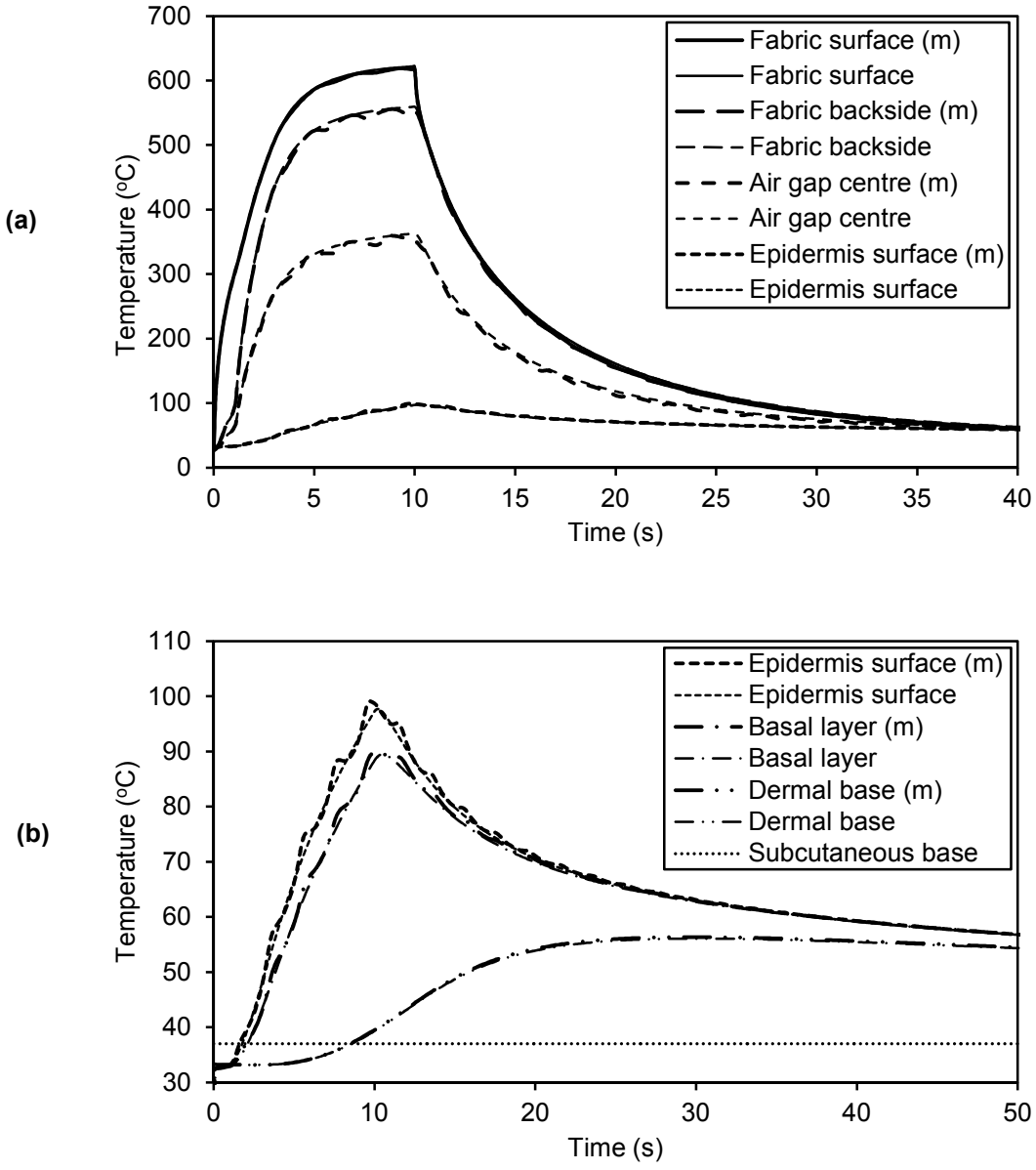

Figure 3. Influence of the fabric periodic movement on the temporal temperature distribution within the clothing system: (a) fabric and air gap, (b) skin.

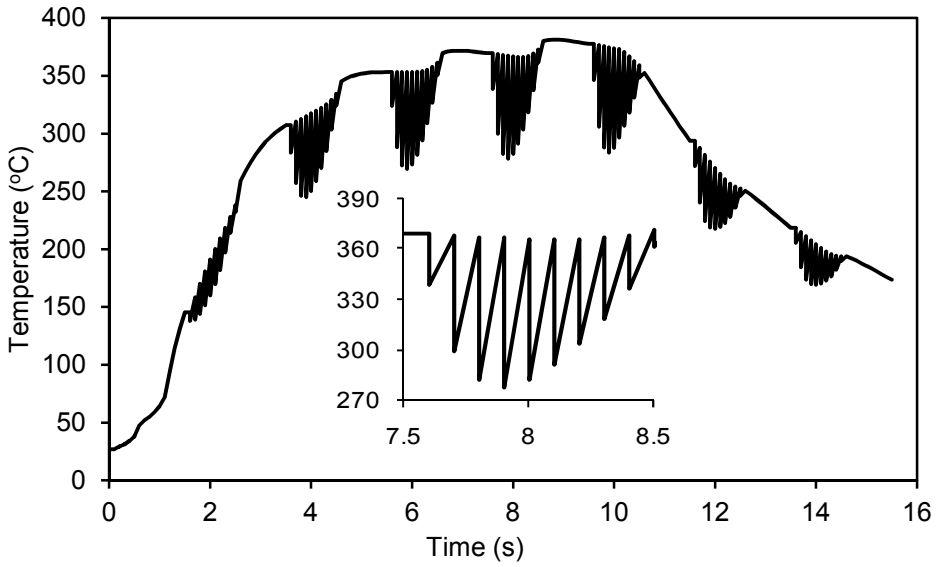

Figure 4. The cooling effect of the entering air on the air gap centre temperature.

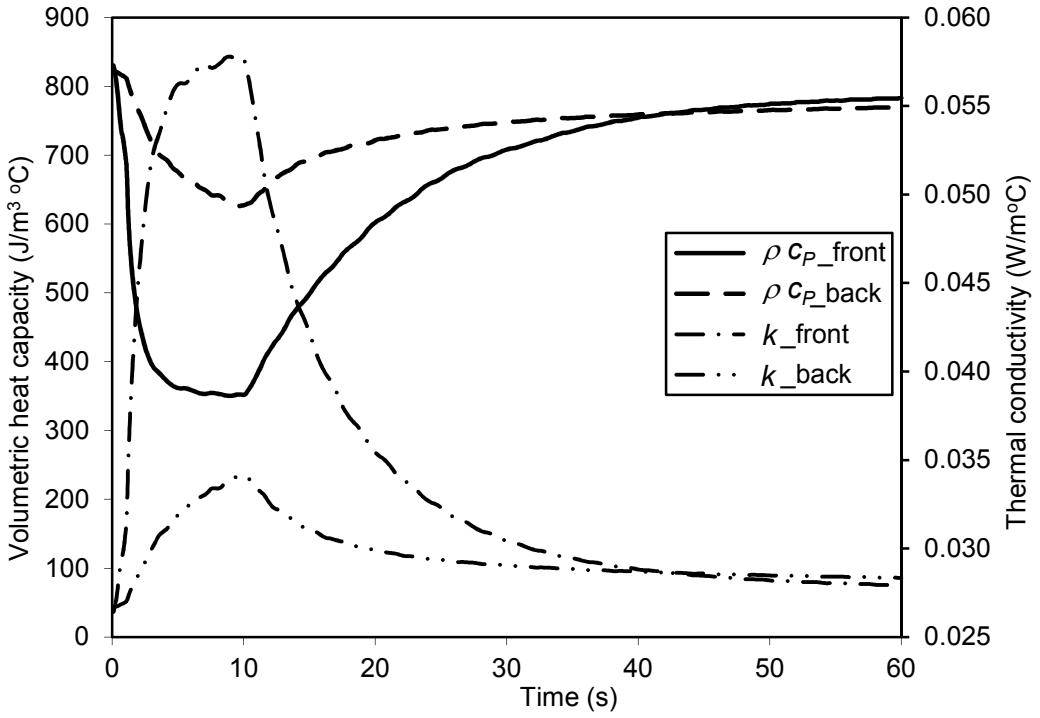

Figure 5. The variation in the air gap thermal conductivity and volumetric heat capacity.

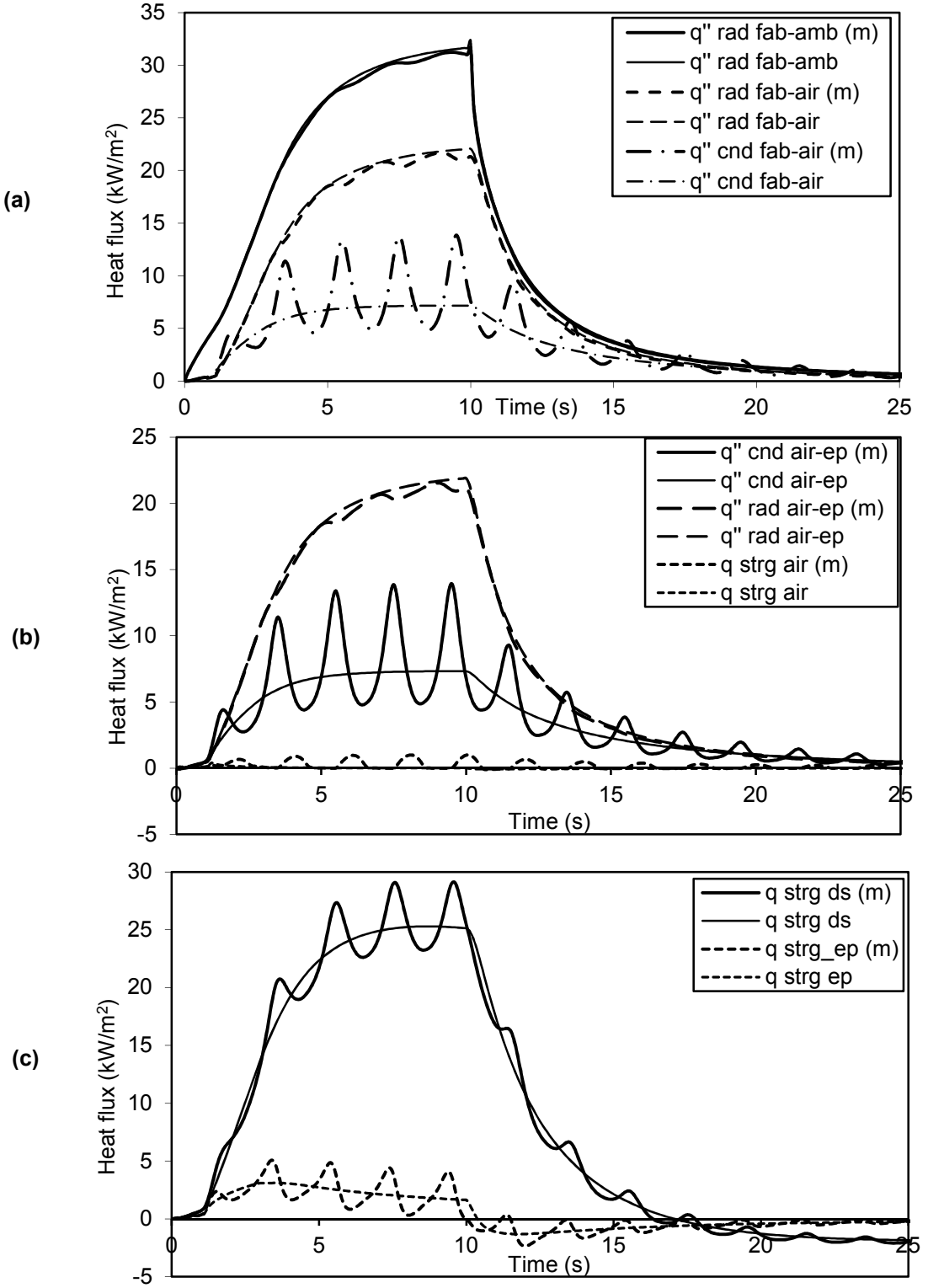

Figure 6. Influence of the fabric periodic movement on the protective clothing system energy balance: (a) fabric, (b) air gap, (c) skin.

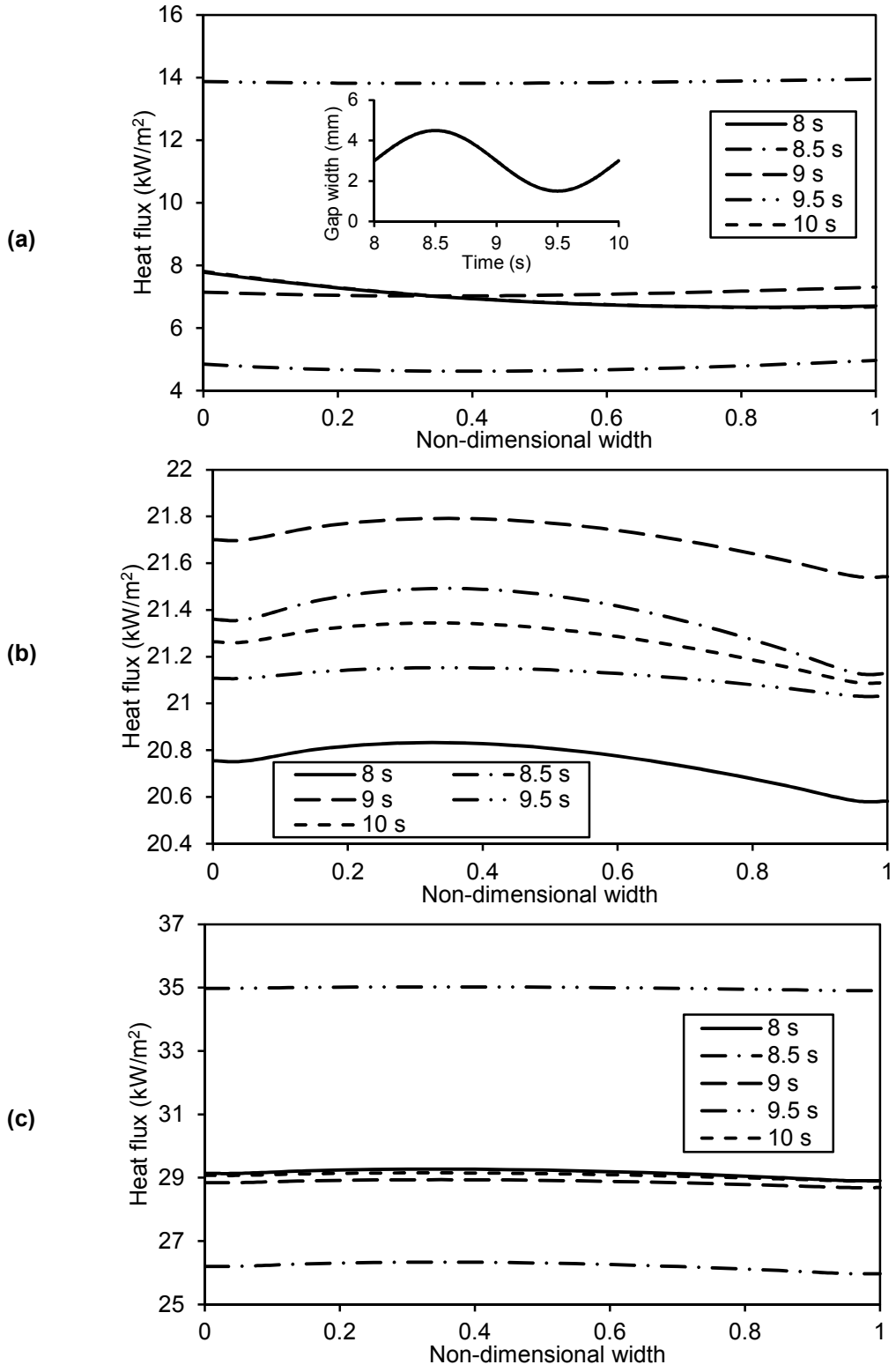

Figure 7. Influence of the fabric periodic movement on heat transfer across the air gap through one cycle: (a) conductive heat flux, (b) radiative heat flux, (c) total heat flux.

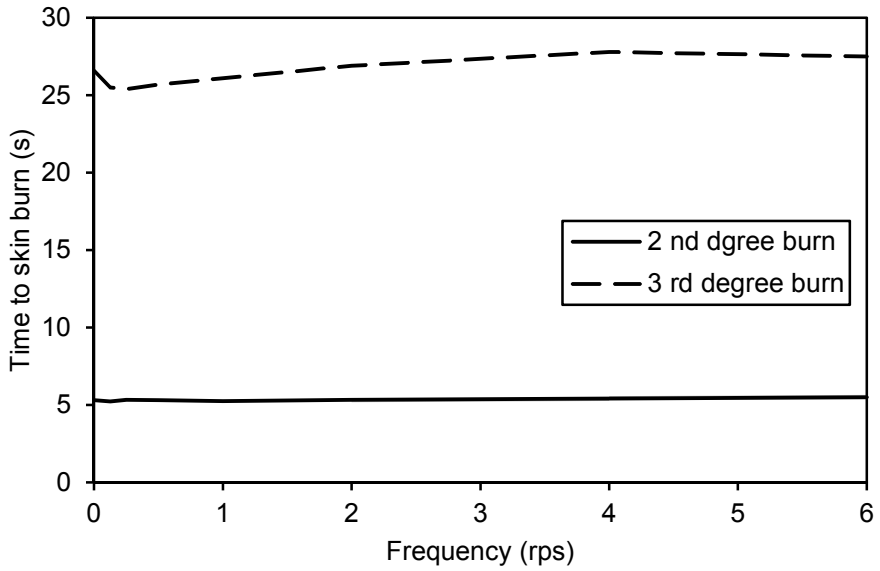

Figure 8. Influence of the fabric movement frequency on skin burn predictions.

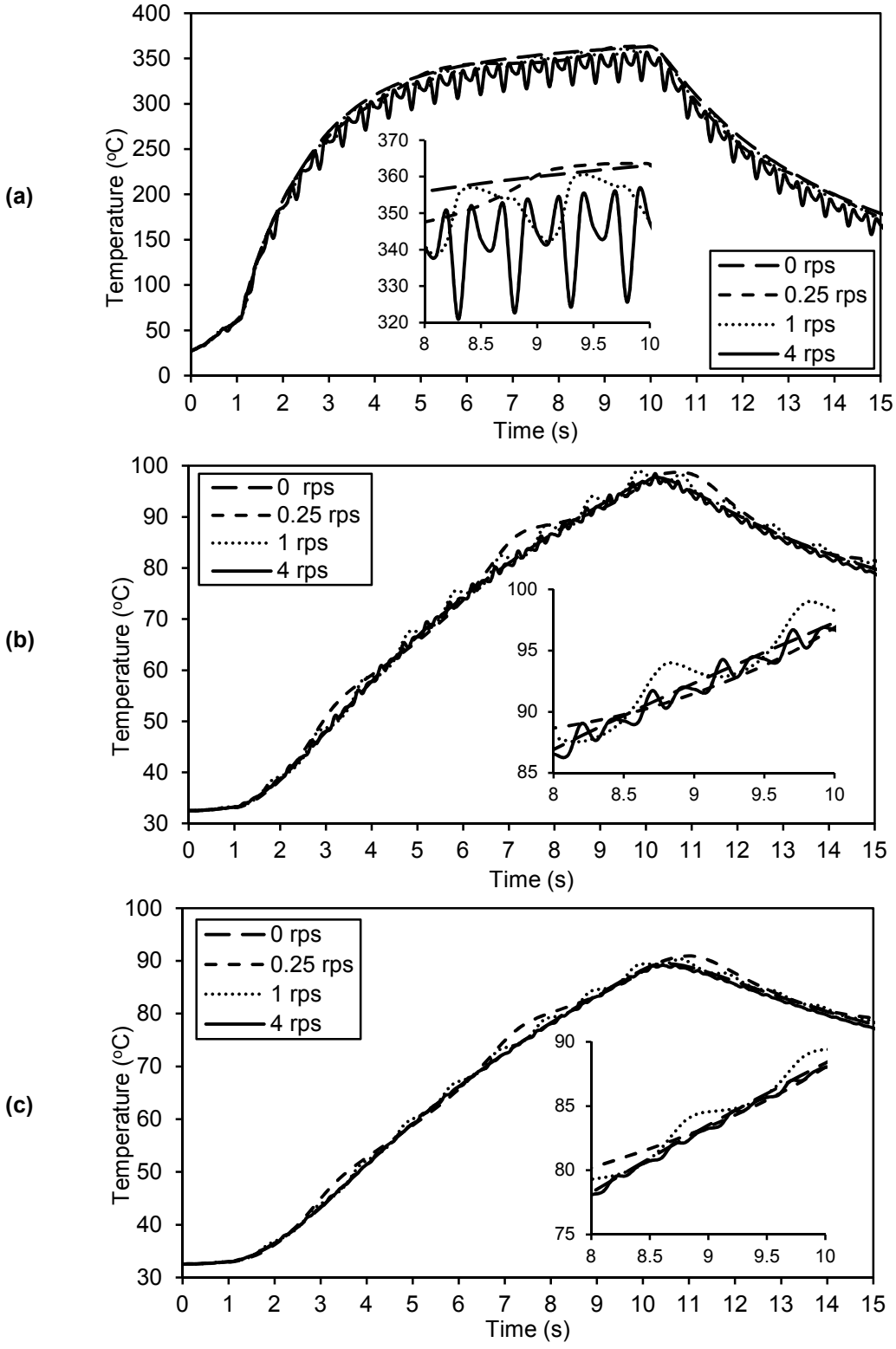

Figure 9. The effect of the fabric movement frequency on the protective clothing system temperature: (a) air gap centre, (b) epidermis surface, (c) dermal base.

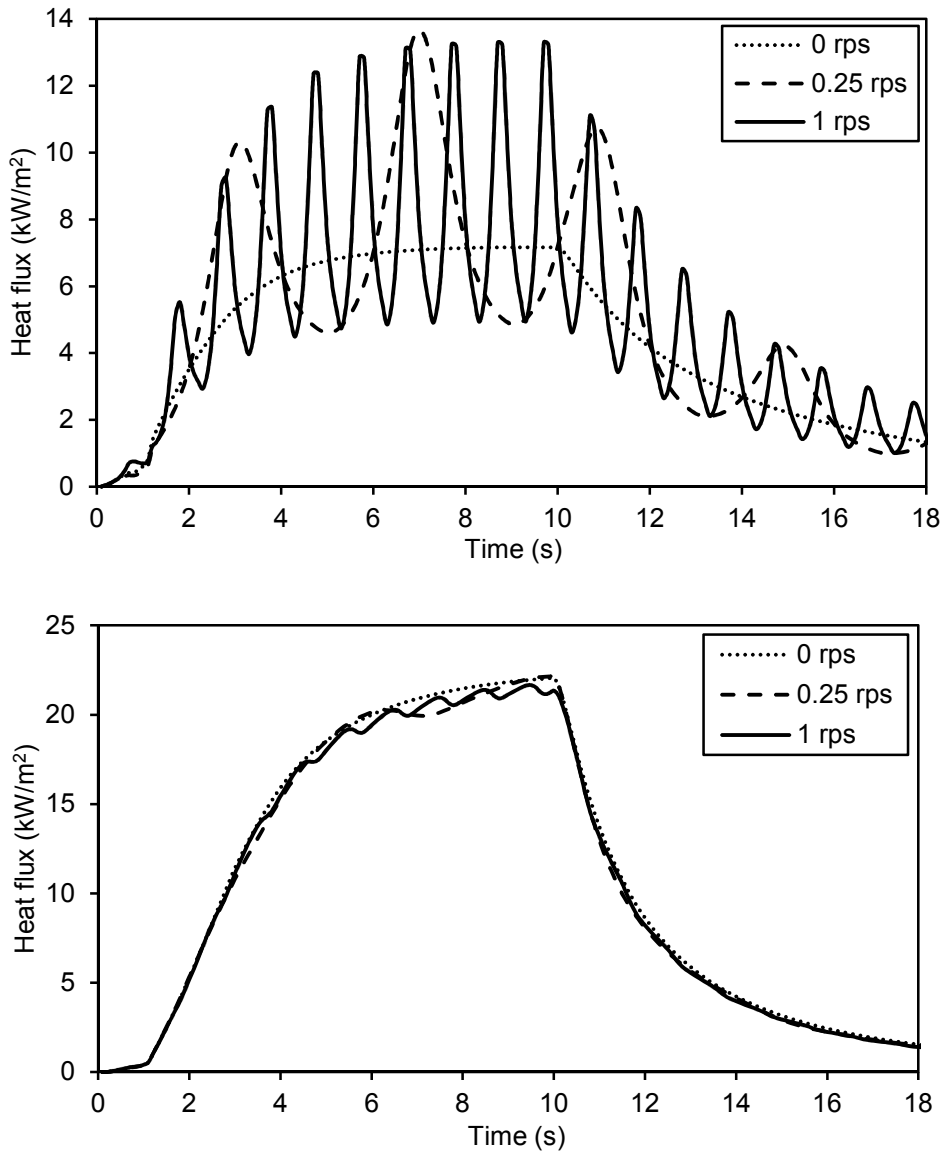

Figure 10. The effect of the fabric movement frequency on the energy transfer across the air gap: (a) conductive heat flux at fabric-air interface, (b) emitted radiation from the fabric backside.

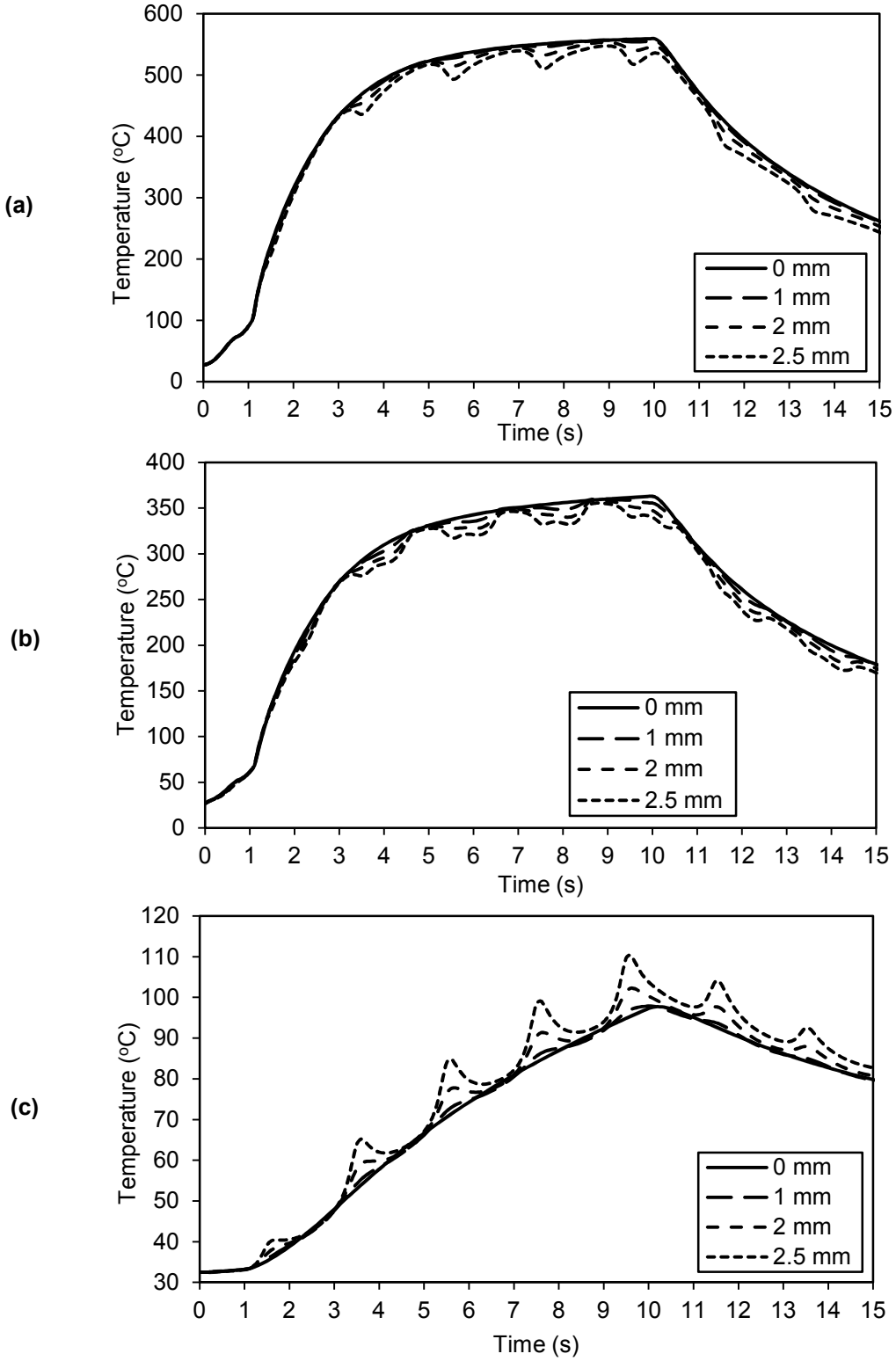

Figure 11. Influence of the fabric movement amplitude on the air gap temperature: (a) fabric backside, (b) air gap centre, (c) epidermis surface.

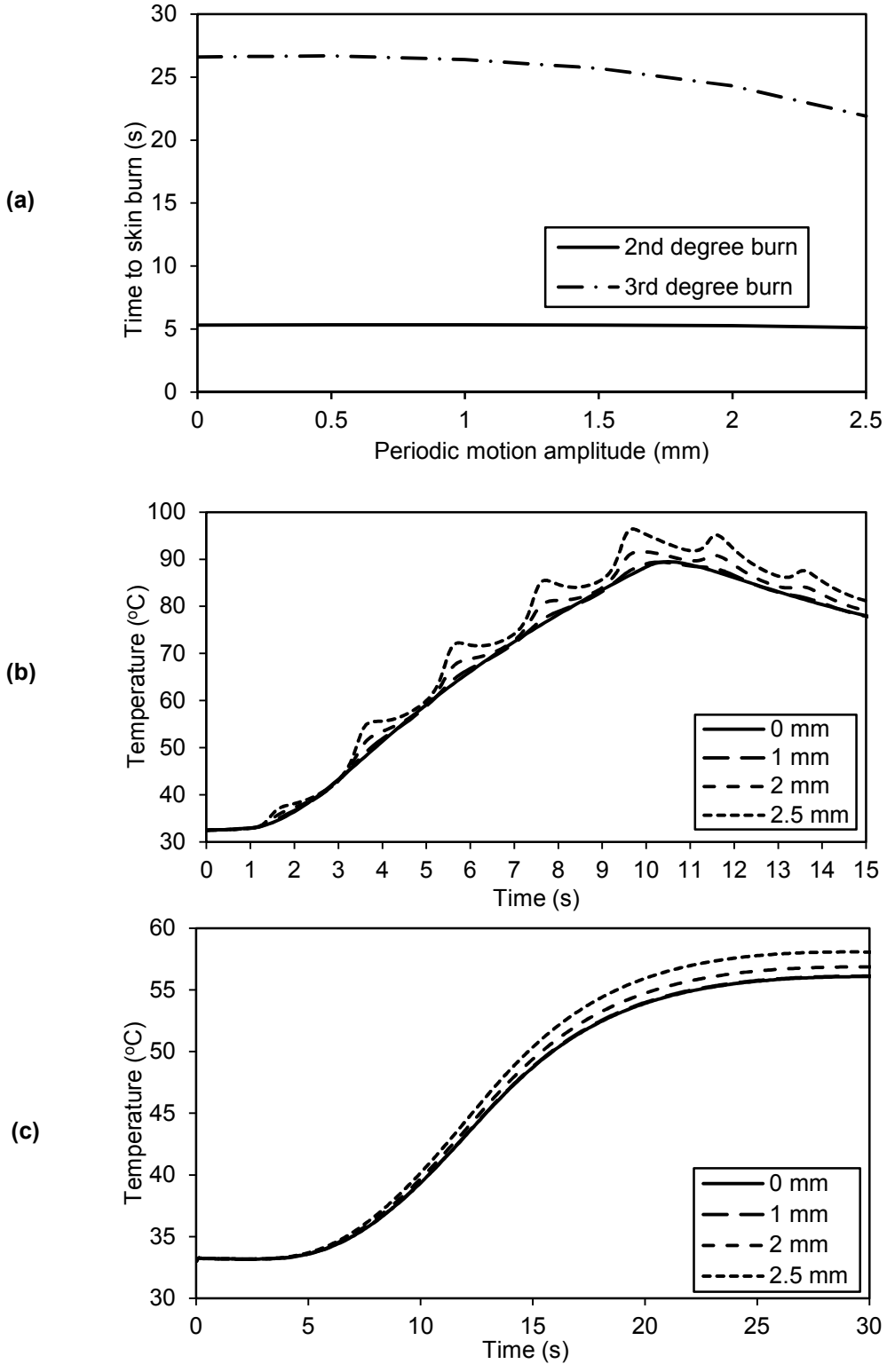

Figure 12. Influence of the fabric movement amplitude on skin burn predictions: (a) time to skin burn, (b) Basal layer temperature, (c) Dermal base temperature.

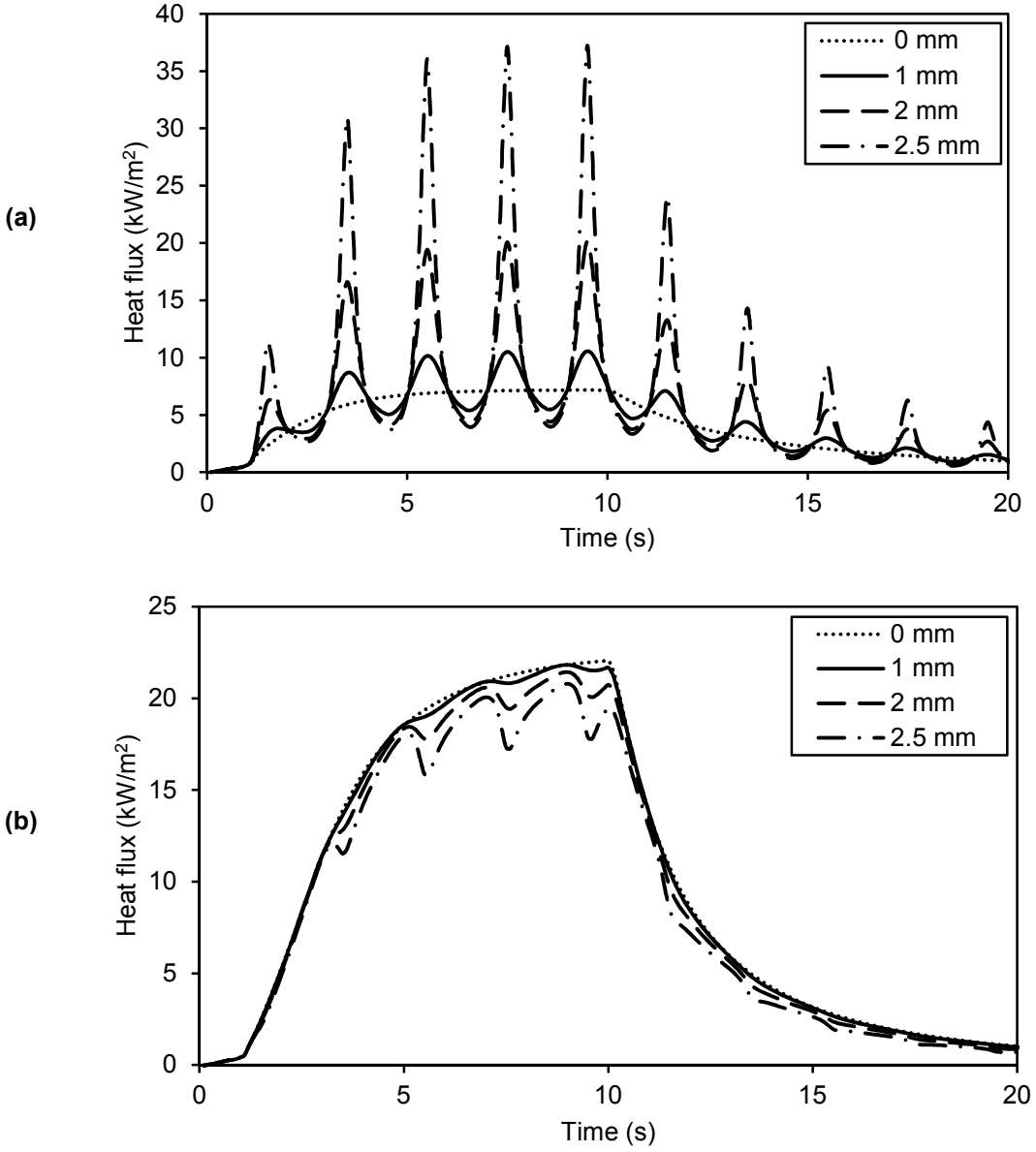

Figure 13. Influence of the movement amplitude on energy transfer across the air gap: (a) conductive heat flux at fabric-air interface, (b) emitted radiation from the fabric backside.

CHAPTER 5

NUMERICAL SIMULATION OF HEAT TRANSFER IN FIREFIGHTERS' PROTECTIVE CLOTHING WITH MULTIPLE AIR GAPS DURING FLASH FIRE EXPOSURE

Submitted as

A. Ghazy and D.J. Bergstrom, Numerical Simulation of Heat Transfer in Firefighters' Protective Clothing with Multiple Air Gaps during Flash Fire Exposure, Numerical Heat Transfer A, 2011.

Contribution of this Chapter to the Thesis

The research work presented in this chapter aims at achieving the fourth objective of the thesis. More specifically, the chapter describes a numerical model for heat transfer in a multiple layer protective clothing system with multiple air gaps between the clothing layers. The model accounts for the conduction-radiation heat transfer in each air gap within the clothing system. The influence of the size of each air gap width on the performance of the clothing was investigated.

Numerical Simulation of Heat Transfer in Firefighters' Protective Clothing with Multiple Air Gaps during Flash Fire Exposure

Ahmed Ghazy and Donald J. Bergstrom

Department of Mechanical Engineering, University of Saskatchewan, Saskatoon, Saskatchewan, Canada

Address correspondence to Donald J. Bergstrom, Department of Mechanical Engineering, University of Saskatchewan, 57 Campus Dr., Saskatoon, SK S7N 5A9, Canada. E-mail: Don.Bergstrom@usask.ca

ABSTRACT

A finite volume model was developed to simulate transient heat transfer in firefighters' protective clothing during flash fire exposure. The model domain consists of three layers of fire-resistant fabrics (outer shell, moisture barrier, and thermal liner) with two air gaps between the clothing layers, the human skin, and the air gap between the clothing and the skin. The model accounts for the combined conduction-radiation heat transfer in the air gaps entrapped between the clothing layers, and between the clothing and the skin. The variation in the air gap properties and energy content during both the exposure and the cool down periods was accounted for. Predictions were obtained for the temperature and heat flux distributions in the fabric layers, skin, and air gaps as a function of time. The influence of each air gap on the clothing performance was investigated as well. The paper demonstrates the importance of accurately modeling the contributions of the air gaps in order to predict the protective clothing performance.

NOMENCLATURE

A	surface area (m^2)

a, b	finite volume discrete equation coefficient, source term
C	heat capacity (J/kg K)
c_P	specific heat at constant pressure (J/kg K)
D_c^l	directional cosine integrated over $\Delta\Omega^l$
$\hat{e}$	unit vector in coordinate direction
G	incident radiation ($W/m^{2)}$
h	convective heat transfer coefficient (W/m^2K)
I	intensity (W/m^2)
k	thermal conductivity (W/mK)
L	thickness (m)
P	pre-exponential factor (1/s)
q''	heat flux (W/m^2)
$\vec{r}$	position vector (m)
R	ideal gas constant (J/mol K)
$\hat{s}$	unit vector in a given direction
S	source function
s	geometric distance (m)
T	temperature (K)
t	time (s)
W	clothing width (m)
y	linear vertical coordinate (m)

Greek Symbols

Ω	solid angle (sr)

θ	polar angle (rad)
φ	quantitative measure of skin damage
ϕ	azimuthal angle (rad)
ΔE	activation energy of skin (J/kmol)
ΔV	volume of control volume (m^3)
$\Delta\Omega^l$	control angle
ε	emissivity
γ	extinction coefficient of the outer shell (1/m)
κ	air gap absorption coefficient (1/m)
ρ	density (kg/m^3) or surface reflectivity
σ	Stefan-Boltzmann constant, 5.67×10^{-8} (W/m^2K^4)
τ	transmissivity
ω	blood perfusion rate (m^3/s)/m^3 of human tissue

Subscripts

air	air gap
amb	ambient conditions
b	human blood / black body
cnv	convection heat transfer
cr	human body core
ep, ds, sc	epidermis , dermis, subcutaneous human skin layers
exp	exposure
fbr	fabric fiber
fl	flame

g	hot gases
lin	thermal liner
msr	moisture barrier
n, s	north, south control volume faces
P	control volume central node
R , rad	radiation heat transfer
shl	outer shell
x, y, z	coordinate directions

Superscript

A	apparent
l	index for direction

1. INTRODUCTION

Municipal firefighters are exposed to a variety of fire exposures of different duration and intensity. Flash fire is one of the possible hazards that firefighters face when extinguishing fires. The typical intensity of flash fire exposure is about 80 kW/m^2 and it lasts for short duration (a few seconds) until the firefighter escapes from the fire location. Firefighters rely on their protective gear to avoid skin burn injuries that are caused by fire exposure. The protective performance of the clothing relates to the energy transfer through the clothing causing burn injury to the human skin on the other side of the clothing.

The typical protective clothing system consists of a single or multi-layer fire resistant fabric, the human skin, and an air gap between the fabric and the skin. Modeling the thermal performance of protective clothing has been extensively reported in the literature during the past decade. Each model in the literature contributes to modeling one of the abovementioned

elements of the protective clothing system. For example, in terms of modeling the fabric, Torvi [1, 2] and Zhu et al. [3] considered heat transfer in single layer fire resistant fabric during local flame and radiant exposure tests, respectively. Mell et al. [4] modeled heat transfer in firefighters' clothing during radiant exposure. Chitrphiromsri et al. [5, 6] and Song et al. [7] modeled coupled heat and mass transfer in firefighters' clothing during a flash fire exposure and local flame test, respectively. Pennes's model [8] was adopted by Chitrphiromsri et al. [5, 6] and Song et al. [9, 10] to model heat transfer in the human skin. Alternatively, Zhu et al. [11] used the thermal wave model of bioheat transfer introduced by Liu et al. [12] to model heat transfer in the human skin. All of these models used Henriques' burn integral [13] to estimate times to receive burn injuries.

The important role of the air gap between the fabric and the skin in the overall performance of protective clothing has been acknowledged by many researchers. Torvi et al. [1, 14] investigated the influence of the air gap width on the protective performance of a single layer fire-resistant fabric during a contact flame bench top test [15]. Three-dimensional body scanning technology was used [9, 10, 16, 17, 18] to determine the distribution and width of air gaps between the protective garment and the manikin body [19]. Sawcyn and Torvi [20] and Talukdar et al. [21] attempted to improve the modeling of the air gap in bench top tests. Ghazy and Bergstrom [22] introduced a numerical model for the transient heat transfer in protective clothing that accounts for the combined conduction-radiation heat transfer between the fabric and the skin. They [23] further investigated the influence of different parameters that affect the combined conduction-radiation heat transfer between the fabric and the skin, and the consequences on the clothing performance.

Often the air gaps entrapped in firefighters' protective clothing are either ignored [5, 6, 7, 24] or only modeled in an approximate way [4, 25]. However, proper modeling for the air gap between protective clothing and the skin [22, 23] has proven significant in predicting the clothing performance. This paper introduces a numerical model for the transient heat transfer in firefighters' protective clothing during flash fire exposure that effectively models the air gaps entrapped in the clothing system. More specifically, the model accounts for the combined conduction-radiation heat transfer in each air gap within the clothing system. In addition, the variation in the thermal properties of each air gap was accounted for during both the exposure and the cool down period. Finally, the paper briefly investigates the influence of each air gap on the overall performance of firefighters' clothing.

2. PROBLEM FORMULATION

Figure 1 shows a firefighting protective clothing system that consists of three different layers of fire-resistant fabric, the human skin which consists of epidermis, dermis, and subcutaneous layers, and an air gap of 1/4 in. (6.35 mm) between the clothing and the skin. The three layers of the fabric are, from the exterior to the interior of the clothing assembly, the outer shell (Kevlar®/PBI), the moisture barrier (breathable PTFE film on NOMEX®), and the thermal liner (Aramid batting quilted to NOMEX®), where two air gaps of 1 mm each separate the three fabric layers. The system is in a horizontal orientation where the outer shell is exposed to flame contact from a lab burner to simulate flash fire exposure.

Energy transfers by both convection and radiation from the flame to the outer shell, while it transfers by conduction through the fabric layers and through the human skin. Combined conduction-radiation is the mode of energy transfer through the two air gaps between the fabric layers and in the air gap between the clothing and the epidermis. Energy loss takes place from

the outer shell to the ambient by radiation during the exposure period and by convection and radiation during the cool down period.

The analysis of the protective clothing system can be divided into seven elements: three fabric layers (outer shell, moisture barrier, and thermal liner), the human skin, and the three air gaps. The energy equations of the seven elements are solved simultaneously where the continuity of temperature and heat flux represents the inner boundary conditions between these elements.

2.1. Heat Transfer in the Outer Shell

The energy equation of the outer shell (Kevlar®/PBI) during the exposure and cool down periods can be written [2, 26] as

$$\rho_{shl} C^{A}_{shl}(T) \frac{\partial T}{\partial t} = \frac{\partial}{\partial y}\left(k_{shl}(T) \frac{\partial T}{\partial y}\right) - \frac{\partial}{\partial y} q^{"}_{rad}(y) \qquad 0 < t \leq t_{exp} \qquad (1a)$$

$$\rho_{shl} c_{P,shl}(T) \frac{\partial T}{\partial t} = \frac{\partial}{\partial y}\left(k_{shl}(T) \frac{\partial T}{\partial y}\right) \qquad t > t_{exp} \qquad (1b)$$

where ρ_{shl}, $c_{P,shl}$, and k_{shl} are the outer shell density, specific heat, and thermal conductivity, respectively, t_{exp} is the exposure duration, C^{A}_{shl} is the outer shell apparent heat capacity [1, 2], and $q^{"}_{rad}(y)$ is the transmitted portion of the radiant heat flux from the flame to the outer shell. Beer's law [27] was employed [1, 2] to account for the absorption of the incident thermal radiation as it penetrates the pores of the fabric, i.e.

$$q^{"}_{rad}(y) = \sigma \varepsilon_g T_g^4 \, exp(-\gamma_{shl} y) \qquad (2)$$

where σ is the Stefan-Boltzmann constant, ε_g is the hot gases emissivity, T_g is the hot gases temperature (K), and γ_{shl} is the extinction coefficient of the outer shell that is given by

$$\gamma_{shl} = \frac{-ln(\tau_{shl})}{L_{shl}} \qquad (3)$$

where τ_{shl} is the outer shell transmissivity and L_{shl} is the outer shell thickness. The Kevlar®/PBI thermal conductivity was determined from the fiber to air fraction in the fabric [1, 2] as follows.

$$k_{shl}(T) = 0.8\, k_{air}(T) + \ 0.2\, k_{fbr}(T) \tag{4}$$

where k_{fbr} and k_{air} are the fiber thermal conductivity and the thermal conductivity of the air contained in the outer shell's pores, respectively.

The boundary conditions for the outer shell energy equation are as follows.

$$-k_{shl}(T)\frac{\partial T_{shl}}{\partial y}\bigg|_{y=0} = h_{fl}\left(T_g - T_{shl(y=0)}\right) - \sigma\varepsilon_{shl}\left(1-\varepsilon_g\right)\left(T^4_{shl(y=0)} - T^4_{amb}\right) \qquad 0 < t \le t_{exp} \tag{5a}$$

$$k_{shl}(T)\frac{\partial T_{shl}}{\partial y}\bigg|_{y=0} = h_{cnv}\left(T_{shl(y=0)} - T_{amb}\right) + \sigma\varepsilon_{shl}\left(T^4_{shl\ (y=0)} - T^4_{amb}\right) \qquad t > t_{exp} \tag{5b}$$

$$-k_{shl}(T)\frac{\partial T_{shl}}{\partial y}\bigg|_{y=L_{shl}} = q''_y(\vec{r})\big|_{y=L_{shl}} - k_{air1}(T)\frac{\partial T_{air1}}{\partial y}\bigg|_{y=L_{shl}} \qquad t > 0 \tag{6}$$

where h_{fl} is the convective heat transfer coefficient from the flame to the outer shell, ε_{shl} is the outer shell emissivity, T_{amb} is the ambient temperature (300 K), and h_{cnv} is the convective heat transfer coefficient from the outer shell to the ambient during the cool down period. The latter is estimated from an empirical correlation for natural convection heat transfer from a horizontal heated plate facing downwards to air at atmospheric pressure [27] as

$$h_{cnv} = 0.59\left(\frac{T_{shl(y=0)} - T_{amb}}{W_{shl}}\right)^{1/4} \tag{7}$$

where W_{shl} is the outer shell width. The emitted radiation from the outer shell backside surface, $q''_y(\vec{r})\big|_{y=L_{shl}}$, will be discussed later in this section.

The outer shell initial condition is

$$T_{shl}(x, t=0) = T_{amb} \tag{8}$$

2.2. Heat Transfer in the First Air Gap

The 1-D transient conduction-radiation heat transfer in the first air gap between the outer shell and the moisture barrier is expressed as

$$\rho_1(T)c_{P,1}(T)\frac{\partial T}{\partial t} = \frac{\partial}{\partial y}\left(k_1(T)\frac{\partial T}{\partial y}\right) - \frac{\partial q''_{R,1}}{\partial y} \tag{9}$$

where ρ_1, $c_{P,1}$, and k_1 are the air density, specific heat, and thermal conductivity in the first air gap, respectively. In order to estimate the divergence of the radiative heat flux through the air gap $\frac{\partial q''_{R,1}}{\partial y}$, the Radiative Transfer Equation (RTE) was solved within the first air gap as described below.

Considering the first air gap to behave as an absorbing and emitting medium, the change in the intensity along a radiation ray path is written [28] as

$$\frac{dI(\vec{r},\hat{s})}{ds} = -\kappa(\vec{r})I(\vec{r},\hat{s}) + \kappa(\vec{r})I_b(\vec{r}) \tag{10}$$

where I is the radiation intensity, which varies with the spatial position $\vec{r}$ and the angular direction $\hat{s}$, κ is the air gap absorption coefficient, s is the geometric distance, and I_b is the black body intensity defined as

$$I_b = \frac{\sigma T^4}{\pi} \tag{11}$$

where σ is the Stephan-Boltzmann constant and T is the medium temperature. The component of $\hat{s}$ in the y-direction is given by

$$\hat{s} = (sin\theta\ sin\phi)\hat{e}_y \tag{12}$$

where $\hat{e}_y$ is the unit vector in the y-direction, θ is the polar angle, and ϕ is the azimuthal angle.

Assuming both the outer shell backside and the moisture barrier front surface to behave as opaque gray surfaces, the boundary conditions for the air gap RTE (Eq. 10) are written as

$$I_{shl}(\vec{r},\hat{s}) = \varepsilon_{shl}(\vec{r})I_{b,shl}(\vec{r}) + \frac{\rho_{shl}(\vec{r})}{\pi}\int_{\hat{s}'\cdot\hat{n}<0} I(\vec{r},\hat{s}')|\hat{s}'\cdot\hat{n}|d\,\Omega' \qquad at\ y = L_{shl} \tag{13}$$

$$I_{msr}(\vec{r},\hat{s}) = \varepsilon_{msr}(\vec{r})I_{b,msr}(\vec{r}) + \frac{\rho_{msr}(\vec{r})}{\pi}\int_{\hat{s}'\cdot\hat{n}<0} I(\vec{r},\hat{s}')|\hat{s}'\cdot\hat{n}|d\,\Omega' \quad at\ y = L_{shl} + L_{air1} \tag{14}$$

where ε_{shl} and ρ_{shl} are the outer shell backside emissivity and reflectivity, ε_{msr} and ρ_{msr} are the moisture barrier front surface emissivity and reflectivity, $\hat{s}'$ is the reflected ray unit direction, $\hat{n}$ is the unit normal to the surface, $d\Omega'$ is the solid angle containing the reflected ray, and $L_{air1}$is the width of the first air gap.

The divergence of the radiative heat flux in Eq. (9) is obtained from the relation

$$\frac{\partial q''_{R,1}}{\partial y} = \kappa\left(4\pi I_b(\vec{r}) - G(\vec{r})\right) \tag{15}$$

where $G(\vec{r})$ is the incident radiation, which is defined as

$$G(\vec{r}) = \int_{4\pi} I(\vec{r},\hat{s})d\,\Omega \tag{16}$$

The radiation heat flux at both sides of the first air gap can be estimated as

$$q''_y(\vec{r})\big|_{y=L_{shl}} = \int_{4\pi} I(\vec{r},\hat{s})(\hat{s}\cdot\hat{e}_y)d\,\Omega\Big|_{y=L_{shl}} \tag{17}$$

$$q''_y(\vec{r})\big|_{y=L_{shl}+L_{air1}} = \int_{4\pi} I(\vec{r},\hat{s})(\hat{s}\cdot\hat{e}_y)d\,\Omega\Big|_{y=L_{shl}+L_{air1}} \tag{18}$$

The boundary conditions for the first air gap energy equation (Eq. (9)) are obtained from the continuity of temperature between the air gap and both the outer shell and the moisture barrier as follows.

$$T_{air1}|_{y=L_{shl}} = T_{shl}|_{y=L_{shl}} \qquad t > 0 \tag{19}$$

$$T_{air1}|_{y=L_{shl}+L_{air1}} = T_{msr}|_{y=L_{shl}+L_{air1}} \qquad t > 0 \tag{20}$$

where T_{msr} is the moisture barrier temperature.

The initial condition for the first air gap is

$$T_{air1}(y, t = 0) = T_{amb} \tag{21}$$

The variation in the thermal properties of the hot gases in the gap with temperature was accounted for using the properties of dry air [29].

2.3. Heat Transfer in the Moisture Barrier

The energy equation for the moisture barrier is written as

$$(\rho c_P)_{msr} \frac{\partial T}{\partial t} = \frac{\partial}{\partial y}\left(k_{msr}(T) \frac{\partial T}{\partial y}\right) \tag{22}$$

where ρ , c_P, and k have their conventional meaning.

The moisture barrier boundary conditions are

$$-k_{msr}(T) \left.\frac{\partial T_{msr}}{\partial y}\right|_{y=L_{shl}+L_{air1}} = q_y^{"}(\vec{r})\big|_{y=L_{shl}+L_{air1}} - k_{air1}(T) \left.\frac{\partial T_{air1}}{\partial y}\right|_{y=L_{shl}+L_{air1}} \qquad t > 0 \tag{23}$$

$$-k_{msr}(T) \left.\frac{\partial T_{msr}}{\partial y}\right|_{y=L_{shl}+L_{air1}+L_{msr}} = q_y^{"}(\vec{r})\big|_{y=L_{shl}+L_{air1}+L_{msr}} - k_{air1}(T) \left.\frac{\partial T_{air1}}{\partial y}\right|_{y=L_{shl}+L_{air1}+L_{msr}} \qquad t > 0 \tag{24}$$

where L_{msr} is the moisture barrier thickness. The radiation heat flux at the backside surface of the moisture barrier $q_y^{"}(\vec{r})\big|_{y=L_{shl}+L_{air1}+L_{msr}}$ can be estimated by solving the Radiative Transfer Equation (RTE) within the second air gap, as it will be discussed later in this section.

The moisture barrier initial condition is

$$T_{msr}(y, t = 0) = T_{amb} \tag{25}$$

2.4. Heat Transfer in the Second Air Gap

The 1-D transient conduction-radiation heat transfer in the second air gap between the moisture barrier and the thermal liner is expressed as

$$\rho_2(T)c_{P,2}(T)\frac{\partial T}{\partial t} = \frac{\partial}{\partial y}\left(k_2(T)\frac{\partial T}{\partial y}\right) - \frac{\partial q_{R,2}^{"}}{\partial y} \tag{26}$$

where ρ_2, $c_{P,2}$, and k_2 are the air density, specific heat, and thermal conductivity in the second air gap, respectively. The divergence of the radiative heat flux through the air gap $\frac{\partial q_{R,2}^{"}}{\partial y}$ is obtained by solving the Radiative Transfer Equation (Eq. 10) over the second air gap using the following boundary conditions.

$$I_{msr}(\vec{r}, \hat{s}) = \varepsilon_{msr}(\vec{r})I_{b,msr}(\vec{r}) + \frac{\rho_{msr}(\vec{r})}{\pi}\int_{\hat{s}'\cdot\hat{n}<0} I(\vec{r}, \hat{s}')|\hat{s}'\cdot\hat{n}|d\,\Omega' \quad at\ y = L_{shl} + L_{air1} + L_{msr} \tag{27}$$

$$I_{lin}(\vec{r}, \hat{s}) = \varepsilon_{lin}(\vec{r})I_{b,lin}(\vec{r}) + \frac{\rho_{lin}(\vec{r})}{\pi}\int_{\hat{s}'\cdot\hat{n}<0} I(\vec{r}, \hat{s}')|\hat{s}'\cdot\hat{n}|d\,\Omega' \quad at\ y = L_{shl} + L_{air1} + L_{msr} + L_{air2} \tag{28}$$

where ε_{msr} and ρ_{msr} are the moisture barrier backside emissivity and reflectivity, ε_{lin} and ρ_{lin} are the thermal liner front surface emissivity and reflectivity, and $L_{air2}$is the second air gap width. The radiation heat flux at both sides of the second air gap is expressed as

$$q_y^{"}(\vec{r})\big|_{y=L_{shl}+L_{air1}+L_{msr}} = \int_{4\pi} I(\vec{r}, \hat{s})(\hat{s}\cdot\hat{e}_y)d\,\Omega\Big|_{y=L_{shl}+L_{air1}+L_{msr}} \tag{29}$$

$$q_y^{"}(\vec{r})\big|_{y=L_{shl}+L_{air1}+L_{msr}+L_{air2}} = \int_{4\pi} I(\vec{r},\hat{s})(\hat{s}\cdot\hat{e}_y)d\,\Omega\Big|_{y=L_{shl}+L_{air1}+L_{msr}+L_{air2}} \tag{30}$$

The boundary conditions for the second air gap energy equation (Eq. (26)) are obtained from the continuity of temperature between the second air gap and both the moisture barrier and the thermal liner as follows.

$$T_{air2}\big|_{y=L_{shl}+L_{air1}+L_{msr}} = T_{msr}\big|_{y=L_{shl}+L_{air1}+L_{msr}} \qquad t>0 \tag{32}$$

$$T_{air2}\big|_{y=L_{shl}+L_{air1}+L_{msr}+L_{air2}} = T_{lin}\big|_{y=L_{shl}+L_{air1}+L_{msr}+L_{air2}} \qquad t>0 \tag{33}$$

where T_{lin} is the thermal liner temperature.

The second air gap initial condition is

$$T_{air2}(y, t=0) = T_{amb} \tag{33}$$

2.5. Heat Transfer in the Thermal Liner

The energy equation of the thermal liner is written as

$$(\rho c_P)_{lin}\frac{\partial T}{\partial t} = \frac{\partial}{\partial y}\left(k_{lin}\frac{\partial T}{\partial y}\right) \tag{34}$$

where ρ , c_P, and k have their conventional meaning.

The thermal liner boundary conditions are

$$-k_{lin}(T)\frac{\partial T_{lin}}{\partial y}\Big|_{y=L_{shl}+L_{air1}+L_{msr}+L_{air2}} = q_y^{"}(\vec{r})\big|_{y=L_{shl}+L_{air1}+L_{msr}+L_{air2}} - k_{air2}(T)\frac{\partial T_{air2}}{\partial y}\Big|_{y=L_{shl}+L_{air1}+L_{msr}+L_{air2}} \qquad t>0 \tag{35}$$

$$-k_{lin}(T)\frac{\partial T_{lin}}{\partial y}\Big|_{y=L_{shl}+L_{air1}+L_{msr}+L_{air2}+L_{lin}} = q_y^{"}(\vec{r})\big|_{y=L_{shl}+L_{air1}+L_{msr}+L_{air2}+L_{lin}} - k_{air3}(T)\frac{\partial T_{air3}}{\partial y}\Big|_{y=L_{shl}+L_{air1}+L_{msr}+L_{air2}+L_{lin}} \tag{36}$$

$$t > 0$$

where L_{lin} is the thickness of the thermal liner. The radiation heat flux at the backside surface of the thermal liner $q_y^{"}(\vec{r})\big|_{y=L_{shl}+L_{air1}+L_{msr}+L_{air2}+L_{lin}}$ can be estimated by solving the Radiative Transfer Equation (RTE) within the third air gap, as it will be discussed later in this section.

The thermal liner initial condition is

$$T_{lin}(y, t = 0) = T_{amb} \tag{37}$$

2.6. Heat Transfer in the Third Air Gap

The 1-D transient conduction-radiation heat transfer in the third air gap between the thermal liner and the skin is expressed as

$$\rho_3(T)c_{P,3}(T)\frac{\partial T}{\partial t} = \frac{\partial}{\partial y}\left(k_3(T)\frac{\partial T}{\partial y}\right) - \frac{\partial q_{R,3}^{"}}{\partial y} \tag{38}$$

where ρ_3, $c_{P,3}$, and k_3 are the air density, specific heat, and thermal conductivity in the third air gap, respectively. The divergence of radiative heat flux through the air gap $\frac{\partial q_{R,3}^{"}}{\partial y}$ is obtained by solving the Radiative Transfer Equation (Eq. 10) over the third air gap using the following boundary conditions:

$$I_{lin}(\vec{r}, \hat{s}) = \varepsilon_{lin}(\vec{r})I_{b,lin}(\vec{r}) + \frac{\rho_{lin}(\vec{r})}{\pi}\int_{\hat{s}'\cdot\hat{n}<0} I(\vec{r}, \hat{s}')|\hat{s}'\cdot\hat{n}|d\,\Omega' \qquad at\ y = L_{shl} + L_{air1} + L_{msr} + L_{air2} + L_{lin} \tag{39}$$

$$I_{ep}(\vec{r}, \hat{s}) = \varepsilon_{ep}(\vec{r})I_{b,ep}(\vec{r}) + \frac{\rho_{ep}(\vec{r})}{\pi}\int_{\hat{s}'\cdot\hat{n}<0} I(\vec{r}, \hat{s}')|\hat{s}'\cdot\hat{n}|d\,\Omega' \qquad at\ y = L_{shl} + L_{air1} + L_{msr} + L_{air2} + L_{lin} + L_{air3} \tag{40}$$

where ε_{lin} and ρ_{lin} are the thermal liner backside emissivity and reflectivity, ε_{ep} and ρ_{ep} are the epidermis surface emissivity and reflectivity, and L_{air3} is the width of the third air gap.

The radiation heat flux at both sides of the third air gap is expressed as

$$q_y^{"}(\vec{r})\big|_{y=L_{shl}+L_{air1}+L_{msr}+L_{air2}+L_{lin}} = \int_{4\pi} I(\vec{r},\hat{s})(\hat{s}\cdot\hat{e}_y)d\,\Omega\Big|_{y=L_{shl}+L_{air1}+L_{msr}+L_{air2}+L_{lin}} \tag{41}$$

$$q_y^{"}(\vec{r})\big|_{y=L_{shl}+L_{air1}+L_{msr}+L_{air2}+L_{lin}+L_{air3}} = \int_{4\pi} I(\vec{r},\hat{s})(\hat{s}\cdot\hat{e}_y)d\,\Omega\Big|_{y=L_{shl}+L_{air1}+L_{msr}+L_{air2}+L_{lin}+L_{air3}} \tag{42}$$

The boundary conditions for the third air gap energy equation (Eq. (38)) are obtained from the continuity of temperature between the air gap and both the thermal liner and the epidermis surface as follows.

$$T_{air3}\big|_{y=L_{shl}+L_{air1}+L_{msr}+L_{air2}+L_{lin}} = T_{lin}\big|_{y=L_{shl}+L_{air1}+L_{msr}+L_{air2}+L_{lin}} \qquad t>0 \tag{43}$$

$$T_{air3}\big|_{y=L_{shl}+L_{air1}+L_{msr}+L_{air2}+L_{lin}+L_{air3}} = T_{ep}\big|_{y=L_{shl}+L_{air1}+L_{msr}+L_{air2}+L_{lin}+L_{air3}} \qquad t>0 \tag{44}$$

where T_{ep} is the epidermis surface temperature.

The initial condition for the third air gap is

$$T_{air3}(y, t=0) = T_{amb} \tag{45}$$

2.7. Heat Transfer in the Human Skin

The human skin consists of epidermis, dermis, and subcutaneous layers where blood perfusion takes place in the latter two layers. The bioheat equation developed by Pennes [8] was employed to model heat transfer in the skin tissues. The energy equations for the three layers of the skin are written as

$$(\rho c_P)_{ep}\frac{\partial T}{\partial t} = \frac{\partial}{\partial y}\left(k_{ep}\frac{\partial T}{\partial y}\right) \tag{46}$$

$$(\rho c_P)_{ds}\frac{\partial T}{\partial t} = \frac{\partial}{\partial y}\left(k_{ds}\frac{\partial T}{\partial y}\right) + (\rho c_P)_b \omega_b (T_{cr} - T) \tag{47}$$

$$(\rho c_P)_{sc}\frac{\partial T}{\partial t} = \frac{\partial}{\partial y}\left(k_{sc}\frac{\partial T}{\partial y}\right) + (\rho c_P)_b \omega_b (T_{cr} - T) \tag{48}$$

where ω_b is the blood perfusion rate within the dermis and subcutaneous layers, T_{cr} is the human core body temperature, and ρ, c_P, and k have their conventional meaning.

The overall skin boundary conditions are

$$-k_{ep}\frac{\partial T_{ep}}{\partial y}\Big|_{y=L_{shl}+L_{air1}+L_{msr}+L_{air2}+L_{lin}+L_{air3}} = q_y^{"}(\vec{r})\Big|_{y=L_{shl}+L_{air1}+L_{msr}+L_{air2}+L_{lin}+L_{air3}}$$
$$-k_{air3}(T)\frac{\partial T_{air3}}{\partial y}\Big|_{y=L_{shl}+L_{air1}+L_{msr}+L_{air2}+L_{lin}+L_{air3}} \qquad t > 0 \tag{49}$$

$$T_{sc}\big|_{y=L_{shl}+L_{air1}+L_{msr}+L_{air2}+L_{lin}+L_{air3}+L_{ep}+L_{ds}+L_{sc}} = T_{cr} \qquad t > 0 \tag{50}$$

where L_{ep}, L_{ds}, L_{sc} are the epidermis, dermis, and subcutaneous layers widths, respectively. The continuity of temperature and heat flux represents the inner boundary conditions between the three skin layers.

A linear temperature distribution between 32.5ºC at the epidermis surface and 37ºC at the subcutaneous base (core body temperature) is assumed as the skin initial condition. Skin burn injury is expected to take place as the basal layer (interface between the epidermis and the dermis layers) temperature reaches 44^{o}C. Henriques integral [13] was employed to predict times to receive skin burn injuries as follows.

$$\varphi = \int_0^t P\, exp\left(-\frac{\Delta E}{RT}\right) dt \tag{51}$$

where the values for the pre-exponential factor P and the activation energy ΔE of the skin were determined by Weaver and Stoll [30] for second degree burn injury. The corresponding values for third degree burn injury were determined by Takata [31]. In order to calculate times for first and second degree burns, the basal layer temperature is used in the above integral, while the dermal base (the interface between the dermis and the subcutaneous) temperature is used in the integral to calculate times to third-degree burn. A first degree burn takes place when φ reaches 0.53, while a second degree burn occurs when φ reaches 1. A third degree burn occurs when φ reaches 1 with the dermal base temperature is used in the above integral.

3. NUMERICAL SOLUTION

The finite volume method [32] was employed in the discretization of the energy equations for the three layers of the clothing (outer shell, moisture barrier, and thermal liner), the three air gaps, and the skin (epidermis, dermis, and subcutaneous) along with their boundary conditions. A fully implicit scheme was used for the temporal discretization. The Gauss-Seidel point-by-point iterative scheme was used to solve the discrete energy equations. The solution procedure proceeds as follows. For each time step, temperatures from the previous time step are used as initial values for the iteration loop. The outer shell backside surface and moisture barrier front surface temperatures are used to solve the RTE through the first air gap. The moisture barrier backside surface and thermal liner front surface temperatures are used to solve the RTE through the second air gap. The thermal liner backside surface and epidermis surface temperatures are used to solve the RTE through the third air gap. Then, the divergence of the radiative heat flux within each air gap is calculated and employed in the energy equation for each air gap. The radiation heat flux at both sides of each air gap is calculated and employed in the boundary condition equations for the two elements surrounding that air gap. For example, the

radiation heat fluxes at the outer shell backside surface and at the moisture barrier front surface are used in the boundary equations for the first air gap. Then new temperatures are calculated by visiting each control volume starting from the outer shell surface and ending with the subcutaneous base. The thermal properties for the outer shell and the three air gaps, the temperature values in the source terms, and the divergence of radiative heat flux are updated based on the current temperature within the iteration loop. The iterative solver continues until the non-dimensional change in the temperature field becomes less than 10^{-5}. Finally both the basal layer and the dermal base temperatures are used in Henriques' integral (Eq. (51)) to predict times to receive skin burn injuries.

The RTE for each air gap was solved along with its boundary conditions using the Finite Volume method [33]. By integrating the RTE over a spatial control volume and a control angle, the 1-D discrete equation using the step scheme is written as

$$a_P^l I_P^l = a_N^l I_N^l + a_S^l I_S^l + b^l \tag{52}$$

where

$$a_N^l = max(-A_n D_{cn}^l, 0), a_S^l = max(-A_s D_{cs}^l, 0) \tag{53}$$

$$a_P^l = max(A_n D_{cn}^l, 0) + max(A_s D_{cs}^l, 0) + \kappa_P \Delta V_P \Delta\Omega^l \tag{54}$$

$$b^l = S_P^l \Delta V_P \Delta\Omega^l \tag{55}$$

$$D_{cn}^l = \int_{\Delta\Omega^l} \left(\hat{s}^l \cdot \hat{e}_y\right) d\Omega, D_{cs}^l = -D_{cn}^l \tag{56}$$

$$\Delta\Omega^l = \int_{\Delta\Omega^l} d\Omega \tag{57}$$

$$S_P^l = \kappa_P I_{b,P} \tag{58}$$

4. RESULTS AND DISCUSSION

The thermophysical properties of the firefighters' clothing used in the simulation are listed in Table 1 along with the burner parameters. The thermophysical properties of the human skin are listed in Table 2. The simulation assumed a contact flame exposure with a nominal heat flux of about 83 kW/m^2 for 10 s followed by 60 s of cool down.

In order to verify the influence of the air gaps entrapped between the clothing layers on the performance of firefighters' clothing, the present model was simplified to the more common assumption of direct contact between the clothing layers. The third air gap of 1/4 in. (6.4 mm) between the clothing and the skin was retained in the simplified model, while the first and second air gaps of 1 mm between the clothing layers were eliminated. Figure 2 shows the comparison between the temperature distributions predicted by the present model and those predicted by the simplified model during both the exposure and the cool down periods. As shown in Figure 2(a), the simplified model (no gaps) under predicted the outer shell surface temperature by about 3% by the end of the exposure period. It also over predicted both the moisture barrier surface temperature by about 10% and the thermal liner surface temperature by about 58%. Clearly these results can be attributed to the neglect of the insulating effect of the air gaps between the clothing layers. Figure 2(b) shows the differences between the present model and the simplified model in predicting the temperature distribution within the skin. The simplified model over predicted the temperature of the epidermis surface and the basal layer during the exposure period; however, this difference gradually vanishes during the cool down period. In contrast, the over prediction in the dermal base temperature increases during the cool down period due to the energy accumulation in the subcutaneous layer during the cool down period [22]. In summary, although the width of the air gaps between the clothing layers look minimal,

their significant role in determining the clothing performance indicates the necessity of modeling the air gaps properly.

The temporal temperature distribution within the firefighters' protective clothing system is illustrated in Figure 3. As shown in Figure 3(a), by the end of the exposure period, the temperature drop across the first, second, and third air gap are about 80°C, 110°C, and 105°C, respectively. Recall that the first and the second air gaps are of 1 mm width each while the width of the third air gap is 6.4 mm. The temperature drop across the first and second air gap compared to that of the third air gap demonstrates the significance of modeling them properly. An increasing delay in the time to reach the maximum temperature before cool down can be realized through clothing layers from the exterior to interior. For example, both sides of the outer shell reach their maximum temperature at the end of the exposure, while the front and back surfaces of the thermal liner reach their maximum temperature 1.5 s and 4.5 s after the end of the exposure, respectively. The temporal temperature distribution through the skin is shown in Figure 3(b). There is almost no significant increase in the skin layer temperatures during the exposure period due to the protection provided by the clothing. However, the rapid increase in the skin temperature during the cool down period reflects the influence of the energy stored in the clothing on its performance. Based on the parameters used in the simulation, skin burn injury would not take place as none of the skin layers reach 44°C (the temperature for feeling pain in the skin) during either the exposure or the cool down periods.

Figure 4 illustrates the spatial temperature distribution in the clothing system during both the exposure and the cool down period. As shown in Figure 4(a), about 75% of the temperature rise in the outer shell layer takes place during the first three seconds of exposure, while there is no significant change in the thermal liner temperature until after the third second of

exposure. During the cool down period, about 50% of the temperature drop in the outer shell takes place during the first ten seconds of the cool down period, while the temperature of the thermal liner keeps on increasing. The third air gap temperature keeps on increasing as well during the first ten seconds of the cool down period, see Figure 4(b). Even by the end of the cool down period (60 s), there is a significant temperature rise in the third air gap temperature. Part of the energy stored in the third air gap will most likely be discharged to the skin. This explains the large increase in the skin temperature during the cool down period that is shown in Figure 4(c).

The variation in the thermal properties of the three air gaps is illustrated by Figure 5. In this figure, front and back refer to the air gap boundaries. Figure 5(a) shows a smaller variation in the volumetric heat capacity of the first and the second air gaps compared to that of the third air gap. This reflects the ratio of their widths. The corresponding variation in the thermal conductivity within the three air gaps is illustrated in Figure 5(b). In general, the variation in the air gap properties during both the exposure and the cool down period is significant and needs to be included in the model.

The energy balance of the system shown in Figure 6, although complex, can provide further insight into the mechanism of heat transfer within firefighters' clothing. The total heat flux of exposure (about 83 kW/m^2) transfers in the form of both convection ($\dot{q}''_{cnv\_fl}$) and radiation ($\dot{q}''_{rad\_fl}$) heat fluxes from the hot gases to the outer shell as shown in Figure 6(a). A portion of this energy is stored in the outer shell ($\dot{q}''_{strg\_shl}$) causing a temperature rise and thermochemical reactions in the outer shell. The remainder of this energy is transferred in the form of radiation ($\dot{q}''_{rad\_shl-amb}$) and convection ($\dot{q}''_{cnv\_shl-amb}$) heat fluxes from the exposed surface of the shell; and in the form of conduction ($\dot{q}''_{cnd\_shl-air1}$) and radiation ($\dot{q}''_{rad\_shl-air1}$) heat fluxes from the backside of the shell to the first air gap. Note that the radiation heat transfer

from the hot gases to the shell (q''_{rad_fl}) takes place only during the exposure period while the convection heat transfer from the outer shell to the ambient ($q''_{cnv\_shl-amb}$) takes place only during the cool down period.

The energy balance for the moisture barrier is illustrated by Figure 6(b). The energy inputs to the moisture barrier are the conduction ($q''_{cnd\_air1-msr}$) and radiation ($q''_{rad\_air1-msr}$) heat fluxes from the first air gap to the front surface of the moisture barrier. A good portion of this energy is stored in the moisture barrier (q''_{strg_msr}) causing the temperature rise in this layer of the clothing. The remainder is transferred in the form of conduction ($q''_{cnd\_msr-air2}$) and radiation ($q''_{rad\_msr-air2}$) heat fluxes from the backside surface of the moisture barrier to the second air gap.

The energy balance of the thermal liner is depicted in Figure 6(c). Energy transfers from the second air gap to the front surface of the thermal liner in the form of conduction ($q''_{cnd\_air2-lin}$) and radiation ($q''_{rad\_air2-lin}$) heat transfer. Energy also transfers from the backside surface of the thermal liner in the form of conduction ($q''_{cnd\_lin-air3}$) and radiation ($q''_{rad\_lin-air3}$) heat transfer to the third air gap. The difference between the input and output is stored in the thermal liner (q''_{strg_lin}) causing a rise in its temperature. Note that the energy transfer from the backside surface of the thermal liner does not begin until the fourth second of exposure, and it keeps on increasing during the first five seconds of the cool down period.

As shown in Figure 6(d), the energy input to the skin is in the form of conduction ($q''_{cnd\_air3-ep}$) and radiation ($q''_{rad\_air3-ep}$) heat transfer at the interface between the third air gap and the epidermis surface. Only a small portion of this energy is stored in the epidermis layer (q''_{strg_ep}) raising its temperature. The rest of this energy is stored in the dermis (q''_{strg_ds}) and

subcutaneous (q''_{strg_sc}) layers. Note, the blood perfusion through the latter two layers has a relatively insignificant influence on the energy transfer through the skin.

Recall that the width of both the first and second air gap was taken as 1 mm to represent the typical spacing between layers. The effect of increasing the first and second air gap widths on the overall heat transfer was investigated as a potential improvement to the performance of firefighters' clothing. The influence of a variation in the width of each of them was studied separately, while the width of the other one was kept at 1 mm. The influence of a variation in the third air gap width on the clothing performance was also investigated where the widths for the first and second air gaps were kept at 1 mm.

Figure 7 illustrates the effect of increasing the first air gap width on the skin temperature. Increasing the first air gap width from 1 mm to 4 mm causes a small reduction in the epidermis surface temperature, the basal layer temperature, and the dermal base temperature as shown in Figures 7(a), 7(b), and 7(c), respectively. It is shown that the reduction in these layers' temperatures decreases as the air gap width increases.

The effect of increasing the width of the second air gap on the skin temperature is illustrated by Figure 8. Similar to the case of the first air gap, increasing the second air gap width from 1 mm to 4 mm causes a small reduction in the skin temperature as shown in Figures 8(a), 8(b), and 8(c). As before, the reduction in the skin temperature decreases as the air gap width increases. A comparison between Figures 7 and 8 shows that increasing the second air gap width has a larger effect on reducing the skin temperature than of increasing the first air gap width.

The width of the third air gap was taken in this study as 1/4 in. (6.4 mm) corresponding to the air gap width of the standard TPP test. The influence of a variation in the third air gap width from 1 mm to 6 mm on the skin temperature is depicted by Figure 9. The variation in the

third air gap width has a similar trend as that of the first and second air gaps. However, the reduction in the skin temperature due to an increase in the third air gap width is higher than for the first or the second air gap widths. This is because of its location directly next to the skin.

5. CONCLUSIONS

A finite volume model for the transient heat transfer in firefighters' protective clothing was developed. The model used a more sophisticated and appropriate analysis for the air gaps entrapped in the clothing system compared to most other models in the literature. The model was employed to explore the transient temperature distribution and energy content of the clothing system. These results provide insight as to the contribution of each layer to the overall protective performance of the clothing system, which in turn could provide a rational basis for improving the clothing performance. The paper investigated the influence of each air gap within the system on the overall performance of the clothing system. The simulation indicates that the influence of the air gaps entrapped in the clothing system on the overall performance increases from the exterior to the interior. For example, the influence of the air gap between the moisture barrier and the thermal liner is greater than that of the air gap between the outer shell and the moisture barrier. The additional protection provided by the clothing as each air gap width increases quickly drops off. However, neglecting the air gaps entrapped in the clothing would dramatically underestimate the clothing protective performance.

REFERNCES

1. D. A. Torvi, Heat Transfer in Thin Fibrous Materials under High Heat Flux Conditions, Ph.D. Thesis, University of Alberta, Edmonton, Alberta, 1997.
2. D.A. Torvi, and J.D. Dale, Heat Transfer in Thin Fibrous Materials under High Heat Flux, Fire Technology, vol. 35, pp. 210-231, 1999.

3. F. Zhu, and W. Zhang, Modeling Heat Transfer for Heat-resistant Fabrics Considering Pyrolysis Effect under an External Heat Flux, J. Fire Sciences, vol. 27, pp. 81-96, 2009.

4. W. E. Mell, and J. R. Lawson, Heat Transfer Model for Fire Fighter's Protective Clothing, Fire Technology, vol. 36, pp. 39-68, 2000.

5. P. Chitrphiromsri, and A.V. Kuznetsov, Modeling Heat and Moisture Transport in Firefighter Protective Clothing during Flash Fire Exposure, Heat Mass Transfer, vol. 41, pp. 206-215, 2005.

6. P. Chitrphiromsri, Modeling of Thermal Performance of Firefighter Protective Clothing during the Intense Heat Exposure, Ph.D. Thesis, North Carolina State University, Raleigh, North Carolina, 2004.

7. G. Song, P. Chitrphiromsri, D. Ding, Numerical Simulation of Heat and Moisture Transport in Thermal Protective Clothing Under Flash Fire Conditions, Int. J. Occupational Safety and Ergonomics, vol. 14(1), pp. 89-106, 2008.

8. H.H. Pennes, Analysis of tissue and arterial blood temperatures in resting human forearm, J. Applied Physiology, vol. 1, pp. 93–122, 1948.

9. G. Song, R.L. Barker, H. Hamouda, A.V. Kuznetsov, P. Chitrphiromsri, and R.V. Grimes, Modeling the Thermal Protective Performance of Heat Resistant Garments in Flash Fire Exposures, Textile Research J., vol. 74, pp. 1033-1040, 2004.

10. G. Song, Modeling Thermal Protection Outfits for Fire Exposures, Ph.D. Thesis, North Carolina State University, Raleigh, North Carolina, 2002.

11. F. Zhu, and W. Zhang, Evaluation of Thermal Performance of Flame-resistant Fabrics Considering Thermal Wave Influence in Human Skin Model, J. Fire Sciences, vol. 24, pp. 465-485, 2006.

12. J. Liu, C. Xu, and X.X. Lisa, New Thermal Wave Aspects on Burn Evaluation of Skin Subjected to Instantaneous Heating, IEEE Transactions on Biomedical Engineering, vol. 46(4), pp. 420-428, 1999.

13. F.C. Henriques, Jr., A.R. Moritz, Studies of thermal injuries I: The conduction of heat to and through skin and the temperatures attained therein. A theoretical and experimental investigation, American J. Pathology, vol. 23, pp. 531–549, 1947.

14. D.A. Torvi, J.D. Dale, and B. Faulkner, Influence of Air Gaps on Bench Top Test Results of Flame Resistant Fabrics, J. Fire Protection Engineering, vol. 10, pp. 1-12, 1999.

15. American Society for Testing Materials, ASTM D 4108-87 Standard Test Method for Thermal Protective Performance of Materials and Clothing by open-Flame Method, West Conshohocken, PA, 1987.

16. I.Y. Kim, C. lee, P. Li, B. D. Corner, and S. Paquette, Investigation of Air Gaps Entrapped in Protective Clothing Systems, Fire and Materials, vol. 26, pp. 121-126, 2002.

17. T. Mah, and G. Song, Investigation of the Contribution of Garment Design to Thermal Protection. Part 1: Characterizing Air Gaps using Three-dimensional body Scanning for Women`s Protective Clothing, Textile Research Journal, vol. 80(13), pp. 1317-1329, 2010.

18. T. Mah, and G. Song, Investigation of the Contribution of Garment Design to Thermal Protection. Part 2: Instrumented Female Mannequin Flash-fire Evaluation System, Textile Research Journal, vol. 80(14), pp. 1473-1487, 2010.

19. American Society for Testing Materials, ASTM F 1930-00 Standard Test Method for Evaluation of Flame Resistant Clothing for Protection Against Flash Fire Simulations Using an Instrumented Thermal Manikin, West Conshohocken, PA, 2000.

20. C.M.J. Sawcyn, D.A. Torvi, Improving Heat Transfer Models of Air Gaps in Bench Top Tests of Thermal Protective Fabrics, Textile Res. J. 79 (2009) 632–644.

21. P. Talukdar, D.A. Torvi, C.J. Simonson and C.M.J. Sawcyn, Coupled CFD and Radiation Simulation of Air Gaps in Bench Top Protective Fabric Tests, Int. J. Heat Mass Transfer, vol. 53, pp. 526-539, 2010.

22. A. Ghazy, D.J. Bergstrom, Numerical Simulation of Transient Heat Transfer in a Protective Clothing System during a Flash Fire Exposure. Numerical Heat Transfer A, vol. 58(9), pp. 702-724, 2010.

23. A. Ghazy, D.J. Bergstrom, Influence of the Air Gap between Protective Clothing and Skin on clothing Performance during Flash Fire Exposure. Heat Mass Transfer, DOI: 10.1007/s00231-011-0791-y.

24. P. Chitrphiromsri, A.V. Kuznetsov, G. Song, R.L. Barker, Investigation of Feasibility of Developing Intelligent Firefighter-Protective Garments Based on the Utilization of a Water-Injection System, Numerical Heat Transfer A, vol. 49, pp. 427–450, 2006.

25. Y.Y. Jiang, E. Yanai, K. Nishimura, H. Zhang, N. Abe, M. Shinohara, K. Wakatsuki, An Integrated Numerical Simulator for Thermal Performance Assessments of Firefighters' Protective Clothing, Fire Safety Journal, vol. 45, pp. 314-326, 2010.

26. D.A. Torvi, and T.G. Threlfall, Heat Transfer Model of Flame Resistant Fabrics During Cooling After Exposure to Fire, J. Fire Technology, vol. 42, pp. 27-48, 2006.

27. J.P. Holman, Heat Transfer, 8th edition, McGraw-Hill Co., 1997.

28. M.F. Modest, Radiative Heat Transfer, 2nd edition, Academic Press, New York, 2003.

29. F.P. Incropera, and D.P. DeWitt, Fundamentals of Heat and Mass Transfer, 5th edition, John Wiley & Sons, Inc., New York, 2002.

30. J.A. Weaver, and A.M. Stoll, Mathematical Model of Skin Exposed to Thermal Radiation, Aerospace Medicine, vol. 40, pp. 24-30, 1969.

31. A.N. Takata, J. Rouse, and T. Stanley, Thermal Analysis Program, I.I.T. Research Institute Report IITRI-J6286, Chicago, 1973.

32. S.V. Patankar, Numerical Heat Transfer and Fluid Flow, Taylor & Francis, Washington, DC, 1980.

33. J. C. Chai and S. V. Patankar, Finite-Volume Method for Radiation Heat Transfer, Advances in Numerical Heat Transfer, editors; W. J. Minkowycz, and E. M. Sparrow, vol. 2, Ch. 4, Taylor & Francis, pp. 109-141, 2000.

Table 1. Clothing and burner parameters [1, 6]

	Property	Value
L_{shl}	Outer shell thickness	0.6 mm
ρ_{shl}	Outer shell density	323 kg/m^3
γ_{shl}	Outer shell extinction factor	0.01
ε_{shl}	Outer shell emissivity	0.9
τ_{shl}	Outer shell transmissivity	0.01
L_{msr}	Moisture barrier thickness	0.85 mm
ρ_{msr}	Moisture barrier density	250 kg/m^3
$c_{P,msr}$	Moisture barrier specific heat	1150 J/kg K
k_{msr}	Moisture barrier thermal conductivity	0.05 W/m K
L_{lin}	Thermal liner thickness	0.95 mm
ρ_{lin}	Thermal liner density	220 kg/m^3
$c_{P,lin}$	Thermal liner specific heat	1300 J/kg K
k_{lin}	Thermal liner thermal conductivity	0.052 W/m K
T_g	Hot gases temperature	2000 K
ε_g	Hot gases emissivity	0.02
h_{fl}	Flame convective heat transfer coefficient	40 W/m^{2}K

Table 2. Human skin thermophysical properties

Property	Epidermis	Dermis	Subcutaneous	Blood
Thickness (m)	8×10^{-5}	2×10^{-3}	1×10^{-2}	-
Density (Kg/m^3)	1200	1200	1000	1060
Specific Heat (J/Kg^oC)	3598	3222	2760	3770
Thermal Conductivity (W/m^oC)	0.255	0.523	0.167	-
Blood Perfusion Rate $(m^3/s)/m^3$ tissue	-	-	-	1.25×10^{-3}

Figure Captions

Figure 1. The multiple layers protective clothing schematic diagram.

Figure 2. Influence of the air gaps between the fabric layers on the temperature within the protective clothing system: (a) fabric layers and (b) skin layers.

Figure 3. The temporal temperature distribution within the protective clothing system: (a) fabric and air gap layers and (b) skin.

Figure 4. The spatial temperature distribution within the protective clothing system: (a) fabric layers and air gaps, (b) third air gap, and (c) skin layers.

Figure 5. The variation in the air properties within the protective clothing system: (a) volumetric heat capacity and (b) thermal conductivity.

Figure 6. The protective clothing system energy balance: (a) outer shell, (b) moisture barrier, (c) thermal liner, and (d) human skin.

Figure 7. Influence of the air gap width between the outer shell and the moisture barrier on the clothing protective performance: (a) epidermis surface temperature, (b) basal layer temperature, and (c) dermal base temperature.

Figure 8. Influence of the air gap width between the moisture barrier and the thermal liner on the clothing protective performance: (a) epidermis surface temperature, (b) basal layer temperature, and (c) dermal base temperature.

Figure 9. Influence of the air gap width between the thermal liner and the skin on the clothing protective performance: (a) epidermis surface temperature, (b) basal layer temperature, and (c) dermal base temperature.

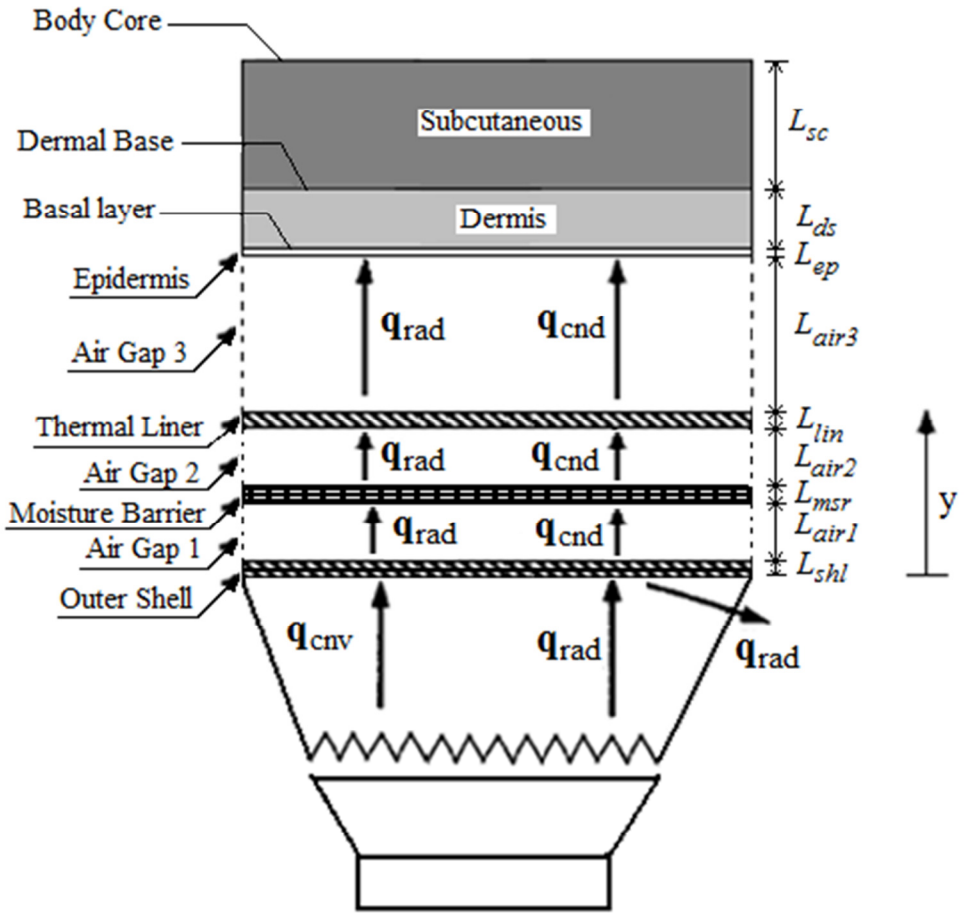

Figure 1. The multiple layers protective clothing schematic diagram.

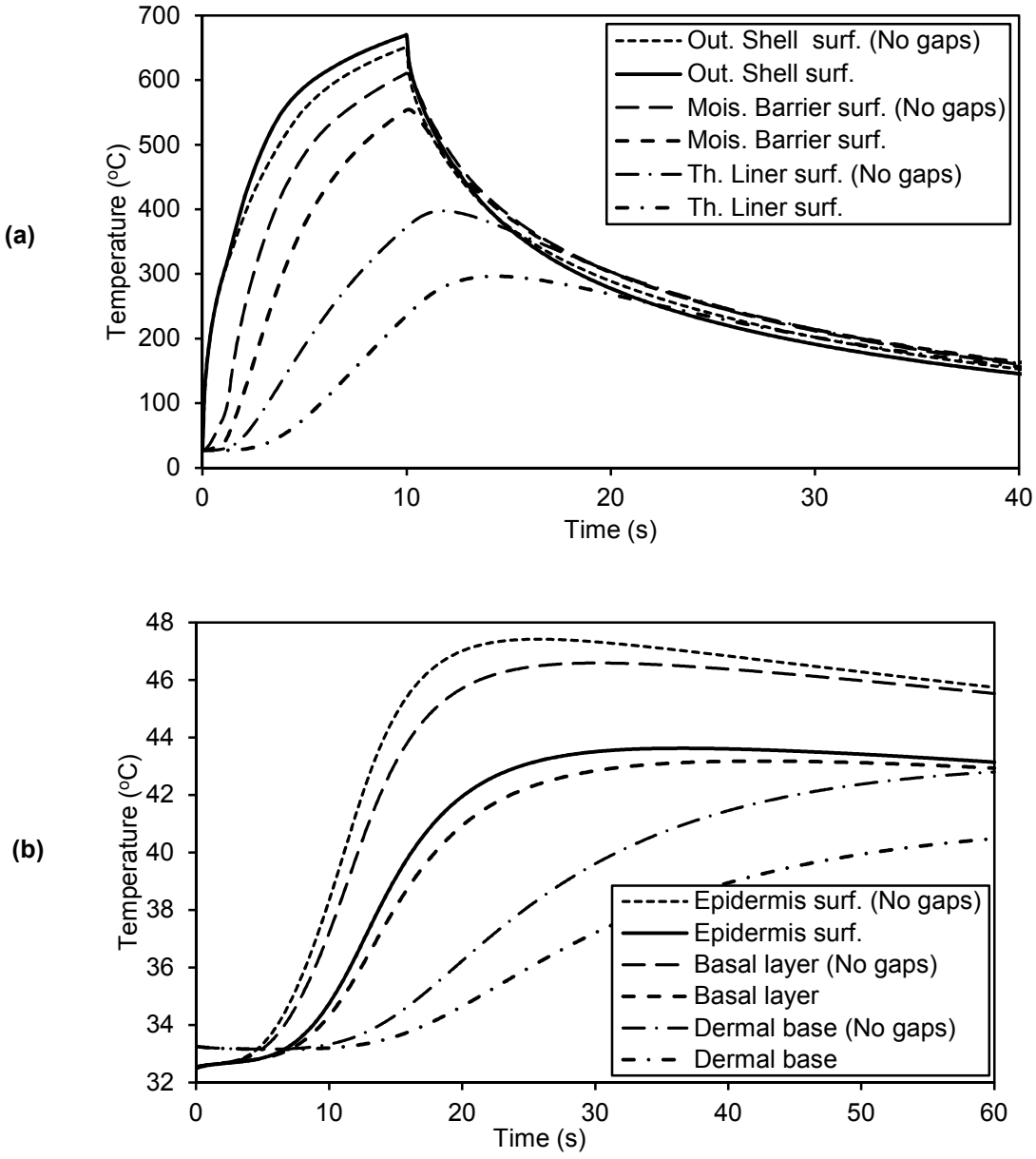

Figure 2. Influence of the air gaps between the clothing layers on the temperature within the protective clothing system: (a) fabric layers and (b) skin layers.

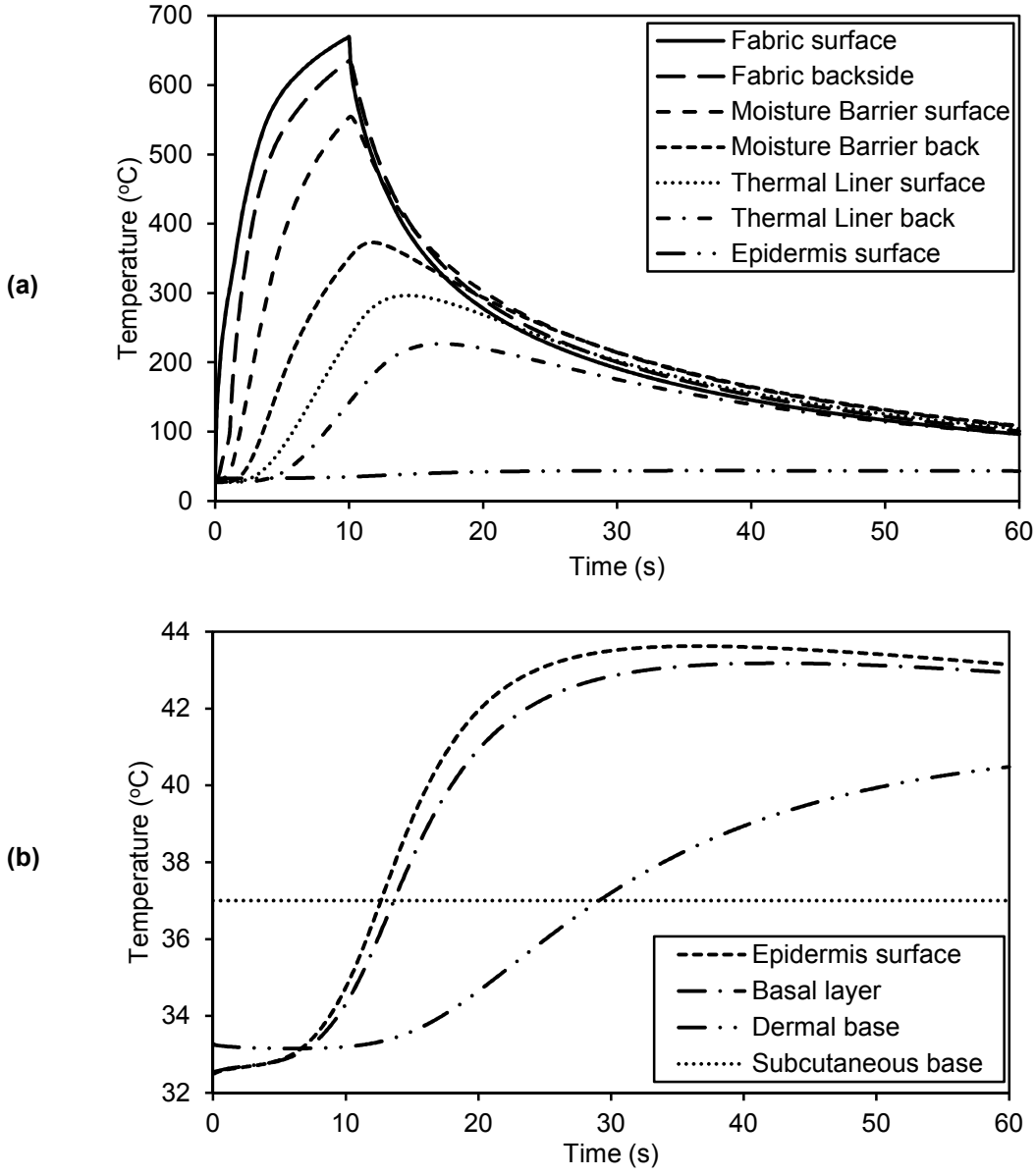

Figure 3. The temporal temperature distribution within the protective clothing system: (a) fabric and air gap layers and (b) skin.

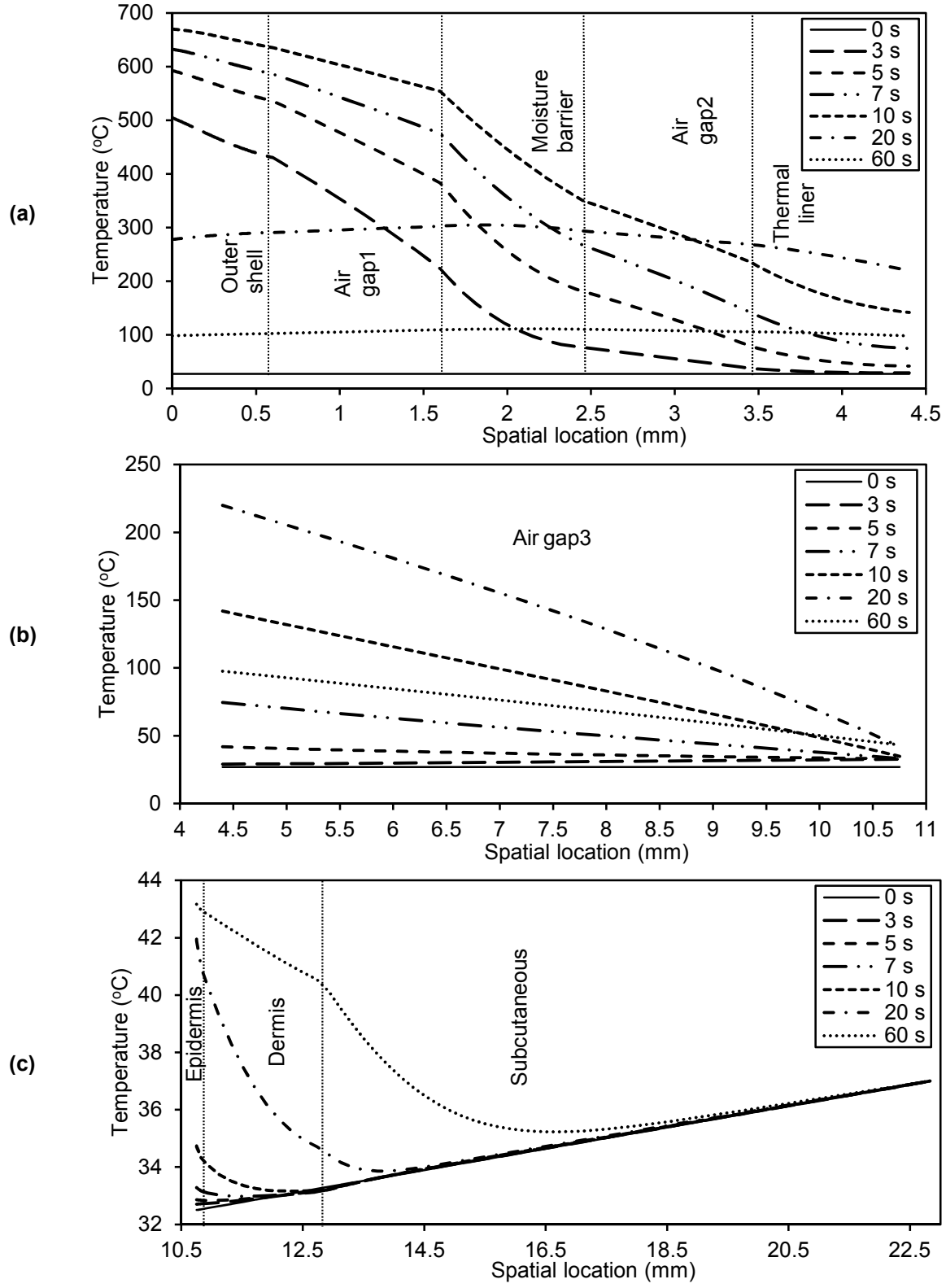

Figure 4. The spatial temperature distribution within the protective clothing system: (a) fabric layers and air gaps, (b) third air gap, and (c) skin layers.

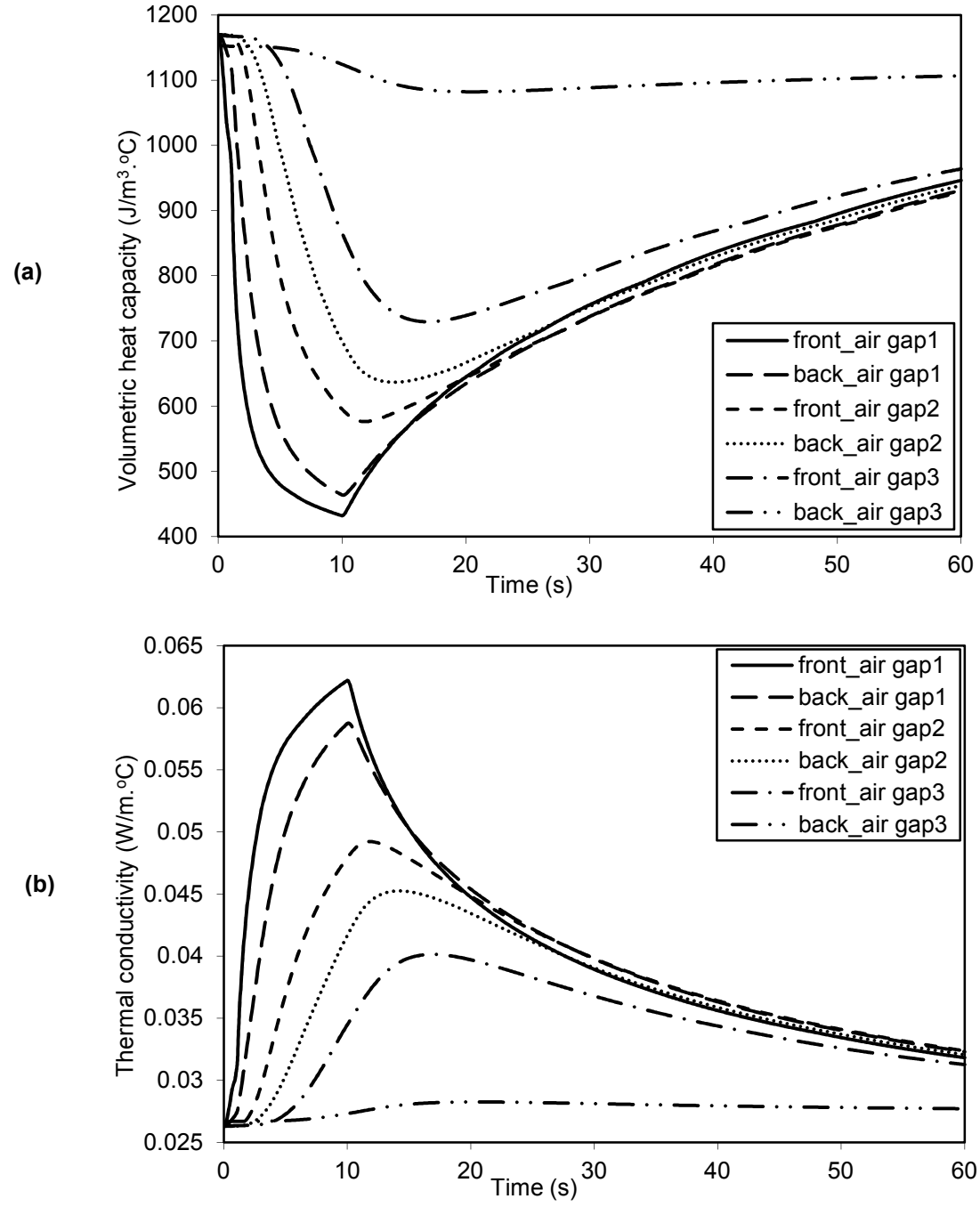

Figure 5. The variation in the air properties within the protective clothing system: (a) volumetric heat capacity and (b) thermal conductivity.

(a)

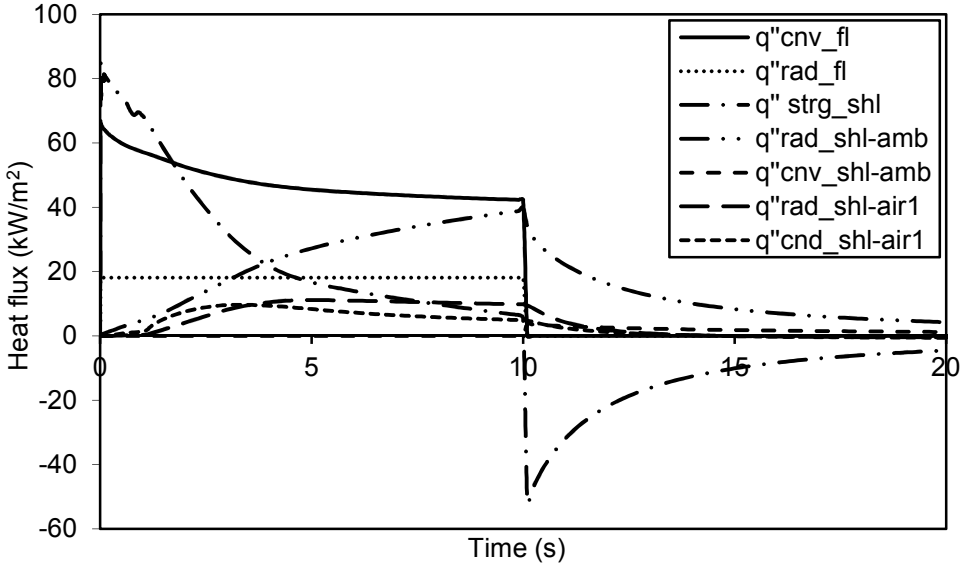
q"cnv_fl
q"rad_fl
q" strg_shl
q"rad_shl-amb
q"cnv_shl-amb
q"rad_shl-air1
q"cnd_shl-air1
Heat flux (kW/m2)
Time (s)
100
80
60
40
20
0
-20
-40
-60
0
5
10
15
20

(b)

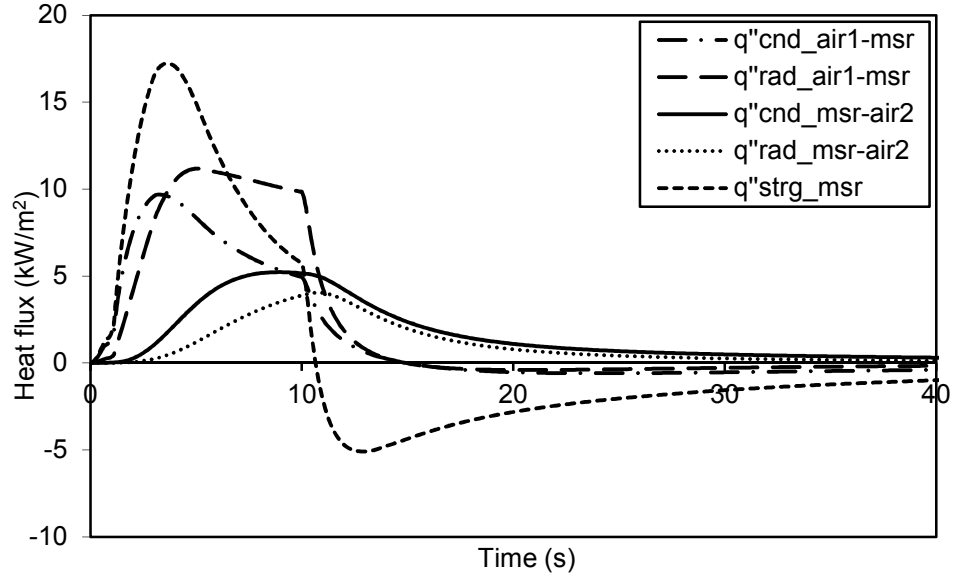
q"cnd_air1-msr
q"rad_air1-msr
q"cnd_msr-air2
q"rad_msr-air2
q"strg_msr
Heat flux (kW/m2)
Time (s)
20
15
10
5
0
-5
-10
0
10
20
30
40

(c)

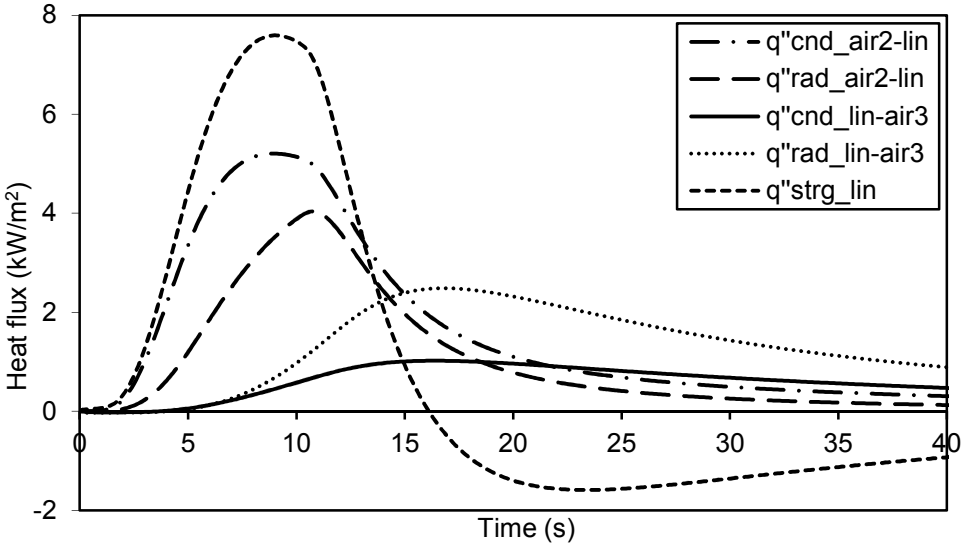
q"cnd_air2-lin
q"rad_air2-lin
q"cnd_lin-air3
q"rad_lin-air3
q"strg_lin
Heat flux (kW/m2)
Time (s)
8
6
4
2
0
-2
0
5
10
15
20
25
30
35
40

(d)

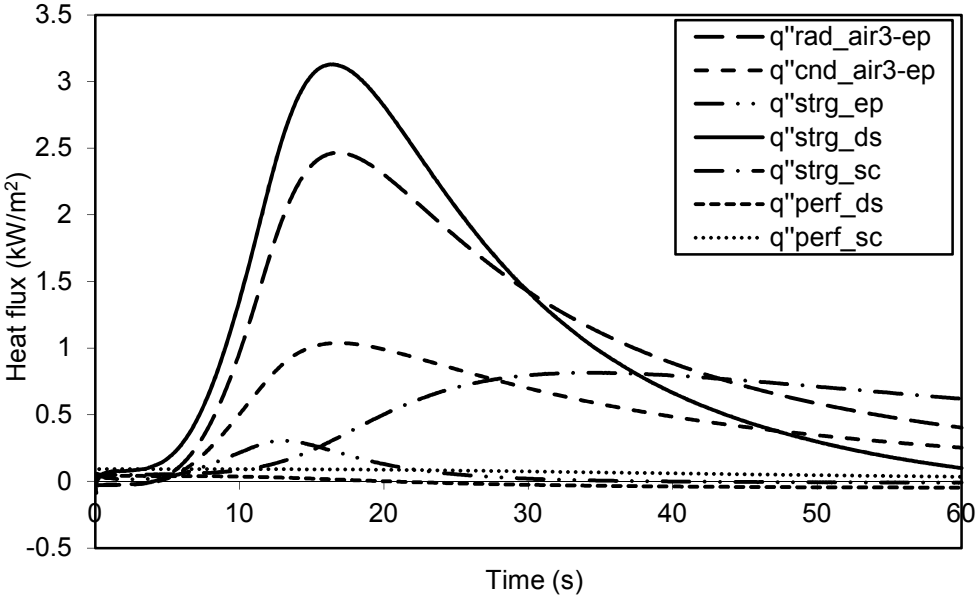

Figure 6. The protective clothing system energy balance: (a) outer shell, (b) moisture barrier, (c) thermal liner, and (d) human skin.

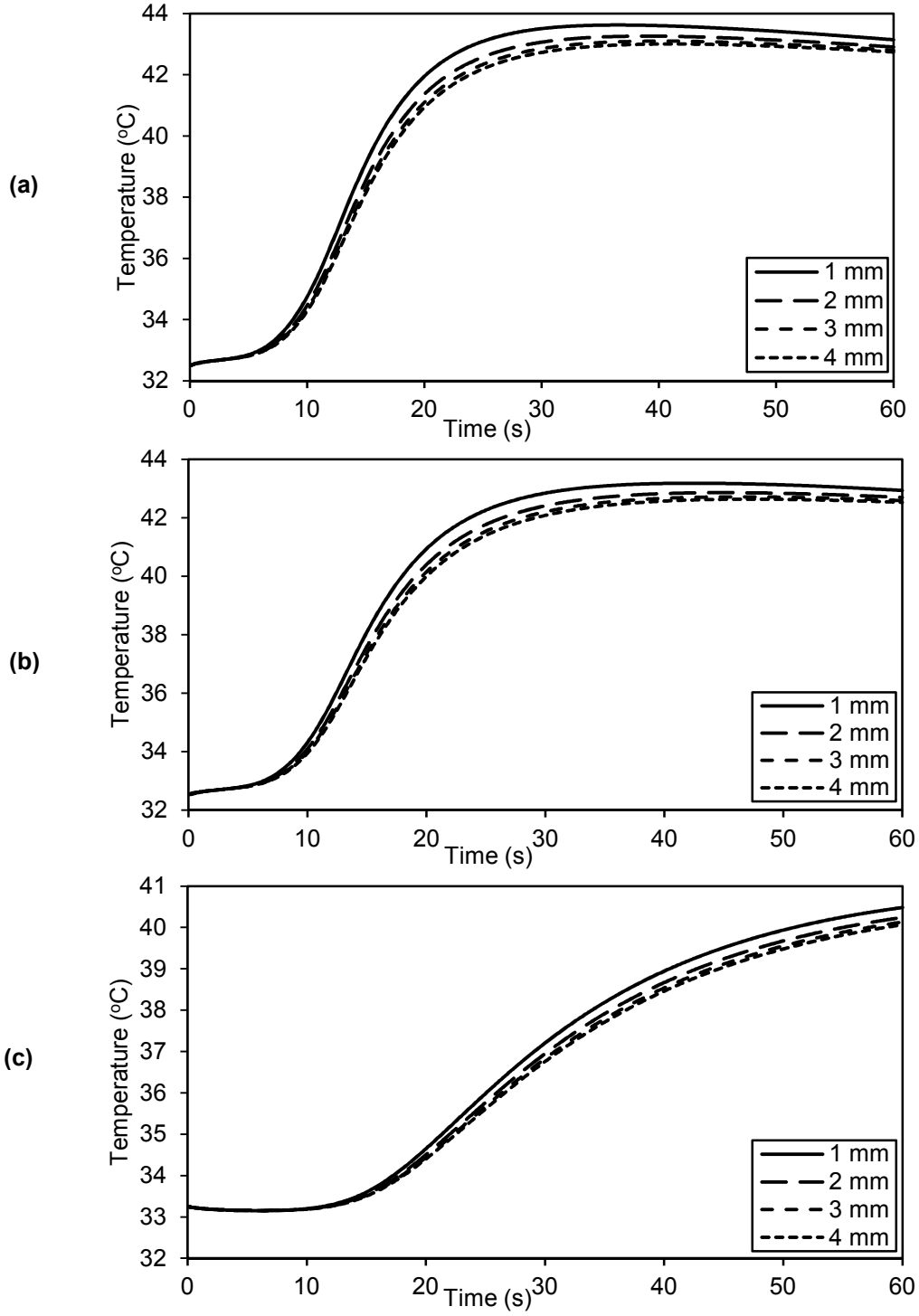

Figure 7. Influence of the air gap width between the outer shell and the moisture barrier on the clothing protective performance: (a) epidermis surface temperature, (b) basal layer temperature, and (c) dermal base temperature.

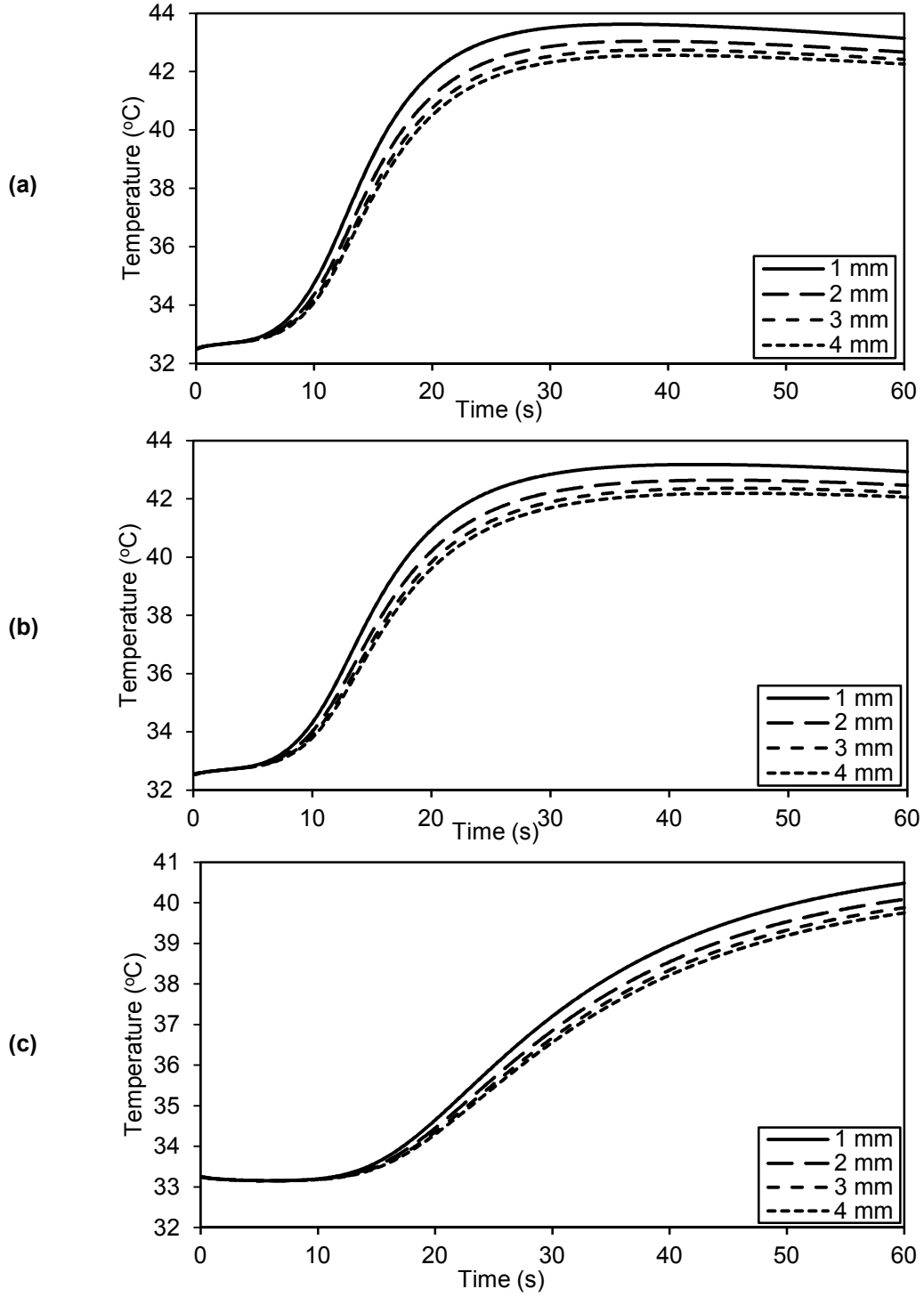

Figure 8. Influence of the air gap width between the moisture barrier and the thermal liner on the clothing protective performance: (a) epidermis surface temperature, (b) basal layer temperature, and (c) dermal base temperature.

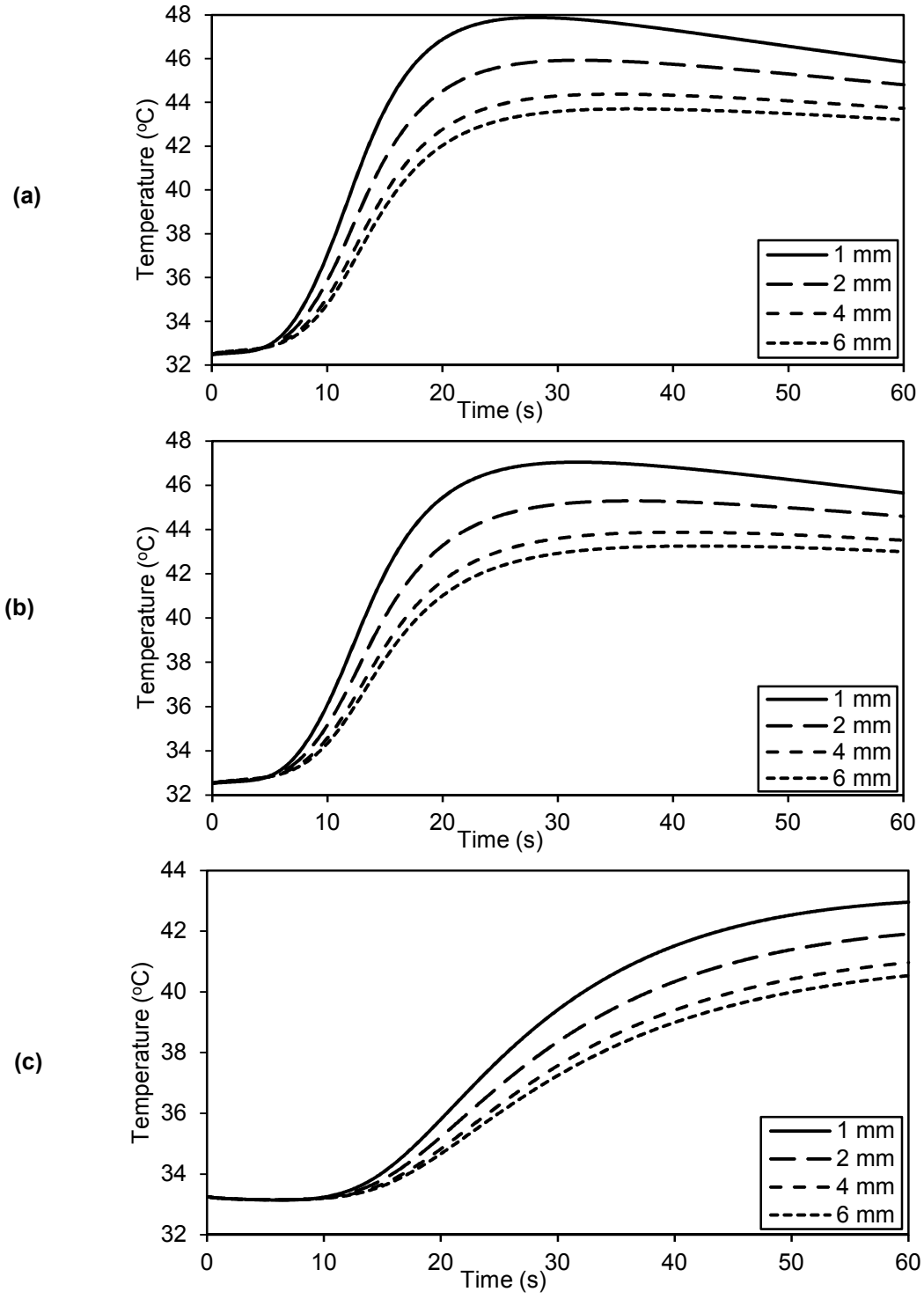

Figure 9. Influence of the air gap width between the thermal liner and the skin on the clothing protective performance: (a) epidermis surface temperature, (b) basal layer temperature, and (c) dermal base temperature.

CHAPTER 6

CONCLUSIONS

1. SUMMARY OF THE THESIS

The air gap between protective clothing and the skin plays a critical role in the protective performance provided by the clothing during flash fire exposure. Numerical models for heat transfer in protective clothing are used for predicting the clothing performance under different fire exposure conditions and scenarios as an alternative to experimental models, which are both costly and time consuming. Moreover, the more realistic the analysis of the air gap in the numerical model, the more reliable the performance of the clothing predicted by the model.

In this research project, the air gap between the protective clothing and the skin was treated as a thermal radiation participating medium because of the hot gas that fills this gap. This required the author to learn and implement the modeling of thermal radiation heat transfer in a thermal radiation participating medium using the finite volume method. Moreover, the modeling and implementation of the combined conduction-radiation heat transfer in enclosures of participating media is the specific expertise which is developed in this research work. The air gap between the protective clothing and the skin represents an enclosure with simultaneously determined boundary conditions since the air gap is located in the middle of the protective clothing system. This added more complexity to the typical problem of the combined conduction-radiation heat transfer in enclosures of participating media.

A 1-D numerical model for transient heat transfer in single layer protective clothing was described in chapter two. The model accounted for the conduction, the radiation absorption, and the thermochemical reactions within the fabric, the combined conduction-radiation heat

transfer through the air gap, and the conduction and blood perfusion within the skin. The model accounted for the temperature dependence of the thermophysical properties within both the fabric and the air gap. The simulation explored the transient temperature distribution within the clothing system as well as the transient energy content of the system. The chapter demonstrated the influence of the air gap model in predicting the performance of the clothing.

Chapter three, which can be considered as a completion of the research work presented in chapter two, further investigated the influence of different clothing parameters on the combined conduction-radiation heat transfer through the gap and on the corresponding protective performance of the clothing. The air gap absorption coefficient was found to have a relatively minimal influence on the temperature distribution within the air gap. On the other hand, it significantly affects the times to receive skin burn injuries, especially third-degree burn. Any reduction in the air gap width below the standard air gap width of 1/4 in. (6.4 mm) has a significant effect on the heat transfer through the air gap and hence on the clothing performance. In addition, the closer the fabric is to the skin, the more influential the reduction in the air gap width. Reducing the fabric backside emissivity was found to be more effective in improving the clothing performance than increasing the fabric thermal resistance by increasing the fabric thickness or using multiple layers.

Chapter four presented a comprehensive study of the influence of the motion of the person wearing the clothing during the act of extinguishing the fire or escaping from the fire location on the heat transfer through the clothing system. The clothing movement was shown to have a significant effect on the heat transfer in the protective clothing especially within the air gap. The influence of the clothing movement on its protective performance is the result of a combination of the periodic reduction in the air gap width and the periodic cooling of the air

within this gap. Increasing the frequency of the fabric movement improves the protection provided by the clothing due to the more frequent inflow of cool air. Increasing the amplitude of the fabric movement reduces the protection provided by the clothing by concentrating the exposure on the skin as a result of the periodic reduction in the air gap width. The greater the fabric movement amplitude, the greater the influence on the clothing performance.

A finite volume model for the transient heat transfer in firefighters' protective clothing with multiple air gaps was described in chapter five. The model accounted for the combined conduction-radiation heat transfer in each air gap within the clothing system. The model was employed to explore the transient temperature distribution and energy content of the clothing system. These results provide insight as to the contribution of each layer to the overall protective performance of the clothing system, which in turn could provide a rational basis for improving the clothing performance. The chapter investigated the influence of each air gap within the clothing system on the overall performance of the clothing. The contribution of the air gap between the moisture barrier and the thermal liner was found to be more influential on the clothing performance than that of the air gap between the outer shell and the moisture barrier. Neglecting the air gaps entrapped in the clothing would dramatically underestimate the clothing protective performance.

2. FUTURE WORK

The research work presented in the thesis demonstrated the critical role of the air gap(s) entrapped in the protective clothing system on the heat transfer through the clothing and hence on its protective performance. In this study the moisture transfer through the clothing, which results from the sweating and/or from water usage in extinguishing the fire was neglected. In addition, the 1-D nature of the model prevented including mass conservation as described in

chapter two, as well as the exploration of aspects of the three-dimensional geometry of the clothing as worn by firefighters. This creates some potential research work to be achieved in the future, as an extension to the research work introduced in this thesis, including the following:

1. To develop a numerical model for the coupled heat and moisture transfer in single layer protective clothing during flash fire exposure that accounts for the heat (conduction-radiation) and moisture transfer in the air gap between the clothing and the skin properly.
2. To further investigate the influence of different clothing parameters on the coupled heat (conduction-radiation) and moisture transfer through the air gap between protective clothing and the skin during flash fire exposure.
3. To develop a numerical model for the coupled heat and mass transfer in multiple layers protective clothing system during flash fire exposure that considers the air gap entrapped between the clothing layers.

A few aspects need to be taken into consideration in order to accomplish the above mentioned research work. First, an expertise in the modeling and implementation of heat and mass (water and vapour) transfer in the fabric as a porous medium should be developed. Second, a study of the variation in the radiation properties of the air gap (specifically, the radiation absorption coefficient) due to the moisture transfer through the air gap should be implemented in order to model the thermal radiation through the air gap. Finally, as was described earlier, modeling the combined conduction-radiation heat transfer in the air gap of protective clothing involved additional levels of complexity compared to the typical combined conduction-radiation problem in enclosures of thermal radiation participating media. One possible limitation to the above mentioned potential research work might be the state of art in the field of coupled heat and mass transfer in enclosures of thermal radiation participating media.

The experimental validation of the numerical models for heat and mass transfer in protective clothing is both a potential research work and a significant limitation for present numerical models. A contact flame bench top test that considers measuring the temperature distribution within the air gap during both the exposure and the cool down periods is a possible approach to further validating the numerical model developed in this thesis. Another bench top test that accounts for the variation in the air gap width due to the fabric motion could be used to validate the numerical study presented in chapter four. And last but not least, the experimental validation of the numerical modeling of heat and mass transfer as proposed in this section should also be considered.